Attitude Stabilization of a Quadrotor Aircraft

by

Stephen J. McGilvray

Under the Supervision of Dr. Abdelhamid Tayebi

A Thesis Submitted in Partial Fulfillment
of the Requirements for the Degree of

Master of Science
in Control Engineering

Lakehead University, Thunder Bay, Ontario, Canada

June 2004

Your file Votre référence
ISBN: 0-612-96982-7
Our file Notre référence
ISBN: 0-612-96982-7

Acknowledgments

Over the past few years I have had the pleasure and privilege of learning from, and collaborating with Dr. Abdelhamid Tayebi during my undergraduate and graduate studies at Lakehead University. He has proven to be a most excellent supervisor and has shown a great dedication to all of his students. I want to thank him for his incredible support and guidance, and for instilling in me a genuine passion for control engineering.

I also want to thank Kailash Bhatia for his contributions and innovative ideas that have graced every project I have worked on at Lakehead University.

I would like to thank my fiancée, Mélanie, for her love and understanding during our entire stay in Thunder Bay.

Finally, I would like to thank my family for their endless love and support.

Stephen J. McGilvray
smcgilvr@lakeheadu.ca

Contents

List of Figures

List of Tables

Chapter 1

Introduction

The quadrotor aircraft has seen a growing interest in the research community over the past few years, with a focus on modeling and control however. Early rotating wing aircraft pioneers designed similar four-rotor aircraft with varied success over a number of years. With the introduction of new lightweight sensors for measuring the attitude and angular velocity of a rigid body, model sized versions of traditional helicopters with autonomous capabilities have emerged, with the advantage of vertical take-off and landing (VTOL) over fixed wing aircraft. The quadrotor aircraft, with its symmetrical design, has a potential advantage with respect to the traditional helicopter in terms of maneuverability and mechanical simplicity. In fact, autonomous unmanned aerial vehicles (UAV's) have gained popularity for their numerous potential applications where human interaction is difficult or hazardous. Attitude stabilization, which could be considered the most important component for flight control, is essential for autonomous or even pilotable aircraft such as the quadrotor, as their designs are inherently unstable. As the literature suggests, a number of control algorithms have been proposed for the attitude control of a rigid body. In this thesis, a control strategy for the attitude stabilization of the quadrotor aircraft as well as some simulation and experimental results are presented.

1.1 Brief Quadrotor History

Over the past one hundred years rotor-crafts have been under extensive research and much time, effort and money have been invested into a wide variety of designs. In the early twentieth century, rotor-craft designs were driven by the desire to build a machine capable of vertical take-off and landing and the ability to hover. After much trial and error, rotor-crafts of all kinds were having limited success at sustained flight. However, it wasn't until the 1930's that significant advances were made involving fully controlled flight.

The four-rotor style aircraft, called the quadrotor, has had a somewhat long and discontinuous history in its research and development. Different variations of the quadrotor design are seen as far back as 1907 with the development of the *Gyroplane* built by Louis and Jacques Breguet in conjunction with Professor Charles Richet (Leishman 2000). This particular model consisted of a square central chassis with an arm attached to each corner supporting a 4-blade biplane rotor. One pair of diagonally opposing rotors rotated in a clockwise direction, while the remaining pair rotated in a counterclockwise direction. Many assisted hover flights were attained at low altitudes however, the aircraft was not practical as it lacked stability and proper control.

In 1922, another quadrotor style aircraft was built by Georges de Bothezat, and was one of the largest helicopters at the time (Leishman 2000; Gessow and Meyers 1967). This machine, which was under contract to the US Army, consisted of two intersecting beams in the shape of an 'x' or a cross with one rotor located at each end. Control of the aircraft was achieved by collective and differential collective thrust control, and cyclic rotor pitch variations for directional control. This particular quadrotor design flew successfully on a number of occasions but at low altitudes and forward speed. Due to its insufficient performance, high cost and the popularity of autogiros at the time, the US military lost interest and withdrew its funding resulting in the demise of the aircraft.

The most successful quadrotor design was flown in 1956 by designer and pilot D. H.

Kaplan, and was funded by the Convertawings company in Amityville, New York. This quadrotor differed from the previous designs in that the rotors were placed in an 'H' configuration. This was an appealing design because the need for cyclic pitch control was eliminated, and various combinations of collective pitch changes between the four rotors yielded a highly controllable aircraft (Gablehouse 1969). The project endured successful testing and development until military support for the Quadrotor was lost after spending cutbacks. However, ideas from the design and control system were used for future vertical short take-off and landing (VSTOL) aircraft designs utilizing four ducts, fans or jets. Currently there is no commercially available quadrotor style aircraft for human flight, and the available literature suggests that this was the last pilot carrying pure quadrotor aircraft to fly.

After many years, and technological advances in sensor capability such as the Micro-Electro-Mechanical-Systems (MEMS) packages for gyroscopes and accelerometers, a renewed interest in the quadrotor design has emerged in the form of smaller model sized operational aircraft. In fact, just recently a Canadian company named RC Toys in Saskatoon, Saskatchewan developed a commercially available quadrotor aircraft model for remote control (RC) enthusiasts (http://www.rctoys.com). This particular quadrotor, dubbed the Draganflyer, is driven by four electrically powered DC motors, with a rigid 'x' frame similar to the 1922 de Bothezat design. With lightweight, inexpensive onboard piezoelectric gyroscopes, the angular velocity of the aircraft is used as a feedback to a simple derivative controller to aid the remote pilot in stabilizing and flying the quadrotor aircraft. However, for inexperienced RC pilots, the first few flights can be quite challenging and require time and patience. Even with experience, a stable hover is virtually unattainable without constant control corrections, and a dedicated focus.

During the past few years, a growing interest in the quadrotor design has been seen, focusing on modeling and control (Hamel *et al.* 2002; Pounds *et al.* 2002; Castillo *et al.* 2003; Altuğ *et al.* 2002). This has been mainly due to the fact that it is now possible to control a model version, such as the Draganflyer, thanks to smaller

lightweight gyroscopes. However, it is important to highlight the motivation driving this recent quadrotor research, considering the traditional helicopter has enjoyed reasonable success for both pilotable and scale model designs.

1.2 Motivation

In recent years, UAV's have received a lot of attention for both fixed wing and rotating wing aircraft for a number of potential applications, and are essential where human interaction is difficult or hazardous. Some examples include high building and monument investigation, reconnaissance and surveillance, movie filming, search and rescue aid and meteorological surveys. Reasonable success has been achieved with fixed wing UAV's however, a great interest has been placed on scale model versions of traditional helicopters for their ability to hover and maneuver in confined or restricted areas, and for vertical take-off and landing ability. The interest in traditional scale model autonomous helicopters has been seen in a number of publications including (Shim *et al.* 1998; Avila Vilchis *et al.* 2003; Frazzoli *et al.* 2000; Mahony and Hamel 2001; Mahony *et al.* 1999).

However, the question remains: *Are there considerable advantages, such as controllability, maneuverability and efficiency that make the quadrotor design desirable over a traditional design, on even a scale model?* Although no experimental testing has been done here to draw quantitative comparisons between the two different designs, the following discussion will help illustrate some of the more obvious differences affecting performance.

There are a number of interesting observations to be made when comparing a quadrotor design with a traditional helicopter. For example, a traditional helicopter compensates the reactive torque produced from the main rotor by using a tail rotor to eliminate unwanted yaw motion. This energy spent on the tail rotor makes no contribution to the upward thrust of the aircraft. Comparatively, the reactive torques generated by the rotors of the quadrotor aircraft are effectively canceled as two rotors

rotate in one direction, and the other two rotate in the opposite direction, and all energy exerted from the four rotors contributes to upward thrust. A traditional helicopter must also consider unwanted gyroscopic torques during maneuvering, whereas the quadrotor, during trimmed flight has the gyroscopic torques canceled due to its configuration (Castillo *et al.* 2003).

Traditional helicopters require a relatively large main rotor, while the quadrotor utilizes four rotors which may be designed quite smaller in comparison, and driven at higher velocities helping to reduce mechanical vibrations and increase efficiency. Additionally, traditional helicopters have somewhat complicated mechanisms for achieving controlled flight. Control of the upward thrust is accomplished by governing and maintaining a constant main rotor speed while varying the pitch angle of the rotor blades, termed collective pitch, effectively increasing the thrust. Although the model version of the quadrotor used for experimental testing has fixed pitch rotor blades, a pilotable sized version could also use collective pitch to obtain control of the thrust. It begins to get mechanically complicated for a traditional helicopter when considering cyclic pitch of the main rotor. Essentially, cyclic pitch control is the ability to tilt the main rotor gear in the direction of desired flight. This mechanism is not necessary for the quadrotor, as controlled flight is achieved by variations in thrust between the four rotors, reducing mechanical complexities.

From a maneuverability perspective, the quadrotor has a clear advantage. Since the aircraft is symmetrical, there is technically no front, rear, right or left. This means the quadrotor has the ability to initiate and maintain flight in any given direction the same as it would for forward flight. A traditional helicopter however, cannot fly to the left or right, while maintaining the same orientation, with the same rigor as forward flight. Again due to its configuration, the quadrotor is capable of fantastic aerobatic maneuvers. A traditional helicopter, while still agile, is somewhat constrained by its physical configuration.

1.3 The Attitude Stabilization Problem

Attitude stabilization could be considered the single most important component of flight control for any aircraft. Many aircraft are inherently unstable in their design, making them much more maneuverable, yet difficult to control. Flight control of a quadrotor aircraft on a scale model or pilotable version is virtually impossible without the aid of a feedback controller. Similarly, UAV's and autonomous aircraft of any kind must be able to stabilize their attitude before controlled flight is attained.
It should be noted that attitude control is not limited to aircraft alone. In fact, the attitude control problem is the same for any rigid body and has been investigated by several researchers (Crouch 1984; Wie *et al.* 1989; Wen and Kreutz-Delgado 1991; Joshi *et al.* 1995; Lizarraide and Wen 1996). This includes for example, aircraft, mobile/walking robots, or underwater vehicles.

One challenge for the attitude stabilization problem arises from the need to use the attitude of the rigid body as feedback in the control algorithm. The angular velocity of the rigid body may not be simply integrated to obtain the attitude of the body, as they are linked dynamically and nonlinearly (Crouch 1984; Joshi *et al.* 1995). A number of other challenges are faced when considering the attitude stabilization problem. For instance, a global representation of the rigid body attitude is essential for full control, but is not always possible. Attitude representation can be achieved by a number of methods including Euler angles, quaternions, or the Direction Cosine Matrix, each with disadvantages including singularities, redundancies, and computational challenges (Wertz 1978; Hughes 1986; Spong and Vidyasagar 1989). Without a global mathematical representation of the aircraft attitude it is impossible to design a global control solution which can stabilize the aircraft from any attitude. However, most existing controllers are based on the four parameter quaternion representation which can be used to describe all possible orientations of the rigid body while avoiding the singularities existing in the aforementioned representations (Kane 1973; Ickes 1970).

A number of control algorithms guaranteeing global asymptotic stability, and under restricted conditions, local exponential stability for the attitude control problem, have been proposed in (Wen and Kreutz-Delgado 1991), however, only asymptotic stability is guaranteed for the other papers in the literature (Joshi *et al.* 1995; Wie *et al.* 1989; Lizarraide and Wen 1996). Most of the existing control algorithms are based on PD feedback control with Coriolis torques compensation, where the proportional action is in terms of the vector-quaternion, and the derivative action is in terms of the angular velocity of the rigid body.

In Chapter 3, the dynamical model for the quadrotor aircraft is developed in detail. With the exception of the gyroscopic term, the model equations reduce to the well known model for the dynamics of a rigid body. Chapter 4 shows the development of two main theorems: Theorem 1, developed using a Lyapunov function described in (Tayebi and McGilvray 2004), is model-dependent and guarantees global exponential stability for this problem. This theorem is based on the compensation of the gyroscopic and Coriolis torques, and has a PD^2 feedback structure, where the proportional action is in terms of the vector-quaternion, and the two derivative actions are in terms of the airframe angular velocity, and the vector-quaternion velocity. Theorem 2 is based on the classical model-independent PD controller and provides asymptotic stability for this problem. Modifications to both control algorithms will be discussed and will take form by either adding or removing compensation terms for the gyroscopic and Coriolis torques to give good comparisons of each controller developed. The advantage of the model-dependent controller developed in Theorem 1 is not fully evident in the simulation or experimental results, however, in practical applications considering large angles and aggressive maneuvers this controller will provide superior results in terms of disturbance rejection and attitude stabilization mostly due to the compensation of the gyroscopic and coriolis torques, and the additional vector-quaternion velocity feedback term.

A control algorithm has been developed to control the altitude of the aircraft once under attitude stabilization. This is an interesting feature as it allows a pilot to hover

the aircraft hands-free once a desired altitude has been chosen. Also, the solution to the attitude set-point regulation problem has been proposed by simply using the attitude error of the Euler angles to produce the quaternion used for feedback. Simulations have been performed for both theorems and their modified counterparts. These include stabilization from initial angles, as well as altitude stabilization, and attitude set-point regulation performance. In the chapter following the simulation results, the experimental setup of a model quadrotor aircraft is described while details regarding attitude measurement and sensor fusion are presented. In fact, the attitude measurement of the quadrotor aircraft proved to be most challenging. Finally, experimental results have been performed on both theorems and modified theorems, and the results are given in graphical format.

Chapter 2

Attitude Representation

Attitude representation of a rigid body in three dimensional space can be achieved by a number of methods, each having its advantages and disadvantages. By using one of the many parameterization methods, we strive to transform a set of orthonormal reference axes in inertial space to a set of axes attached to the aircraft. The methods to be described here are important for the approach taken in the development of a control solution for the quadrotor attitude stabilization as will be seen in the coming chapters. There are many existing methods including the direction cosine matrix, Euler angles, quaternions, Gibbs vector and Euler axis/angle representation. Each parameterization method serves the same purpose of attitude representation, but each has its advantages and disadvantages such as the number of parameters required or existing singularities.

Consider an inertially fixed frame $\mathcal{I}$ described by three orthonormal unit vectors $\hat{x}_\mathcal{I}$, $\hat{y}_\mathcal{I}$ and $\hat{z}_\mathcal{I}$, and a body-attached frame $\mathcal{A}$ attached to the aircraft with origin at the center of mass described by three orthonormal unit vectors $\hat{x}_\mathcal{A}$, $\hat{y}_\mathcal{A}$ and $\hat{z}_\mathcal{A}$ as seen in Figure 2.1. The main objective of each attitude representation method is to relate the frame $\mathcal{I}$ to the frame $\mathcal{A}$ through some transformation. Ideally, we would like to be able to represent the attitude of a rigid body with as few parameters as possible, avoiding singular conditions. However, mathematical manipulation of a potential representation must also be considered. Also, some representations give

clear physical meanings to their quantities, while others have no easily identifiable meaning.

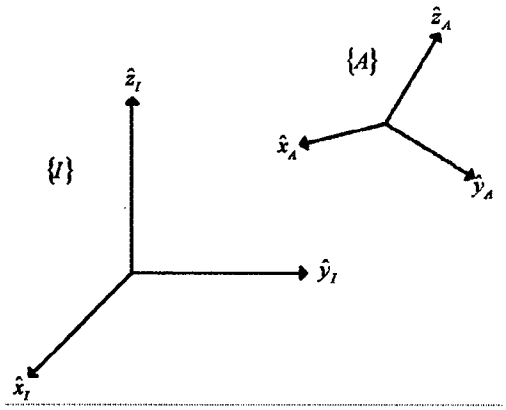

Figure 2.1: Inertially Fixed Frame $\mathcal{I}$, and Aircraft Body-Attached Frame $\mathcal{A}$.

2.1 Euler Angles

Representation of the attitude of an aircraft using Euler angles is one of the more common methods employed for this task. Interpretation of the Euler angles generally has a clear physical meaning and can be visualized with ease, making this method advantageous over others. Given the fact that only three parameters are required to represent the aircraft attitude gives this method another advantage. However, disadvantages that arise from using this method are evident when numerical computations are required to calculate successive rotations, as no convenient product rule exists. The Euler angles are generally described as three successive rotations about the inertial frame or body-attached frame axes. (Spong and Vidyasagar 1989; Wertz 1978; Hughes 1986). All rotations herein are taken in the direction using the right-hand rule, therefore when looking at an axis of rotation, the rotation is in the counter-clockwise direction. It should be noted however, that these notations are not uniform, and in many cases vary in the literature. When specifying the Euler angle representation, it is important to state the order of rotations and whether these rotations were made

around the inertial frame axes, or the body-attached frame axes. The Euler angles may be specified in many different sequences. In fact, for any given orientation there exist 12 possible axis sequences divided into two classes (Wertz 1978), and paired for descriptive purposes. These are given as follows

Class1:

$$\text{Pair 1: } x-y-z,\ z-y-x$$
$$\text{Pair 2: } y-z-x,\ x-z-y$$
$$\text{Pair 3: } z-x-y,\ y-x-z$$

Class2:

$$\text{Pair 4: } z-x-z,\ x-z-x$$
$$\text{Pair 5: } x-y-x,\ y-x-y$$
$$\text{Pair 6: } y-z-y,\ z-y-z$$

For a sequence in Class 1, each rotation is given about a unique axis. When these rotations are taken around the inertial frame axes there are of course 6 possible outcomes. When rotated about the body-attached frame axes the same six orientations are represented, but each sequence now represents the orientation its pair represented for the inertial frame reference rotations. For example, rotations in the $x-y-z$ sequence about the *inertial frame* axes give the same orientation as using the same rotations in the $z-y-x$ sequence about the *body-attached frame* axes.

The sequences described in Class 2 are all given with the third axis identical to the first. This indicates, for example, a rotation first about the $\hat{z}_{\mathcal{I}}$ axis, followed by a rotation about the $\hat{x}_{\mathcal{I}}$ axis, and finally another rotation about the $\hat{z}_{\mathcal{I}}$ axis.

Classically, Euler angles are given specifically as a $z-y-z$ sequence about the body-attached frame axes (Spong and Vidyasagar 1989; Hughes 1986), but any sequence described above can be considered Euler angles since the principle is the same. Class 2 sequences are not well suited to describing the attitude of an aircraft due to a singularity that occurs when the second rotation $\theta = 0$ (or $\theta = 180°$), which happens

to be at the flight reference orientation. It is obvious that when the second rotation $\theta = 0$, the axis of rotation for the first rotation ϕ and the third rotation ψ in the given sequence is the same axis for the inertial frame and for the body-attached frame (they are parallel). This means only a combination of the first and third rotational quantities $\phi + \psi$ is known reducing these two degrees of freedom to one. Although this singularity cannot be avoided using Euler angle representation, it can be moved to a more convenient location by choosing a Class 1 sequence.

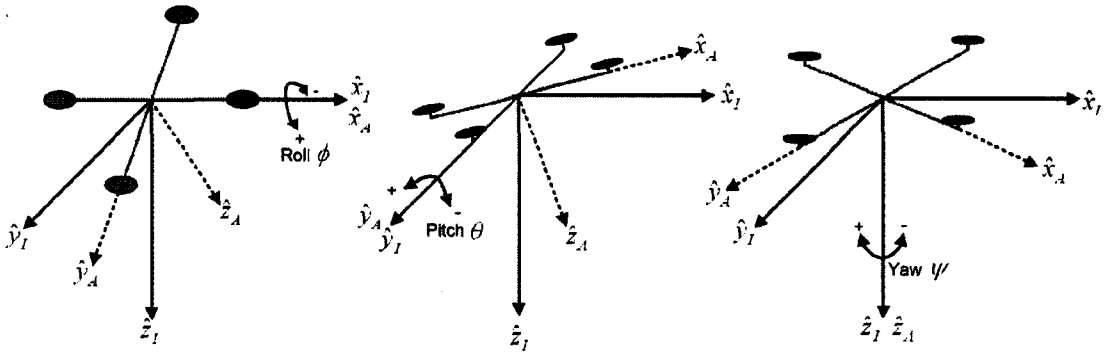

Figure 2.2: Roll, Pitch and Yaw Aircraft Planar Rotations

The $x - y - z$ sequence about the inertial frame axes is known as roll - pitch - yaw rotations (Spong and Vidyasagar 1989). This means the aircraft orientation is defined as a roll ϕ about $\hat{x}_{\mathcal{I}}$, followed by a pitch θ about $\hat{y}_{\mathcal{I}}$, followed by a yaw ψ about $\hat{z}_{\mathcal{I}}$ in this given order. The illustration seen in Figure (2.2) gives a clear example of roll, pitch and yaw movements of the quadrotor aircraft, where the front of the aircraft is indicated by the solid colour rotor. As mentioned previously, the same representation is achieved by using the $z - y - x$ sequence about the body-attached frame axes. Choosing the roll - pitch - yaw sequence from Class 1, moves the singularity. In some applications, the aircraft will never operate near this condition. However, this singularity must not be forgotten or ignored for control algorithms requiring global representation of the aircraft attitude free of singularities.

2.2 Direction Cosine Matrix (DCM)

The direction cosine matrix (DCM), also known as the rotation matrix R, is considered the fundamental quantity which represents the attitude of a rigid body in 3 dimensional space, and belongs to the set of matrices of order three $SO(3)$. In fact, successive rotations are easily computed by matrix multiplication of principal rotation matrices, and any number of rotations can be combined to produce a single rotation matrix defining the attitude of a rigid body. However, the rotation matrix R contains 9 terms, an obvious disadvantage when considering attitude feedback control.
Consider an inertial frame $\mathcal{I}$, and a body-attached frame $\mathcal{A}$ as seen in Figure (2.1). The rotation matrix which transforms the inertial frame to the body-attached frame attached to the aircraft is expressed as

$$R(\hat{x}_{\mathcal{I}} \quad \hat{y}_{\mathcal{I}} \quad \hat{z}_{\mathcal{I}}) \;=\; (\hat{x}_{\mathcal{A}} \quad \hat{y}_{\mathcal{A}} \quad \hat{z}_{\mathcal{A}})$$

and can therefore be defined as

$$R = \begin{pmatrix} \hat{x}_{\mathcal{A}} \cdot \hat{x}_{\mathcal{I}} & \hat{y}_{\mathcal{A}} \cdot \hat{x}_{\mathcal{I}} & \hat{z}_{\mathcal{A}} \cdot \hat{x}_{\mathcal{I}} \\ \hat{x}_{\mathcal{A}} \cdot \hat{y}_{\mathcal{I}} & \hat{y}_{\mathcal{A}} \cdot \hat{y}_{\mathcal{I}} & \hat{z}_{\mathcal{A}} \cdot \hat{y}_{\mathcal{I}} \\ \hat{x}_{\mathcal{A}} \cdot \hat{z}_{\mathcal{I}} & \hat{y}_{\mathcal{A}} \cdot \hat{z}_{\mathcal{I}} & \hat{z}_{\mathcal{A}} \cdot \hat{z}_{\mathcal{I}} \end{pmatrix} \tag{2.1}$$

Consider a rotation of the rigid body about the $\hat{z}_{\mathcal{I}}$ axis by the angle ψ. This implies $\hat{z}_{\mathcal{I}}$ remains orthogonal to $\hat{x}_{\mathcal{A}}$ and $\hat{y}_{\mathcal{A}}$, and $\hat{z}_{\mathcal{A}}$ remains orthogonal to $\hat{x}_{\mathcal{I}}$ and $\hat{y}_{\mathcal{I}}$ and of course $\hat{z}_{\mathcal{I}}$ and $\hat{z}_{\mathcal{A}}$ remain parallel therefore yielding

$$\begin{aligned} \hat{z}_{\mathcal{I}} \cdot \hat{x}_{\mathcal{A}} &= 0 \\ \hat{z}_{\mathcal{I}} \cdot \hat{y}_{\mathcal{A}} &= 0 \\ \hat{z}_{\mathcal{A}} \cdot \hat{x}_{\mathcal{I}} &= 0 \\ \hat{z}_{\mathcal{A}} \cdot \hat{y}_{\mathcal{I}} &= 0 \\ \hat{z}_{\mathcal{I}} \cdot \hat{z}_{\mathcal{A}} &= 1. \end{aligned}$$

Using the fact that, given two unit vectors $\hat{u}$ and $\hat{v}$ we may write

$$\begin{aligned} \hat{u} \cdot \hat{v} &= \|\hat{u}\| \cdot \|\hat{v}\| cos\theta \\ &= cos\theta, \end{aligned}$$

gives

$$\begin{aligned}
\hat{x}_{\mathcal{A}} \cdot \hat{x}_{\mathcal{I}} &= cos\psi \\
\hat{y}_{\mathcal{A}} \cdot \hat{y}_{\mathcal{I}} &= cos\psi \\
\hat{x}_{\mathcal{A}} \cdot \hat{y}_{\mathcal{I}} &= cos(\psi + \tfrac{\pi}{2}) = -sin\psi \\
\hat{y}_{\mathcal{A}} \cdot \hat{x}_{\mathcal{I}} &= cos(\psi - \tfrac{\pi}{2}) = sin\psi.
\end{aligned}$$

Therefore we can construct the principal rotation matrix for a rotation about the $\hat{z}$ axis by ψ as

$$R_{z,\psi} = \begin{pmatrix} c_\psi & -s_\psi & 0 \\ s_\psi & c_\psi & 0 \\ 0 & 0 & 1 \end{pmatrix} \tag{2.2}$$

where the shorthand notation used is as follows: $c_x = cos(x)$, $s_x = sin(x)$, $x \in \{\phi, \theta, \psi\}$.

Similarly, the principal rotation matrices for a rotation about the $\hat{x}$ axis and for a rotation about the $\hat{y}$ axis are constructed and given as

$$R_{x,\phi} = \begin{pmatrix} 1 & 0 & 0 \\ 0 & c_\phi & -s_\phi \\ 0 & s_\phi & c_\phi \end{pmatrix} \tag{2.3}$$

$$R_{y,\theta} = \begin{pmatrix} c_\theta & 0 & s_\theta \\ 0 & 1 & 0 \\ -s_\theta & 0 & c_\theta \end{pmatrix} \tag{2.4}$$

It should be noted that considering R is a *real orthogonal* matrix requires the transpose to be equal to the inverse, *i.e.*, $R^T = R^{-1}$.

For a given orientation, represented by any Euler angle sequence, using either the inertial or body-attached frame as a reference, the resulting rotation matrix will give the same quantifiable result, and is computed by matrix multiplication of (2.2), (2.3) and (2.4). The order of multiplication follows the Euler angle sequence when rotations are taken about the body-attached frame axes, and in reverse order when taken about the inertial frame axes.

The rotation matrix for the Euler angle $x-y-z$ sequence or roll-pitch-yaw about the inertial frame axes, to be used throughout this report, is calculated as follows

$$\begin{aligned} R &= R_{z,\psi}R_{y,\theta}R_{x,\phi} \\ &= \begin{pmatrix} c_\psi & -s_\psi & 0 \\ s_\psi & c_\psi & 0 \\ 0 & 0 & 1 \end{pmatrix} \begin{pmatrix} c_\theta & 0 & s_\theta \\ 0 & 1 & 0 \\ -s_\theta & 0 & c_\theta \end{pmatrix} \begin{pmatrix} 1 & 0 & 0 \\ 0 & c_\phi & -s_\phi \\ 0 & s_\phi & c_\phi \end{pmatrix} \\ &= \begin{pmatrix} c_\theta c_\psi & c_\psi s_\theta s_\phi - s_\psi c_\phi & c_\psi s_\theta c_\phi + s_\psi s_\phi \\ c_\theta s_\psi & s_\psi s_\theta s_\phi + c_\psi c_\phi & s_\psi s_\theta c_\phi - c_\psi s_\phi \\ -s_\theta & s_\phi c_\theta & c_\phi c_\theta \end{pmatrix} \end{aligned} \tag{2.5}$$

For a given rotation matrix

$$R = \begin{pmatrix} R_{11} & R_{12} & R_{13} \\ R_{21} & R_{22} & R_{23} \\ R_{31} & R_{32} & R_{33} \end{pmatrix}$$

it may be necessary to extract the Euler angles corresponding to the orientation represented by R. For the $x-y-z$ sequence about the inertial frame axes as described by (2.5), it is possible to extract the Euler angles from the given matrix R as described in (Spong and Vidyasagar 1989; Akella *et al.* 2003; Wertz 1978) as follows

$$\begin{pmatrix} \phi \\ \theta \\ \psi \end{pmatrix} = \begin{pmatrix} tan^{-1}(\frac{R_{32}}{R_{33}}) \\ sin^{-1}(-R_{31}) \\ tan^{-1}(\frac{R_{21}}{R_{11}}) \end{pmatrix} \begin{Bmatrix} 0 \leq \phi < 360^\circ \\ -90^\circ \leq \theta \leq 90^\circ \\ 0 \leq \psi < 360^\circ \end{Bmatrix} \tag{2.6}$$

Similarly, using the Class 2 Euler angle sequence $z-x-z$ as an example, the corresponding Euler angles are extracted using

$$\begin{pmatrix} \phi \\ \theta \\ \psi \end{pmatrix} = \begin{pmatrix} tan^{-1}(\frac{R_{31}}{R_{32}}) \\ cos^{-1}(R_{33}) \\ tan^{-1}(\frac{R_{13}}{-R_{23}}) \end{pmatrix} \begin{Bmatrix} 0 \leq \phi < 360^\circ \\ 0 \leq \theta \leq 180^\circ \\ 0 \leq \psi < 360^\circ \end{Bmatrix} \tag{2.7}$$

If we were to restrict the Class 1 representation and make it valid only for $-90° < \theta < +90°$, it will avoid the singularity existing when $\theta = \pm 90°$. Of course, to obtain a full unrestricted 360° unique non-singular representation, other methods must be considered. The quaternion representation, for example, reduces not only the number of parameters used for attitude representation, but avoids singularities inherent with the rotation matrix. However, the quaternion representation also has drawbacks associated with it that will be discussed in the coming section.

2.3 Quaternion Representation

The quaternion is yet another method of representing the orientation of a rigid body in space. Using the minimum number of parameters to globally represent orientation, with only four, makes this method advantageous over the rotation matrix. Additionally, the quaternion is free from singularities making this the method of choice (Wen and Kreutz-Delgado 1991; Kane 1973; Klumpp 1976; Wie *et al.* 1989; Joshi *et al.* 1995; Tayebi and McGilvray 2004).

The quaternion is also known as *Euler Parameters*, or *Euler Symmetric Parameters* because, as indicated by (Wertz 1978; Hughes 1986), the term quaternion was coined by Hamilton and strictly speaking this type of attitude representation can only be referred to as quaternions if Hamilton's notation is used. However, the following notation has been used extensively for aircraft attitude representation, and will continue to be referred to as the quaternion herein.

The quaternion is defined as

$$Q = \begin{pmatrix} q_0 \\ q \end{pmatrix} = \begin{pmatrix} q_0 \\ q_1 \\ q_2 \\ q_3 \end{pmatrix} = \begin{pmatrix} cos\frac{\gamma}{2} \\ \hat{k}_x sin\frac{\gamma}{2} \\ \hat{k}_y sin\frac{\gamma}{2} \\ \hat{k}_z sin\frac{\gamma}{2} \end{pmatrix} \tag{2.8}$$

where γ represents a rotation about an axis defined by the unit vector $\hat{k} = (\hat{k}_x\ \hat{k}_y\ \hat{k}_z)$, q_0 represents the scalar portion of the quaternion, and q represents the vector

portion of the quaternion herein called the *vector-quaternion.* Considering that general angular displacement has only three degrees of freedom, the four-parameter set is therefore not independent, and is subject to the constraint

$$q_0^2 + q_1^2 + q_2^2 + q_3^2 \equiv q^T q + q_0^2 = 1. \tag{2.9}$$

Any number of successive rotations represented by quaternions may be multiplied to give one quaternion for the resulting orientation, similar to the rotation matrix. This is achieved through the quaternion multiplication (Hughes 1986; Wertz 1978) given as

$$Q\bar{Q} = \begin{pmatrix} q_0\bar{q}_0 - q^T\bar{q} \\ q_0\bar{q} + \bar{q}_0 q + q \times \bar{q} \end{pmatrix} \tag{2.10}$$

where Q and $\bar{Q}$ are two quaternions such that $Q = \begin{pmatrix} q_0 \\ q \end{pmatrix}$ and $\bar{Q} = \begin{pmatrix} \bar{q}_0 \\ \bar{q} \end{pmatrix}$, and $\times$ denotes the cross product. However, it may also be convenient to express the quaternion multiplication in matrix form (Wertz 1978) given as

$$Q\bar{Q} = \begin{pmatrix} \bar{q}_0 & \bar{q}_3 & -\bar{q}_2 & \bar{q}_1 \\ -\bar{q}_3 & \bar{q}_0 & \bar{q}_1 & \bar{q}_2 \\ \bar{q}_2 & -\bar{q}_1 & \bar{q}_0 & \bar{q}_3 \\ -\bar{q}_1 & -\bar{q}_2 & -\bar{q}_3 & \bar{q}_0 \end{pmatrix} \begin{pmatrix} q_0 \\ q_1 \\ q_2 \\ q_3 \end{pmatrix} \tag{2.11}$$

The rotation matrix can be expressed in terms of the quaternion (Wertz 1978; Hughes 1986) as follows

$$R(Q) = \begin{pmatrix} q_0^2 + q_1^2 - q_2^2 - q_3^2 & 2(q_1q_2 + q_3q_0) & 2(q_1q_3 - q_2q_0) \\ 2(q_1q_2 - q_3q_0) & q_0^2 - q_1^2 + q_2^2 - q_3^2 & 2(q_2q_3 + q_1q_0) \\ 2(q_1q_3 + q_2q_0) & 2(q_2q_3 - q_1q_0) & q_0^2 - q_1^2 - q_2^2 + q_3^2 \end{pmatrix} \tag{2.12}$$

Therefore using (2.12) we can transform a given quaternion representation into the rotation matrix equivalent. However, if it is desirable to use the quaternion to represent aircraft orientation, one must consider that the mathematical model for the attitude dynamics for most rigid body problems include the use of the rotation matrix. Therefore, a transformation from the rotation matrix to the quaternion may

also be necessary.

Consider the relation between the rotation matrix R and the quaternion Q, made through Rodriguez formula as described in (Spong and Vidyasagar 1989; Hughes 1986) and given as

$$\begin{aligned} R &= I + 2q_0 S(q) + 2S(q)^2 \\ &= I + sin\gamma S(\hat{k}) + (1 - cos\gamma)S(\hat{k})^2 \end{aligned} \tag{2.13}$$

where $S(\hat{v})$ is defined as the skew symmetric matrix for a given vector $\hat{v} = (v_1, v_2, v_3)$ given as

$$S(\hat{v}) = \begin{pmatrix} 0 & -v_3 & v_2 \\ v_3 & 0 & -v_1 \\ -v_2 & v_1 & 0 \end{pmatrix} \tag{2.14}$$

A method of extracting the quaternion from R is presented in (Klumpp 1976), and shown in (Lizarraide and Wen 1996) as follows

$$S(q) = \frac{1}{2\sqrt{1 + trR}}(R - R^T), \tag{2.15}$$

where one can obtain q from $S(q)$, and finally q_0 by using (2.9).

The above method is mathematically equivalent to the transformation discussed in (Wertz 1978; Hughes 1986) given as

$$\begin{aligned} q_0 &= \pm\tfrac{1}{2}(1 + R_{11} + R_{22} + R_{33})^{1/2} \\ q &= \tfrac{1}{4q_0}\begin{pmatrix} R_{23} - R_{32} \\ R_{31} - R_{13} \\ R_{12} - R_{21} \end{pmatrix}. \end{aligned} \tag{2.16}$$

These transformations are valid provided that $q_0 \neq 0$. Numerical inaccuracies can also arise when q_0 is close to zero. For the condition where $q_0 = 0$, the vector-quaternion q is determined by (Hughes 1986)

$$q = \begin{pmatrix} \pm(\frac{1+R_{11}}{2})^{1/2} \\ \pm(\frac{1+R_{22}}{2})^{1/2} \\ \pm(\frac{1+R_{33}}{2})^{1/2} \end{pmatrix}. \tag{2.17}$$

It should be noted that there is a sign ambiguity present in the quaternion representation. By inspection of (2.12), it can be easily seen that by changing the sign of all four quaternion parameters has no effect on the outcome of the rotation matrix R. For example, the quaternion (q_0, q) leads to the same orientation as $(-q_0, -q)$. However, this ambiguity can be resolved by using the following differential equations (Hughes 1986; Wen and Kreutz-Delgado 1991)

$$\begin{aligned} \dot{q} &= \tfrac{1}{2}(S(q) + q_0 I_{3\times 3})\Omega, \\ \dot{q}_0 &= -\tfrac{1}{2} q^T \Omega, \end{aligned} \tag{2.18}$$

where $I_{3\times 3}$ is a 3×3 identity matrix, and Ω is the angular velocity of the rigid body.

Assuming most aircraft are likely to use sensors to measure the Euler angles, either directly or indirectly, a transformation of the Euler angles to the quaternion is convenient. The quaternion may be computed from given Euler angles using the following formula

$$\begin{pmatrix} q_0 \\ q \end{pmatrix} = \begin{pmatrix} cos(\frac{\phi}{2})cos(\frac{\theta}{2})cos(\frac{\psi}{2}) + sin(\frac{\phi}{2})sin(\frac{\theta}{2})sin(\frac{\psi}{2}) \\ sin(\frac{\phi}{2})cos(\frac{\theta}{2})cos(\frac{\psi}{2}) - cos(\frac{\phi}{2})sin(\frac{\theta}{2})sin(\frac{\psi}{2}) \\ cos(\frac{\phi}{2})sin(\frac{\theta}{2})cos(\frac{\psi}{2}) + sin(\frac{\phi}{2})cos(\frac{\theta}{2})sin(\frac{\psi}{2}) \\ cos(\frac{\phi}{2})cos(\frac{\theta}{2})sin(\frac{\psi}{2}) - sin(\frac{\phi}{2})sin(\frac{\theta}{2})cos(\frac{\psi}{2}) \end{pmatrix} \tag{2.19}$$

In fact, (2.19) is obtained by using the quaternion multiplication given in (2.10), *i.e.*,

$$\begin{pmatrix} q_0 \\ q \end{pmatrix} = Q_\psi Q_\theta Q_\phi \tag{2.20}$$

where Q_ψ, Q_θ and Q_ϕ represent the quaternions for the roll (ϕ), pitch (θ) and yaw (ψ) angles respectively, and using (2.8), *i.e.*,

$$Q_\phi = \begin{pmatrix} cos(\frac{\phi}{2}) \\ sin(\frac{\phi}{2}) \\ 0 \\ 0 \end{pmatrix}, Q_\theta = \begin{pmatrix} cos(\frac{\theta}{2}) \\ 0 \\ sin(\frac{\theta}{2}) \\ 0 \end{pmatrix}, Q_\psi = \begin{pmatrix} cos(\frac{\psi}{2}) \\ 0 \\ 0 \\ sin(\frac{\psi}{2}) \end{pmatrix} \tag{2.21}$$

Note that the order of rotation follows the same rules as the rotation matrix (multiply quaternions in direct order of Euler angle sequence for rotations about the body-attached frame, and in reverse order for rotations about the inertial frame).

In summary, the quaternion provides a non-singular representation of the attitude of a rigid body, and is prefered to the rotation matrix because of its more compact form, requiring only four parameters as opposed to nine. Successive rotations are also calculated using a multiplication method involving no trigonometric functions, reducing the complexity of the computations. Physically, there are no sensors that can be mounted to directly give the quaternions representing the attitude of the quadrotor aircraft. The sensors involved will yield, indirectly, the Euler angles of the aircraft, and since the quaternion representation is desirable for the feedback control design, the transformation from Euler angles to quaternion, provided in this chapter, is necessary.

Chapter 3

The Quadrotor Model

The quadrotor aerial robot under examination consists of a rigid cross frame with four rotors; one attached at each end of the frame and geared to a DC permanent magnet motor as seen in Figure (3.1). The design is symmetrical and therefore the quadrotor has no obvious front or rear however, to avoid confusion the front rotor on the physical model is indicated by a different colour. One significant difference between this aircraft and a traditional helicopter is how dynamic flight is achieved. A traditional helicopter uses cyclic pitch control to slightly change the degree of the axis of rotation of the main rotor gear, allowing the aircraft to pitch and roll. Collective pitch control is used to change the pitch angle of the actual rotor blades, and if done while the speed is maintained constant, will control the thrust of the main rotor. However, the quadrotor model has neither collective nor cyclic pitch capabilities. This creates a much simpler aircraft in terms of actuator control as cyclic and collective pitch of a rotor creates mechanical complexities and challenges in the design. Therefore, variations in thrust to each rotor are applied by varying the rotor speed. This particular design allows for vertical take-off and landing flight similar to a traditional helicopter. Basic flight maneuvers are not entirely obvious, and are explained in detail in the following section.

3.1 Properties of Flight

As seen in Figure (3.1) the front and rear rotors, numbered 1 and 3 rotate in a counter-clockwise direction, while the left and right rotors, numbered 2 and 4 rotate in a clockwise direction. The rotors spin only in the direction indicated, and will not reverse direction. Of course this limits the possibility of 'upside down' flight, or some aggressive maneuvers requiring positive and negative thrust capabilities from the rotors.

To understand the properties of flight of the quadrotor, first consider a static attitude

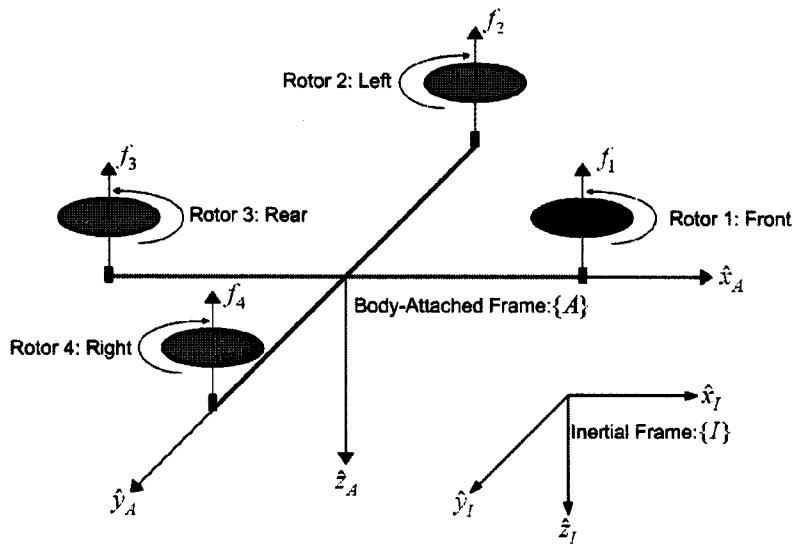

Figure 3.1: Quadrotor Model

at zero, or hover orientation. Vertical flight is achieved by increasing (decreasing) the speed of each rotor by the same proportion. This will increase (decrease) the overall thrust applied to the airframe allowing the aircraft to ascend (descend).

The roll motion of the quadrotor is achieved by increasing the thrust to rotor 2 (4) and decreasing the thrust to rotor 4 (2) to obtain a positive (negative) roll to the right

(left). Similarly, the pitch motion of the quadrotor is achieved by increasing the thrust to rotor 1 (3) and decreasing the thrust to rotor 3 (1) to obtain a positive (negative) pitch up (down). For both the roll and the pitch motion, the thrust increase to one rotor is exactly proportional to the thrust decrease for the opposite rotor to maintain the same overall thrust, since the overall thrust is simply the sum of the thrust from the four rotors.

The yaw motion of the quadrotor, similar to a traditional helicopter, takes advantage of the effects of the reactive torque. On a traditional helicopter, the reactive torque from the main rotor is applied to the airframe in the opposite direction to the spin of the rotor, causing the aircraft to yaw. However, the tail rotor compensates for this reactive torque, and once in equilibrium no yaw motion is present. The quadrotor aircraft has a combined reactive torque from all four rotors. The reactive torques from rotors 1 and 3 combine to create a positive yaw torque, while the reactive torques from rotors 2 and 4 combine to create a negative yaw torque. Therefore, when the sum of the reactive torques from rotors 1 and 3 equals that of rotors 2 and 4, there is no yaw action. When a yaw motion is desired, the rotor pair 1 and 3 (2 and 4) increase (decrease) by the same proportion while the rotor pair 2 and 4 (1 and 3) decrease (increase) by the same proportion. This will result in a yaw motion in the positive (negative) direction without pitching or rolling the aircraft, and while still maintaining the same overall aircraft thrust.

3.2 Dynamical Model

The dynamical model of the quadrotor aircraft as described in (Hamel *et al.* 2002; Tayebi and McGilvray 2004) is based on using Newton's equations of motion. The quadrotor dynamical model described in (Castillo *et al.* 2003) has been derived using the Lagrangian approach however, the result is nearly identical to the model derived using Newton's equations. In fact, the first approach has been taken here, and is developed as follows:

Let $\mathcal{I} = \{\hat{x}_\mathcal{I}, \hat{y}_\mathcal{I}, \hat{z}_\mathcal{I}\}$ denote a right-hand inertially fixed frame where $\hat{z}_\mathcal{I} = (0, 0, 1)^T$ is a vertical vector pointing towards the earth, and $\mathcal{A} = \{\hat{x}_\mathcal{A}, \hat{y}_\mathcal{A}, \hat{z}_\mathcal{A}\}$ denotes a right-hand inertial body-attached frame with origin at the center of mass. Using Newton's equations of motion, a dynamical model for the quadrotor is given as (Hamel *et al.* 2002)

$$\dot{p} = v, \tag{3.1}$$

$$\dot{v} = g\hat{z}_\mathcal{I} - \frac{1}{m}TR\hat{z}_\mathcal{I}, \tag{3.2}$$

$$\dot{R} = RS(\Omega), \tag{3.3}$$

$$I_f\dot{\Omega} = -\Omega \times I_f\Omega - G_a + \tau_a, \tag{3.4}$$

$$I_r\dot{\omega}_i = \tau_i - Q_i, \quad i \in \{1, 2, 3, 4\} \tag{3.5}$$

where the vector $p = (x, y, z)^T$ denotes the position of the origin of the body-attached frame $\mathcal{A}$ at the center of mass of the quadrotor expressed in the inertial frame $\mathcal{I}$, the vector v denotes the linear velocity of the origin of $\mathcal{A}$ expressed in $\mathcal{I}$, g denotes the acceleration due to gravity, m denotes the mass of the aircraft, T denotes the total thrust applied to the airframe by the four rotors, $R \in SO(3)$ denotes the rotation matrix which describes the orientation of the body-attached frame $\mathcal{A}$ expressed in $\mathcal{I}$. The vector Ω denotes the angular velocity of the quadrotor expressed in the body-attached frame $\mathcal{A}$, $S(\Omega)$ denotes the skew-symmetric matrix associated to Ω such that $S(\Omega)V = \Omega \times V$ for any vector $V \in \mathbb{R}^3$, where $\times$ denotes the vector cross-product. $I_f \in \mathbb{R}^{3\times3}$ denotes the constant inertia matrix around the center of mass, G_a denotes the gyroscopic torques applied to the airframe from the four rotors, τ_a denotes the torques applied to the airframe by the four rotors. I_r, ω_i, τ_i and Q_i denote the rotor inertia, the rotor velocity, the torque and reactive torque generated by the rotor i, respectively.

The thrust applied to the airframe from the four rotors is given by

$$T = \sum_{i=1}^{4} |f_i| = b\sum_{i=1}^{4} \omega_i^2, \tag{3.6}$$

where $f_i = -b\omega_i^2 \hat{z}_{\mathcal{I}}$ is the lift generated by the rotor i in free air, and b is a proportionality constant dependent on factors such as the density of air, the number, shape, radius and pitch of the rotor blades as described in (Hamel *et al.* 2002; Prouty 1995) in more detail.

The rotation matrix describing the orientation of the quadrotor aircraft is developed from the Euler $x-y-z$ sequence about the inertial frame axes as described in (2.5) and is given as

$$R = \begin{pmatrix} c_\theta c_\psi & c_\psi s_\theta s_\phi - s_\psi c_\phi & c_\psi s_\theta c_\phi + s_\psi s_\phi \\ c_\theta s_\psi & s_\psi s_\theta s_\phi + c_\psi c_\phi & s_\psi s_\theta c_\phi - c_\psi s_\phi \\ -s_\theta & s_\phi c_\theta & c_\phi c_\theta \end{pmatrix} \tag{3.7}$$

The Euler angles representing the roll, pitch and yaw orientation of the quadrotor are denoted as ϕ, θ and ψ.

Equation (3.4) equates the airframe torques $I_f\dot{\Omega}$ to the applied airframe torques τ_a with the subtraction of the Coriolis torques $(\Omega \times I_f\Omega)$ and gyroscopic torques G_a where the gyroscopic torques are given as

$$G_a = \sum_{i=1}^{4} I_r(\Omega \times \hat{z}_{\mathcal{I}})(-1)^{i+1}\omega_i, \tag{3.8}$$

and the airframe torques applied by the rotors are given as

$$\begin{aligned} \tau_a^1 &= db(\omega_2^2 - \omega_4^2) \\ \tau_a^2 &= db(\omega_1^2 - \omega_3^2) \\ \tau_a^3 &= \kappa(\omega_1^2 + \omega_3^2 - \omega_2^2 - \omega_4^2) \end{aligned} \tag{3.9}$$

where d denotes the distance from the rotor center to the center of mass of the aircraft at the origin of the body-attached frame $\mathcal{A}$, and κ denotes a proportionality constant also dependent on a number of factors as described for the constant b.

The reactive torque generated by the rotor i, in free air, due to rotor drag is given by

$$Q_i = \kappa\omega_i^2. \tag{3.10}$$

The dynamical equation describing the angular attitude given by (3.3), may also be described in terms of the roll-pitch-yaw Euler angles by the following kinematic equation (Crouch 1984; Rehbinder and Hu 2003; Rehbinder and Hu 2000)

$$\begin{pmatrix} \Omega_1 \\ \Omega_2 \\ \Omega_3 \end{pmatrix} = \begin{pmatrix} \dot{\phi} \\ 0 \\ 0 \end{pmatrix} + \begin{pmatrix} 1 & 0 & 0 \\ 0 & c_\phi & -s_\phi \\ 0 & s_\phi & c_\phi \end{pmatrix} \begin{pmatrix} 0 \\ \dot{\theta} \\ 0 \end{pmatrix}$$

$$+ \begin{pmatrix} 1 & 0 & 0 \\ 0 & c_\phi & -s_\phi \\ 0 & s_\phi & c_\phi \end{pmatrix} \begin{pmatrix} c_\theta & 0 & s_\theta \\ 0 & 1 & 0 \\ -s_\theta & 0 & c_\theta \end{pmatrix} \begin{pmatrix} 0 \\ 0 \\ \dot{\psi} \end{pmatrix} \tag{3.11}$$

$$= \begin{pmatrix} 1 & 0 & -s_\theta \\ 0 & c_\phi & s_\phi c_\theta \\ 0 & -s_\phi & c_\phi c_\theta \end{pmatrix} \begin{pmatrix} \dot{\phi} \\ \dot{\theta} \\ \dot{\psi} \end{pmatrix}$$

Inversion of the above matrix gives

$$\begin{pmatrix} \dot{\phi} \\ \dot{\theta} \\ \dot{\psi} \end{pmatrix} = \begin{pmatrix} 1 & sin\phi tan\theta & cos\phi tan\theta \\ 0 & cos\phi & -sin\phi \\ 0 & sin\phi sec\theta & cos\phi sec\theta \end{pmatrix} \begin{pmatrix} \Omega_1 \\ \Omega_2 \\ \Omega_3 \end{pmatrix} \tag{3.12}$$

where Ω_1,Ω_2 and Ω_3 represent the angular velocity of the aircraft around the body-attached frame $\hat{x}_\mathcal{A}$, $\hat{y}_\mathcal{A}$ and $\hat{z}_\mathcal{A}$ axes respectively. It is clear that the above kinematic equation is only valid for $-90° < \theta < 90°$. It is also apparent from the above equation that for a single planar rotation about one axis, when starting with zero initial angles, the angular velocity about the body-attached axis is linear with respect to the inertial frame axis. However, for any combination of angles and angular velocity, the result is truly nonlinear. This is important to consider for practical implementation, as gyroscopic sensors mounted on the orthonormal axes measure the angular velocity of the aircraft rotations around the body-attached frame axes, and do not directly represent the Euler angle velocity, however it may be necessary to quantify the angular

velocity of the Euler angles of the aircraft, making this relationship essential.

The model equations given in (3.1) - (3.5) describe the dynamical model for the quadrotor aircraft, but are not much different from the model of a traditional helicopter seen in (Mahony and Hamel 2001; Mahony *et al.* 1999; Frazzoli *et al.* 2000). In fact, the first four equations of the quadrotor model, with the exception of the gyroscopic torque term G_a is almost identical to the model proposed in (Mahony and Hamel 2001).

Again, with exception of the gyroscopic torque G_a, equations (3.3) and (3.4) describe the attitude dynamics of a rigid body in three dimensional space. The input to these two equations τ_a, represents the torque applied around the three primary axes of rotation. The model does not become specific to the quadrotor aircraft until the equation for τ_a is defined in (3.9) and equation (3.5) is introduced.

As previously mentioned, the development of the quadrotor model as described in (Castillo *et al.* 2003) yields a similar result while taking a somewhat different approach. The general idea, using a Lagrangian approach, considers the translational kinetic energy, the rotational kinetic energy, and the gravitational potential energy and is given as

$$\begin{aligned} L(c,\dot{c}) &= K_t + K_r - P_g \\ &= \tfrac{1}{2} m \dot{p}^T \dot{p} + \tfrac{1}{2} \dot{\eta}^T I_f \dot{\eta} - mgz \end{aligned} \tag{3.13}$$

where K_t, K_r and P_g represent the translational kinetic energy, rotational kinetic energy, and the gravitational potential energy. The vector $\eta = (\psi, \theta, \phi)$ represents the Euler angles, while $c = (p, \eta)$.

Further development of the model which includes the full quadrotor dynamics, uses the Euler-Lagrange equations with external generalized force and yields

$$m\ddot{p} = T \begin{pmatrix} -sin\theta \\ cos\theta sin\phi \\ cos\theta cos\phi \end{pmatrix} + \begin{pmatrix} 0 \\ 0 \\ -mg \end{pmatrix} \tag{3.14}$$

$$I_f\ddot{\eta} \;=\; -C(\eta,\dot{\eta})\dot{\eta} + \tau_a, \tag{3.15}$$

where $C(\eta,\dot{\eta})$ is defined as containing the Coriolis and gyroscopic terms. From inspection it is clear to see that (3.15) is representing the same dynamics as (3.4) given in the original model development. Similarly, the dynamics represented by (3.14) are also described by the original model in (3.2).

Some possible disadvantages could arise from the use of this particular dynamical model. Specifically, there is no development of a unique gyroscopic term, only a combined Coriolis and gyroscopic term. In fact, compensation of these individual terms is necessary for a more rigorous control design as will be seen in a coming chapter.

Chapter 4

Control Design

The main objective of the controllers to be developed in this chapter, is to stabilize the attitude of the quadrotor aircraft. Additional objectives include the stabilization of the quadrotor aircraft to a desired altitude, and developing a solution to the attitude set-point regulation problem.

The attitude stabilization objective has been met and is presented in two theorems listed as Theorem 1, and Theorem 2. The controller in Theorem 1 is model-dependent and slightly more complex however, it guarantees exponential stability, while the controller in Theorem 2 is model-independent and guarantees asymptotic stability.

The general attitude stabilization control design will be divided into two main sections. The first section deals with the design of the airframe torques τ_a. The second section will show the development of the control design for the rotor torques τ_i.

Additional sections are presented in this chapter which include the development of an altitude controller, and a solution to the attitude set-point regulation problem.

4.1 Airframe Torques Design

Considering the model equations (3.3) and (3.4), and using τ_a as an input, the objective is to design a controller to stabilize the attitude of the quadrotor aircraft

to a hover orientation. Depending on the attitude representation under consideration, this hover orientation is at the equilibrium point given by $(\phi, \theta, \psi, \Omega) = 0$ or $(R = I, \Omega = 0)$, which is equivalent to $(q = 0, q_0 = \pm 1, \Omega = 0)$.

Recalling the definition for the quaternion given in (2.8), we can see that a rotation by $\gamma = 0$ around $\hat{k}$ corresponds to $q_0 = 1$, and a rotation by $\gamma = 360°$ around $\hat{k}$ corresponds to $q_0 = -1$, but actually represents the same physical equilibrium point at $R = I$. To avoid this redundancy, the control design has been developed while restricting the Euler roll-pitch-yaw angles, and the equivalent rotation angle γ around $\hat{k}$ between $-180°$ and $180°$. This restricts the scalar portion of the quaternion to $0 \leq q_0 \leq 1$ avoiding the redundancy previously mentioned.

The first theorem, developed in (Tayebi and McGilvray 2004), is given as follows:

4.1.1 Theorem 1

Consider the quadrotor model equations (3.3) and (3.4) under the following control law

$$\tau_a = (\Omega \times I_f \Omega) + G_a + I_f \dot{\bar{\Omega}} - \Gamma_2 \tilde{\Omega} - \Gamma_3 q, \tag{4.1}$$

where

$$\begin{aligned} \tilde{\Omega} &= \Omega - \bar{\Omega} \\ \bar{\Omega} &= -\Gamma_1 q \end{aligned}$$

and using equation (2.18) for the quaternion derivative we have

$$\begin{aligned} \dot{\bar{\Omega}} &= -\Gamma_1 \dot{q} \\ &= -\tfrac{1}{2}\Gamma_1 (S(q) + q_0 I_{3\times 3})\Omega. \end{aligned}$$

The control design parameters Γ_1, Γ_2 and Γ_3 are as follows: Γ_1 is a 3×3 symmetric positive definite matrix, Γ_2, and Γ_3 are 3×3 diagonal positive definite matrices when the matrix defining the aircraft inertia I_f is diagonal. If I_f is not diagonal, the matrix Γ_2 must be a 3×3 symmetric positive definite matrix, and $\Gamma_3 = \alpha I_{3\times 3}$ where α is a positive scalar.

Therefore, considering the above, the equilibrium point described by $(R = I, \Omega = 0)$

is globally exponentially stable.

Proof of Theorem 1

The control law given in (4.1) has been developed using the backstepping method for nonlinear control design. The following details will show how the control law was developed.

Recall the differential equations for the quaternion given in (2.18). The first objective is to force $q \to 0$ and $q_0 \to 1$ as $t \to \infty$, by using $\bar{\Omega}$ as a virtual control variable. The second objective is to force the error term given as $\tilde{\Omega} = \Omega - \bar{\Omega}$ to zero by using τ_a as the control input.

Consider the following positive definite Lyapunov function candidate

$$V_1 = q^T q + (q_0 - 1)^2. \tag{4.2}$$

Using the quaternion constraint (2.9), the above reduces to

$$V_1 = 2(1 - q_0),$$

whose time derivative is given as

$$\dot{V}_1 = -2\dot{q}_0.$$

Substituting for $\dot{q}_0$ in (2.18) gives

$$\dot{V}_1 = q^T \Omega. \tag{4.3}$$

The virtual control variable is now designed as

$$\bar{\Omega} = -\Gamma_1 q$$

and substituting this into (4.3) we have

$$\dot{V}_1 = -q^T \Gamma_1 q, \tag{4.4}$$

which is negative semi-definite. However, to realize this result, we must now ensure that $\Omega \to \bar{\Omega}$ as $t \to \infty$ which is achieved by forcing $\tilde{\Omega} \to 0$.

The angular velocity error is defined as

$$\tilde{\Omega} = \Omega - \bar{\Omega},$$

whose time derivative is given by

$$\dot{\tilde{\Omega}} = \dot{\Omega} - \dot{\bar{\Omega}}. \tag{4.5}$$

Using $\dot{\Omega}$ from the model equation (3.4) into the above gives

$$\dot{\tilde{\Omega}} = I_f^{-1}((-\Omega \times I_f\Omega) - G_a + \tau_a) - \dot{\bar{\Omega}}. \tag{4.6}$$

A second positive definite Lyapunov function candidate is given as

$$V_2 = \frac{1}{2}\tilde{\Omega}^T\Gamma_3^{-1}I_f\tilde{\Omega} \tag{4.7}$$

whose time derivative is given by

$$\dot{V}_2 = \tilde{\Omega}'^T\Gamma_3^{-1}I_f\dot{\tilde{\Omega}}. \tag{4.8}$$

Using $\dot{\tilde{\Omega}}$ from (4.5) into (4.8) above gives

$$\begin{aligned} \dot{V}_2 &= \tilde{\Omega}'^T\Gamma_3^{-1}I_f((I_f^{-1}(-\Omega \times I_f\Omega) - G_a + \tau_a) - \dot{\bar{\Omega}}) \\ &= \tilde{\Omega}^T\Gamma_3^{-1}(-(-\Omega \times I_f\Omega) - G_a + \tau_a) - I_f\dot{\bar{\Omega}}). \end{aligned} \tag{4.9}$$

Now, combining the two Lyapunov functions gives

$$\begin{aligned} V &= V_1 + V_2 \\ &= 2(1 - q_0) + \tfrac{1}{2}\tilde{\Omega}'^T\Gamma_3^{-1}I_f\tilde{\Omega}, \end{aligned} \tag{4.10}$$

whose time derivative is given as

$$\dot{V} = q'^T(\tilde{\Omega} + \bar{\Omega}) + \tilde{\Omega}'^T\Gamma_3^{-1}(-(\Omega \times I_f\Omega) - G_a + \tau_a - I_f\dot{\bar{\Omega}}). \tag{4.11}$$

Finally, the input τ_a appears in the above equation allowing the control law given in (4.1) to be designed. Using this control law and substituting it into (4.11) above yields

$$\dot{V} = -q^T\Gamma_1 q - \tilde{\Omega}^T\Gamma_3^{-1}\Gamma_2\tilde{\Omega}, \tag{4.12}$$

which is negative semi-definite.

The proof for the exponential convergence is shown as follows: Using the constraint $\|q_0\| \leq 1$ stated previously, and the quaternion restriction given in (2.9), we have

$$\|q\|^2 = 1 - q_0^2 \geq 1 - q_0 \tag{4.13}$$

Therefore, V can be bounded as follows

$$V \leq max\{2, \frac{\lambda_{max}(\Gamma_3^{-1} I_f)}{2}\}(\|q\|^2 + \|\tilde{\Omega}\|^2). \tag{4.14}$$

Similarly $\dot{V}$ can be bounded as follows

$$\dot{V} \leq -min\{\lambda_{min}(\Gamma_1), \lambda_{min}(\Gamma_3^{-1}\Gamma_2)\}(\|q\|^2 + \|\tilde{\Omega}\|^2). \tag{4.15}$$

Therefore, using (4.14) and (4.15) above, we can conclude that

$$\dot{V} \leq -\beta V, \tag{4.16}$$

where $\beta = \frac{min\{\lambda_{min}(\Gamma_1), \lambda_{min}(\Gamma_3^{-1}\Gamma_2)\}}{max\{2, 0.5\lambda_{max}(\Gamma_3^{-1} I_f)\}}$, with $\lambda_{min}(*)$ and $\lambda_{max}(*)$ denote, respectively, the minimum and maximum eigenvalue of $(*)$.

It should be noted that control law (4.1) developed in Theorem 1 can be rewritten in the following form:

$$\tau_a = \Omega \times I_f \Omega + G_a - (\Gamma_3 + \Gamma_2\Gamma_1)q - \Gamma_2\Omega - I_f\Gamma_1\dot{q}. \tag{4.17}$$

From the rearranged control law above, we can see clearly that we have direct compensation for the Coriolis and gyroscopic torques. The remaining terms could be thought of as a PD^2 feedback (Tayebi and McGilvray 2004), as we have proportional feedback from the vector-quaternion q, derivative feedback from the angular velocity term Ω, and an additional derivative feedback from the vector-quaternion velocity $\dot{q}$.

If we consider the quadrotor aircraft to have an attitude such that (ϕ, θ, ψ) are close to zero, and Ω is relatively small, the Coriolis and gyroscopic torques will also be sufficiently small, and can be neglected. The elimination of these terms from the

control law reduces the complexity of the controller, while still guaranteeing local stability (Tayebi and McGilvray 2004). The new controller is given as follows:

$$\tau_a = I_f\dot{\tilde{\Omega}} - \Gamma_2\tilde{\Omega} - \Gamma_3 q, \tag{4.18}$$

and will be referred to as Modified Theorem 1.

As previously mentioned, both control laws given in Theorem 1 and Modified Theorem 1 rely on the knowledge of the airframe inertia I_f, and are therefore considered model-dependent. In the following section, it will be shown that the classical PD feedback controller, without Coriolis and gyroscopic torques compensation and therefore model-independent, can provide asymptotic stability for the attitude stabilization problem for the quadrotor aircraft. This classical PD feedback controller, developed in (Tayebi and McGilvray 2004), is given as follows:

4.1.2 Theorem 2

Consider the quadrotor model equations (3.3) and (3.4) under the following control law

$$\tau_a = -\Gamma_4\Omega - \alpha q, \tag{4.19}$$

where Γ_4 is a 3×3 symmetric positive definite matrix and α is a positive scalar parameter. Then, the equilibrium point $(R = I, \Omega = 0)$ is globally asymptotically stable.

Proof of Theorem 2

Consider the following positive definite Lyapunov function candidate

$$V = \alpha q^T q + \alpha(q_0 - 1)^2 + \frac{1}{2}\Omega^T I_f \Omega. \tag{4.20}$$

Using the quaternion constraint (2.9), the above reduces to

$$V = 2\alpha(1 - q_0) + \frac{1}{2}\Omega^T I_f \Omega, \tag{4.21}$$

whose time derivative is given as

$$\begin{aligned} \dot{V} &= -2\alpha\dot{q}_0 + \tfrac{1}{2}\Omega^T I_f\dot{\Omega} + \tfrac{1}{2}\dot{\Omega}^T I_f\Omega \\ &= -2\alpha\dot{q}_0 + \Omega^T I_f\dot{\Omega}, \end{aligned} \tag{4.22}$$

and using (2.18) for $\dot{q}_0$ we have

$$\begin{aligned} \dot{V} &= -2\alpha(-\tfrac{1}{2}q'^{T}\Omega) + \Omega'^{T} I_f \dot{\Omega} \\ &= \alpha q^T \Omega + \Omega^T I_f \dot{\Omega}. \end{aligned} \tag{4.23}$$

Rearranging model equation (3.4) to get

$$\dot{\Omega} = I_f^{-1}(-\Omega \times I_f \Omega) - I_f^{-1} G_a + I_f^{-1} \tau_a \tag{4.24}$$

and using the above into (4.23) gives

$$\dot{V} = \alpha q^T \Omega + \Omega^T((-\Omega \times I_f \Omega) - G_a + \tau_a). \tag{4.25}$$

It is clear from the above terms that $\Omega^T(-\Omega \times I_f \Omega) = 0$ and $-\Omega^T G_a = -\Omega^T \sum_{i=1}^{4} I_r(\Omega \times \hat{z}_{\mathcal{I}})(-1)^{i+1}\omega_i = 0$ due to the fact that the dot product of two orthogonal vectors is equal to zero. Therefore we are left with

$$\dot{V} = \alpha q^T \Omega + \Omega^T \tau_a. \tag{4.26}$$

Using the control law (4.19) into the above gives

$$\dot{V} = -\Omega^T \Gamma_4 \Omega \tag{4.27}$$

which is negative semi-definite. Therefore, from (4.21) and (4.27) we can conclude that Ω, q and q_0 are bounded. Using La Salle's invariance theorem we can show that the equilibrium point $(q = 0, q_0 = \pm 1, \Omega = 0)$ is asymptotically stable.

In fact, it is obvious from (4.21) and (4.27) that $\lim_{t\to\infty} \Omega(t) = 0$, which leads to $\lim_{t\to\infty} \dot{\Omega}(t) = 0$. From the above, and using the model equation (3.4) we have $\lim_{t\to\infty} \tau_a(t) = 0$, and using control law (4.19) we have $\lim_{t\to\infty} q(t) = 0$. Finally, using (2.9), we can conclude that $\lim_{t\to\infty} q_0(t) = \pm 1$.

Theorem 2 guarantees asymptotic stability of the equilibrium point $(q = 0, q_0 = \pm 1, \Omega = 0)$. However, the speed of convergence, or the way in which these variables will converge has not been determined. In fact, it is possible that Theorem 2 will provide exponential convergence for the variables in question, but this is not guaranteed, and is not proven mathematically.

It is quite obvious from control law (4.19) that there is no compensation for the Coriolis and gyroscopic torques, unlike the control law developed in Theorem 1. However, the addition of the compensation terms for the Coriolis and gyroscopic torques to control law (4.19), while adding complexity to the controller, will still provide global asymptotic stability. Consider the new control law:

$$\tau_a = (\Omega \times I_f \Omega) + G_a - \Gamma_4 \Omega - \bar{\alpha} q \tag{4.28}$$

where Γ_4 and $\bar{\alpha}$ are 3×3 diagonal positive definite matrices when I_f is diagonal. However, when I_f is not diagonal, Γ_4 must be a 3×3 symmetric positive definite matrix and $\bar{\alpha} = \alpha I_{3\times 3}$, where α is a positive scalar. The above controller will be referred to as Modified Theorem 2.

The control law developed in Theorem 2 is model-independent, therefore no knowledge of the model parameters is necessary. However, the addition of the compensation terms for the Coriolis and gyroscopic torques in Modified Theorem 2 again requires the knowledge of the quadrotor aircraft inertia I_f. The main reason to propose the Modified Theorem 1 is to be able to compare a reduced complexity controller with the controller proposed in Theorem 1. Similarly, Modified Theorem 2, although more complex, gives a controller with which to compare experimentally and in simulation to help understand the importance of the Coriolis and gyroscopic torques compensation, and allows to explore the benefits of using a matrix gain $\bar{\alpha}$ as opposed to a scalar gain α used in the control law in Theorem 1.

The controller proposed in Theorem 2 is a classical PD feedback controller, where the proportional feedback is in terms of the quaternion, and the derivative feedback is in terms of the angular velocity Ω. This controller is similar to the control law proposed in (Joshi *et al.* 1995; Lizarraide and Wen 1996; Wie *et al.* 1989). As stated previously, the advantage of the control law proposed in Theorem 2 is its simplicity, and the fact that no knowledge of the model parameters is required. However, the control law proposed in Theorem 1 has the advantage of guaranteed exponential stability, and the ability to use a matrix gain Γ_3 as opposed to a scalar gain for the quaternion feedback, adding more flexibility to the controller.

4.2 Rotor Torques Design

The control inputs to the entire set of model equations (3.1)-(3.5) are the rotor torques τ_i. To design the rotor torques, the desired rotor velocity $\omega_{d,i}$ must be determined, and one requirement necessary to obtain the desired rotor velocities is the total thrust T. The desired rotor velocity may then be obtained from (3.6) and (3.9), that is $\bar{\omega}_d = M^{-1}\mu$, with $\bar{\omega}_d = (\omega_{d,1}^2, \omega_{d,2}^2, \omega_{d,3}^2, \omega_{d,4}^2)^T$, $\mu = (\tau_a^1, \tau_a^2, \tau_a^3, T)^T$ and

$$M = \begin{pmatrix} 0 & db & 0 & -db \\ db & 0 & -db & 0 \\ \kappa & -\kappa & \kappa & -\kappa \\ b & b & b & b \end{pmatrix} \tag{4.29}$$

where M is nonsingular as long as $db\kappa \neq 0$.

Now, the objective is to design a controller to force $\omega_i \rightarrow \omega_{d,i}$ as $t \rightarrow \infty$ by using τ_i as the control input. First, the rotor speed error is defined as

$$\tilde{\omega}_i = \omega_i - \omega_{d,i}, \tag{4.30}$$

whose time derivative is given as

$$\dot{\tilde{\omega}}_i = \dot{\omega}_i - \dot{\omega}_{d,i}. \tag{4.31}$$

Using model equation (3.5) and the above we have

$$I_r\dot{\tilde{\omega}}_i = \tau_i - Q_i - I_r\dot{\omega}_{d,i} \tag{4.32}$$

Therefore, a control law may be developed (Tayebi and McGilvray 2004) from the above equation as follows:

$$\tau_i = Q_i + I_r\dot{\omega}_{d,i} - k_i\tilde{\omega}_i, \tag{4.33}$$

where k_i, $i \in \{1, 2, 3, 4\}$ are four positive design parameters. Applying the above controller to (4.32) gives

$$\dot{\tilde{\omega}}_i = \frac{-k_i}{I_r}\tilde{\omega}_i, \tag{4.34}$$

which shows the exponential convergence of ω_i to $\omega_{d,i}$ as $t \rightarrow \infty$. This means the convergence of the quadrotor airframe torques to the desired values will be achieved leading to the stabilization of the quadrotor aircraft to the desired equilibrium point.

The physical quadrotor under consideration is powered by four voltage controlled permanent magnet DC motors. Therefore, it is necessary to relate the designed rotor torque τ_i to the appropriate motor voltage. Assuming negligible armature inductance, the mathematical model of the motor (Fitzgerald *et al.* 1990) is given by

$$V_i = R_a I_a + K_m \omega_{m,i}, \tag{4.35}$$

where R_a, I_a, K_m and ω_m are the motor resistance, armature current, motor constant, and the motor speed respectively. The equation for the motor torque is given as follows

$$\tau_m = K_m I_a. \tag{4.36}$$

The rotor torque τ_i can be related to the motor torque $\tau_{m,i}$, using the gear ratio K_g as follows

$$\tau_{m,i} = \frac{\tau_i}{K_g}. \tag{4.37}$$

Similarly, the rotor speed ω_i can be related to the motor speed $\omega_{m,i}$ using the gear ratio K_g to give

$$\omega_{m,i} = K_g \omega_i. \tag{4.38}$$

Using (4.36), (4.37) and (4.38) into (5.5) gives an equation for the motor voltage in terms of the rotor torque, rotor speed, and known constants, and is given as

$$V_i = R_a \frac{\tau_i}{K_m K_g} + K_m K_g \omega_i. \tag{4.39}$$

Since the four motors are the same, the parameters and constants remain the same. Now that the motor voltage has been determined, it can be converted into a PWM signal to control each motor.

Note that for better transient performance, the convergence rate of the actual rotor speed ω_i to the desired rotor speed $\omega_{d,i}$ should be faster than the convergence rate

of the aircraft attitude to the desired orientation. This is somewhat obvious as the rate of convergence of the aircraft attitude hinges upon the convergence of ω_i to $\omega_{d,i}$. Essentially, one must ensure that $\frac{k_i}{I_r}$ defined in (4.34) is greater than β defined in (4.16).

4.3 Altitude Control Design

Controlling the altitude of the quadrotor aircraft can be achieved assuming the aircraft has been stabilized to a hover attitude at $R = I$. Recall in the previous section, a value for the total thrust T is necessary to calculate the desired rotor velocities. When not under altitude control, the total thrust T is user defined, however, it is possible to design a linear feedback controller using the thrust as a control input to the system, and control the altitude of the quadrotor aircraft (Tayebi and McGilvray 2004). The objective is to stabilize the altitude of the aircraft to the desired altitude $z \rightarrow z_d$ as $t \rightarrow \infty$. From (3.1) and (3.2), *i.e.*, assuming that $R \approx I$ and eliminating the x and y coordinates, one can obtain

$$\begin{aligned} \dot{z} &= v_z \\ \dot{v}_z &= u \end{aligned} \tag{4.40}$$

where $u = g - \frac{T}{m}$. We can design a controller of the form

$$T = m\left(g + \bar{k}_1 z + \bar{k}_2 v_z - \bar{k}_3 \int (z_d - z(\tau))d\tau\right), \tag{4.41}$$

where $\bar{K} = [\bar{k}_1, \bar{k}_2, -\bar{k}_3]$ are designed to ensure that $(A - B\bar{K})$ is stable, where

$$A = \begin{pmatrix} 0 & 1 & 0 \\ 0 & 0 & 0 \\ -1 & 0 & 0 \end{pmatrix}, B = \begin{pmatrix} 0 \\ 1 \\ 0 \end{pmatrix}.$$

Under a well designed attitude stabilization controller, this altitude controller will allow the quadrotor aircraft to hover autonomously at a given desired altitude. This is interesting for a number of reasons; the addition of a simple pilot interface could make use of an auto-pilot hover feature when there are no commands being given to

the aircraft. Additionally, achieving an accurate altitude may also be an objective and can be made possible by this linear feedback controller.

4.4 Attitude Set-Point Regulation

The physical quadrotor aircraft can be flown by pilot input in conjunction with the attitude stabilization control algorithm. In fact, if the pilot wishes to stabilize the aircraft at a desired orientation $(\phi_d, \theta_d, \psi_d)$, this may be achieved by first defining an error vector for the Euler angles given as

$$\begin{pmatrix} \tilde{\phi} \\ \tilde{\theta} \\ \tilde{\psi} \end{pmatrix} = \begin{pmatrix} \phi - \phi_d \\ \theta - \theta_d \\ \psi - \psi_d \end{pmatrix}. \tag{4.42}$$

Recall that each attitude controller guarantees asymptotic or exponential stability of the equilibrium point $(q = 0, q_0 = \pm 1, \Omega = 0)$. Hence, if the quaternion used in the feedback is generated from the error vector (4.42), one can conclude that

$$\lim_{t \to \infty} \begin{pmatrix} \tilde{\phi}(t) \\ \tilde{\theta}(t) \\ \tilde{\psi}(t) \end{pmatrix} = \begin{pmatrix} 0 \\ 0 \\ 0 \end{pmatrix}, \tag{4.43}$$

and therefore

$$\lim_{t \to \infty} \begin{pmatrix} \phi(t) \\ \theta(t) \\ \psi(t) \end{pmatrix} = \begin{pmatrix} \phi_d \\ \theta_d \\ \psi_d \end{pmatrix}. \tag{4.44}$$

The desired Euler angles from the pilot may come in the form of numerical input, or from a control stick. This gives the pilot the ability to maneuver the quadrotor aircraft with precise attitude control, and with a spring-loaded self zeroing control stick, for example, the pilot may let go of the control stick at anytime and the attitude controller will ensure the quadrotor aircraft will stabilize at the desired hover orientation.

Chapter 5

Determination of Model Parameters

The knowledge of certain model parameters is necessary for use in simulations and experiments involving the quadrotor aircraft. Of course some parameters, such as acceleration due to gravity, require little if any measurement or experimentation to determine, while others such as the inertia of the airframe require a slightly more complex experimental approach to obtain a reasonable estimate of the parameter value. Although Theorem 2 discussed in Chapter 4 is model-independent, the inclusion of the motor torques design makes it necessary to know some parameters for the control feedback, therefore both Theorem 1 and 2 require some knowledge of the model parameters.

A controller which can provide good performance while requiring little knowledge of the model parameters is ideal. However, it is not always possible to design model-independent controllers, and becomes even more difficult once the actuators have been considered. In fact, a robust design should be able to accommodate for errors in the determination of the parameters while still guaranteeing stability. With this in mind, the determination of the model parameters has been performed to obtain reasonable estimates.

Table (5.1), presented below, gives all of the necessary model parameters for both

simulation and experimentation. Each section following will give details on how the parameters were obtained. The following parameters, not previously defined, I_{f_ϕ}, I_{f_θ} and I_{f_ψ} denote the inertia of the airframe in the roll, pitch and yaw rotational directions, *i.e.*, $I_f = diag(I_{f_\phi}, I_{f_\theta}, I_{f_\psi})$. In fact, I_f is assumed to be diagonal to simplify the result.

Parameter	Description	Value	Units
g	Gravity	9.81	m/s^2
m	Mass	0.468	kg
d	Distance	0.225	m
I_r	Rotor Inertia	3.357×10^{-5}	$kg \cdot m^2$
I_{f_ϕ}	Roll Inertia	4.856×10^{-3}	$kg \cdot m^2$
I_{f_θ}	Pitch Inertia	4.856×10^{-3}	$kg \cdot m^2$
I_{f_ψ}	Yaw Inertia	8.801×10^{-3}	$kg \cdot m^2$
R_a	Motor Resistance	0.67	Ω
k_m	Motor Constant	4.25×10^{-3}	$N \cdot m/A$
k_g	Gear Ratio	5.6	
b	Proportionality Constant	2.923×10^{-5}	
κ	Proportionality Constant	1.120×10^{-6}	

Table 5.1: Quadrotor Aircraft Model Parameters

5.1 Basic Model Parameters

Some parameters that require little to no measurement are described in this section. The acceleration due to gravity is given as $g = 9.81m/s^2$ while the distance from the rotor center to the center of mass of the aircraft has been measured as $d = 0.225m$. The mass was determined by simply weighing the aircraft on a scale and was found to be $m = 0.468kg$. The gear ratio linking the motor to the rotor was measured by counting the number of teeth on each gear and is given as $k_g = 5.6$. The average

armature resistance of the four motors was measured with an ohmmeter to be $R_a = 0.67\Omega$.

5.2 Airframe and Rotor Inertia

The calculation of the inertia for any 3-dimensional geometrically complex object can be extremely difficult. However, there exists experimental methods that can yield relatively accurate results, and is some cases is the only option to obtain a reasonable inertia estimate. The airframe inertia, denoted as $I_f = diag(I_{f_\phi}, I_{f_\theta}, I_{f_\psi})$, can be determined through experimentation. Due to symmetry only two moments of inertia need to be measured, as the inertia around the roll I_{f_ϕ} and pitch I_{f_θ} axes is identical. The experiment involves making a pendulum of the aircraft to find the mass moment of inertia as described in (Riley and Sturges 1996). The natural frequency of oscillation of the pendulum, combined with setup measurements allows the mass moment of inertia to be determined about the point of oscillation. By using the parallel axis theorem, the mass moment of inertia about the center of mass can be calculated from the previously measured information.

There are two possible pendulum designs that could yield the necessary information to calculate the mass moment of inertia. The first is a compound pendulum which requires the object, or in this case the aircraft, to oscillate on a vertical plane about a fixed point on the aircraft. The second is a tri-suspension torsional pendulum which requires a special circular platform to be suspended from 3 guides. The aircraft is placed on the platform, and the rotational oscillations are measured on a horizontal plane. Inertia estimates require oscillation frequencies to be recorded for both the platform alone, and the combination of the platform and aircraft combined. However, the complexity of the torsional pendulum, and the difficulty in obtaining the roll or pitch inertia with this method made choosing the compound pendulum experiment an easy choice.

The compound pendulum experiment setup is quite simple and involves hanging the

aircraft from one end of the airframe, and allowing it to swing around the axis of interest. An example of this setup can be seen in Figure 5.1 below. The mass moment

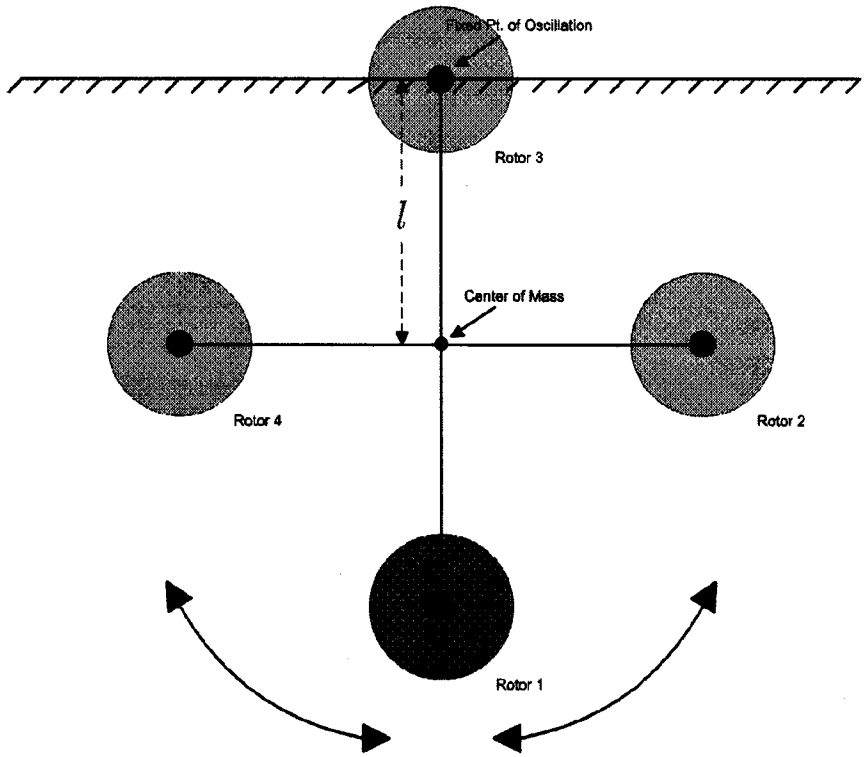

Figure 5.1: Quadrotor Compound Pendulum - Oscillating Around Yaw Axis

of inertia can then be determined from

$$J_G = \frac{mgl}{\omega_n^2} - ml^2 \tag{5.1}$$

where J_G denotes the inertia around the center of gravity, m denotes the aircraft mass, g denotes acceleration due to gravity, l denotes the distance from the center of gravity to the point of oscillation, ω_n denotes the natural frequency of oscillation. In fact, (5.1) has been obtained using the parallel axis theorem where

$$J_G = J_O - ml^2 \tag{5.2}$$

where J_O represents the mass moment of inertia around the point of oscillation. The above has been obtain using the fact that

$$\tau = mglsin\theta,$$

and Newton's second law of rotation given as

$$\Sigma\tau = J\ddot{\theta},$$

which gives

$$J\ddot{\theta} = -mglsin\theta.$$

Considering only small angles of θ we can assume $sin\theta \simeq \theta$ therefore giving

$$\ddot{\theta} - \frac{mgl}{J}\theta = 0, \tag{5.3}$$

and comparing (5.3) with a standard form second order differential equation for simple harmonic motion given as

$$\ddot{\theta} + \omega_n^2\theta = 0,$$

we have

$$J_O = \frac{mgl}{\omega_n^2}. \tag{5.4}$$

The mass m and the length l remain constant for determining both the inertia around the pitch axis I_{f_θ} and the inertia around the yaw axis I_{f_ψ}. The mass of the aircraft was determined with a scale and is given as $m = 0.468kg$. The length from the point of oscillation to the center of gravity was found to be $l = 0.29m$, and the acceleration due to gravity g is given as $g = 9.81m/s^2$. Experimental testing yielded results given in Table 5.2. Using a timer and starting the oscillations by hand, a time was recorded for exactly 4 cycles for 7 separate trials. To determine the natural frequency of oscillation $\omega_{n,\psi}$ for the yaw axis, the highest (trial 3) and lowest (trial 4) measurements have been disregarded. The average time for the remaining trials is then found to be $\tau_{ave,\psi} = 4.78$s, which yields a natural frequency of $\omega_{n,\psi} = 5.26$rad/s. Using (5.1) the mass moment of inertia I_{f_ψ} is found to be

$$I_{f_\psi} = \frac{(0.468)(9.81)(0.29)}{(5.26)^2} - (0.468)(0.29)^2 = 8.801 \times 10^{-3}kg \cdot m^2$$

To determine the natural frequency of oscillation $\omega_{n,\theta}$ for the pitch axis, the highest (trial 2) and lowest (trial 5) measurements have been disregarded. The average time for the remaining trials is then found to be $\tau_{ave,\theta} = 4.58$s, which yields a natural

Trial	$\tau_{4cycles,\psi}$ (sec)	$\tau_{4cycles,\theta}$ (sec)
1	4.82	4.55
2	4.76	4.68
3	4.74	4.55
4	4.91	4.56
5	4.79	4.46
6	4.77	4.62
7	4.76	4.62

Table 5.2: Oscillation Time Trials, Airframe (sec)

frequency of $\omega_{n,\theta} = 5.49\text{rad/s}$. Using (5.1) the mass moment of inertia I_{f_θ} is found to be

$$I_{f_\theta} = \frac{(0.468)(9.81)(0.29)}{(5.49)^2} - (0.468)(0.29)^2 = 4.856 \times 10^{-3} kg \cdot m^2$$

Subsequently, due to symmetry, we can conclude that the mass moment of inertia around the roll axis is identical to that around the pitch axis giving

$$I_{f_\phi} = I_{f_\theta} = 4.856 \times 10^{-3} kg \cdot m^2$$

Therefore the mass moment of inertia for the aircraft is given as

$$I_f = diag(I_{f_\phi}, I_{f_\theta}, I_{f_\psi}) = diag(4.856, 4.856, 8.801) \times 10^{-3}.$$

The mass moment of inertia of each rotor blade I_r has also been determined using the same compound pendulum method. The mass m and the length l are given as $m = 0.00671kg$, and $l = 0.15m$ respectively. Experimental testing yielded results given in Table 5.3. Again, using a timer and starting the oscillations by hand, a time was recorded for exactly 4 cycles for 7 separate trials. To determine the natural frequency of oscillation $\omega_{n,r}$ for the rotor blade, the highest (trial 6) and lowest (trial 7) measurements have been disregarded. The average time for the remaining trials is then found to be $\tau_{ave,r} = 3.436\text{s}$, which yields a natural frequency of $\omega_{n,r} = 7.31\text{rad/s}$.

Trial	$\tau_{4cycles,rotor}$ (sec)
1	3.43
2	3.47
3	3.47
4	3.40
5	3.41
6	3.48
7	3.39

Table 5.3: Oscillation Time Trials, Rotor Blade (sec)

Using (5.1) the mass moment of inertia I_r is found to be

$$I_r = \frac{(0.00671)(9.81)(0.15)}{(7.31)^2} - (0.00671)(0.15)^2 = 3.357 \times 10^{-5} kg \cdot m^2$$

5.3 Motor Constant

To determine the proportionality constant κ in the coming section, the motor constant k_m is first required. A direct approach has been taken to measuring and calculating the motor constant as will be detailed below. Assuming that the current drawn by one motor can be measured, we can write

$$\tau_m = k_m \cdot I_A, \tag{5.5}$$

where τ_m, k_m and I_A are the motor torque in $N \cdot m$, motor constant in $N \cdot m/A$ and motor current in (A) respectively. The above assumes ideal parameters with no loss due to heat or friction and does not include stored energy. Again, assuming no losses, the electrical input power must be equal to the mechanical output power (Fitzgerald *et al.* 1990) and can be written as

$$V_A I_A = \tau_m \omega_m \tag{5.6}$$

where V_A is the armature voltage and ω_m is the angular velocity of the motor. Rearranging (5.6) and using (5.5) we have

$$\frac{V_A}{\omega_m} = \frac{\tau_m}{I_A} = k_m \tag{5.7}$$

Therefore, the motor constant is determined by driving the motor under no-load conditions, assuming no losses, and recording the angular velocity and back emf or V_A generated at the armature for different motor speeds. The results of the test are seen in Table (5.4). The highest and lowest calculated values are removed and the

V_A (V)	ω_m (rad/s)	k_m $(N \cdot m/A)$
0.5	76.2	0.0066
1.0	187.6	0.0053
1.5	304.9	0.0049
2.0	410.5	0.0049
2.5	519.0	0.0048
3.0	621.6	0.0048
3.5	738.9	0.0047
4.0	850.3	0.0047
4.5	950.0	0.0047
5.0	1055	0.0047

Table 5.4: Required Measurements for Motor Constant Determination

remaining values are averaged to yield $k_m = 0.0049$ $(N \cdot m/A)$.

5.4 Proportionality Constant b

The constant b is dependent on factors such as the density of air, the number, shape, radius and pitch of the rotor blades, and appears in the equation given for airframe torque as

$$T = \sum_{i=1}^{4} |f_i| = b \sum_{i=1}^{4} \omega_i^2$$

An experiment has been performed to determine the value of b, and is detailed below. Initially the quadrotor aircraft was placed on a scale with a fixed hover orientation and the weight was recorded as a reference. Then, by driving all four rotors at the same angular velocity and weighing the structure again, the value for b was obtained as follows

$$b = \frac{T}{4\omega^2}$$

where T is given in Newtons. The value for T is determined by the weight in kg times the acceleration due to gravity g. The experimental results are given in Table (5.5) along with the corresponding calculated value for b. Averaging these calculated values gives a final result $b = 2.923 \times 10^{-5}$.

ω_i (rad/s)	T (N)	b
52.36	0.3139	2.862×10^{-5}
62.83	0.4659	2.951×10^{-5}
73.30	0.6475	3.013×10^{-5}
83.78	0.8044	2.865×10^{-5}
94.25	1.0301	2.899×10^{-5}
104.7	1.3047	2.974×10^{-5}
115.2	1.5696	2.957×10^{-5}
125.6	1.8639	2.954×10^{-5}
136.1	2.0601	2.780×10^{-5}

Table 5.5: Required Measurements for b Determination

5.5 Proportionality Constant κ

The constant κ, appearing in the equation given for reactive torque, is dependent on a number of factors such as the density of air, the number, shape and radius of the rotor blades, but particularly the pitch angle of the blade. To physically measure

this value an experiment must be performed which directly or indirectly measures the reactive torque of the rotors. Initially, one particular method to obtain an estimate of κ was tried without success. This method essentially involved measuring and comparing the increase in current to each motor with loaded tests (rotor blade present), and no-load tests (no rotor blade present). Through some calculation an estimate of κ was determined, but with a large error.

A new experimental method was devised to accurately measure the proportionality constant κ. A simple drawing in Figure 5.2 depicts this particular setup. By rotating

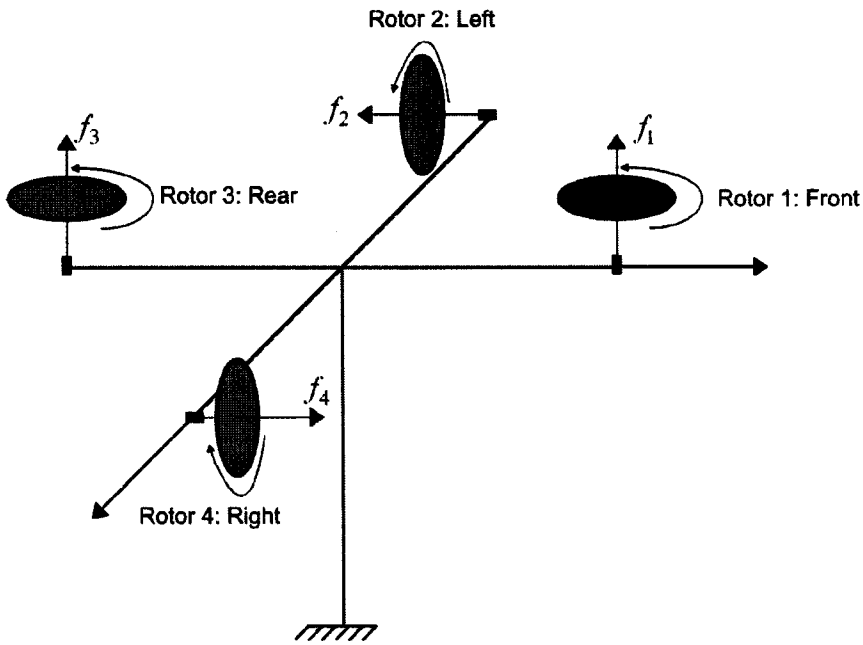

Figure 5.2: Quadrotor Configuration for Measurement of κ

rotors 2 and 4 to generate a combined thrust in the negative yaw direction, and using the combined reactive torques from rotors 1 and 3, an accurate value for κ can be calculated. During experimentation the speed of each rotor was closely monitored, and the aircraft was stabilized by hand on a ball joint base. Once it was determined that the yaw motion was in equilibrium the rotor speeds were recorded. From Figure 5.2 it can be seen that the equation for airframe torques in the yaw direction may

be written as

$$|\tau_{+ve}| = |\tau_{-ve}| = db(\omega_2^2 + \omega_4^2) = \kappa(\omega_1^2 + \omega_3^2) \tag{5.8}$$

Using (5.8) we can isolate κ to get

$$\kappa = db\frac{(\omega_2^2 + \omega_4^2)}{(\omega_1^2 + \omega_3^2)} \tag{5.9}$$

Measured rotor velocities were recorded once the yaw was in equilibrium, and can be seen in Table (5.6), along with the corresponding calculated values for κ. Averaging

ω_1 (rad/s)	ω_2 (rad/s)	ω_3 (rad/s)	ω_4 (rad/s)	κ
1950	750	1715	760	1.1119×10^{-6}
2230	890	1979	850	1.1206×10^{-6}

Table 5.6: Measured Rotor Speeds for κ Determination

the κ values we find $\kappa = 1.12 \times 10^{-6}$.

Therefore, all of the model parameters necessary for both simulations and experimentation have been determined, and the final list is tabulated in Table 5.1. As previously mentioned, the model parameters are not required to be perfectly accurate, as the control design should be able to compensate for any possible inaccuracies.

Chapter 6

Simulation results

To explore the performance of each controller, a number of simulations have been performed in Simulink. The results of each simulation allow a comparison to be made between theorems, helping illustrate similarities or differences in graphical results. All simulations have been performed using the model parameters given in Table 5.1. Controller gains for all theorems tested were obtained through trial and error and are given as follows: $\Gamma_1 = 5I_{3\times3}$, $\Gamma_2 = 0.1I_{3\times3}$, $\Gamma_3 = I_{3\times3}$, $\Gamma_4 = 0.1I_{3\times3}$, $k_i = 0.002$ and $\alpha = 1.3$. The desired thrust for each simulation is given as $T = 15N$. The controller gains for the altitude control law (4.41) are developed in Chapter 7, and are given as $\bar{K} = [20.74, 9.35, -19.49]$.

6.1 Simulation 1

The objective of this simulation is to show the stabilization of the quadrotor attitude from some given initial angles for each proposed theorem. Initial conditions are set for the aircraft angles as roll $\phi = -25°$, pitch $\theta = 25°$ and yaw $\psi = -15°$, and the simulation time is 2 seconds. Simulation 1 has been performed on Theorem 1 (Figures 6.1- 6.6), Modified Theorem 1 (Figures 6.7- 6.12), Theorem 2 (Figures 6.13-

6.18), and Modified Theorem 2 (Figures 6.19- 6.24). For each theorem tested, plots are given for the aircraft angles, the angular velocity of the aircraft and the control effort τ_i of each motor normalized between 0 and 1.

Theorem 1 has guaranteed exponential convergence of the aircraft angles as discussed in the control design, and it can be clearly seen from the simulation results that this has been achieved. The results for Theorem 2 and both Modified Theorem 1 and 2 however, also show very similar results. In fact, it appears from these results that exponential convergence has been achieved by all four controllers tested. This gives an indication that there may exist a mathematical proof which provides local exponential convergence for all Theorems tested.

6.2 Simulation 2

The objective of Simulation 2 is to show the effects of disturbances introduced into the system under closed loop control after the aircraft attitude has stabilized from some given initial angles. The initial aircraft angles are given as roll $\phi = -25°$, pitch $\theta = 25°$ and yaw $\psi = -15°$, and the simulation time is 5 seconds. Each disturbance was introduced to the system for a duration of 0.05 sec. They are given as follows: Roll-Disturbance $= -10°$ at time 2 seconds, Pitch-Disturbance $= -10°$ at time 3 seconds, and Yaw-Disturbance $= 10°$ at time 4 seconds. Simulation 2 has been performed on Theorem 1 (Figures 6.25- 6.30) and Theorem 2 (Figures 6.31- 6.36). Plots are given for the aircraft angles, the angular velocity of the aircraft and the control effort τ_i of each motor normalized between 0 and 1.

Again, from the plots for Theorem 1 and 2 the results are nearly identical. Stabilization from the initial angles is exponential. For each disturbance introduced however, the recovery is rapid but with some overshoot. This slight overshoot could be reduced by adjusting the controller gains if required, but with some compromise to the rise time.

A sharp rise and fall in the control effort can be seen for each disturbance, as expected.

6.3 Simulation 3

The objective of Simulation 3 is to show the stabilization of the quadrotor attitude from some given initial angles to given desired angles. Initial conditions are set for the aircraft angles as roll $\phi = 15°$, pitch $\theta = -15°$ and yaw $\psi = 15°$, and the simulation time is 2 seconds. Desired aircraft angles are given as roll $\phi = -10°$, pitch $\theta = 10°$ and yaw $\psi = -10°$. Simulation 3 has been performed on Theorem 1 (Figures 6.37- 6.42) and Theorem 2 (Figures 6.43- 6.48) and plots are given for the aircraft angles, the angular velocity of the aircraft and the control effort τ_i of each motor normalized between 0 and 1.

The stabilization from the initial angles to the desired angles occurs exponentially and again without much difference between both theorems. The plots are similar for the angles, angular velocity and control effort for both theorems.

6.4 Simulation 4

The objective of Simulation 4 is to show the stabilization of the quadrotor attitude from some given initial angles, and the stabilization of the altitude or z position to a desired altitude. Initial conditions are set for the aircraft angles as roll $\phi = -25°$, pitch $\theta = 25°$ and yaw $\psi = -15°$, and the simulation time is 5 seconds. The desired altitude has been given as $z = 2$ meters. Simulation 4 has been performed on Theorem 1 (Figures 6.49- 6.54) and Theorem 2 (Figures 6.55- 6.60) and plots are given for the aircraft angles, position in space or (x, y, z) coordinates of the aircraft and the control effort τ_i of each motor normalized between 0 and 1.

Each plot for the aircraft angles shows stabilization in an identical fashion as that of Simulation 1, nearly unaffected by the control of the altitude. The position in space plots clearly show the convergence of the quadrotor's altitude to the desired 2 meters in just over 2 seconds. The x and y positions are not controlled and are seen diverging.

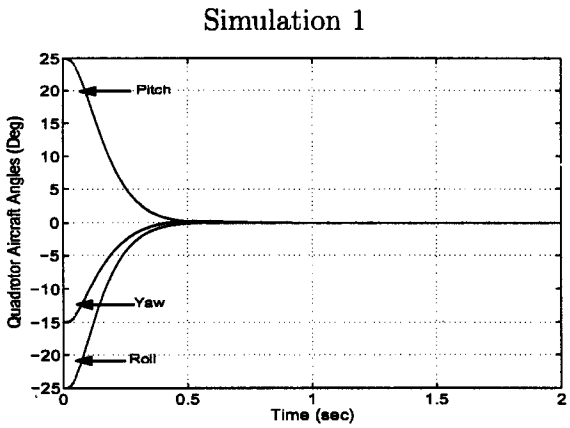

Figure 6.1: Aircraft Angles, Theorem 1

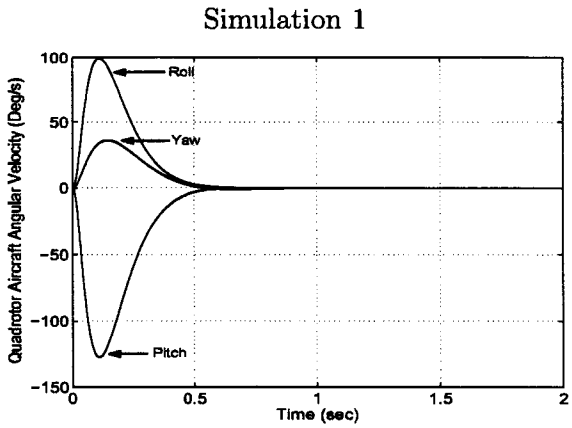

Figure 6.2: Angular Velocity, Theorem 1

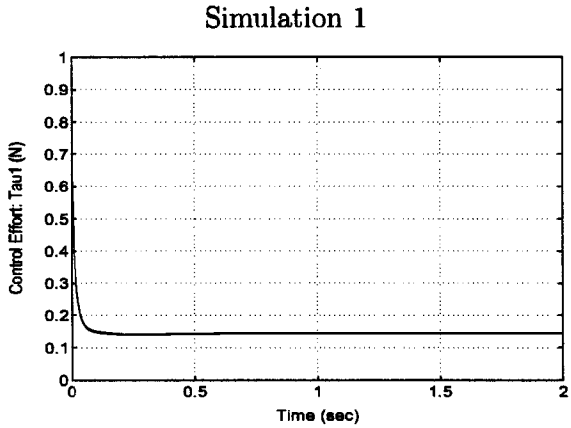

Figure 6.3: Control Effort 1, Theorem 1

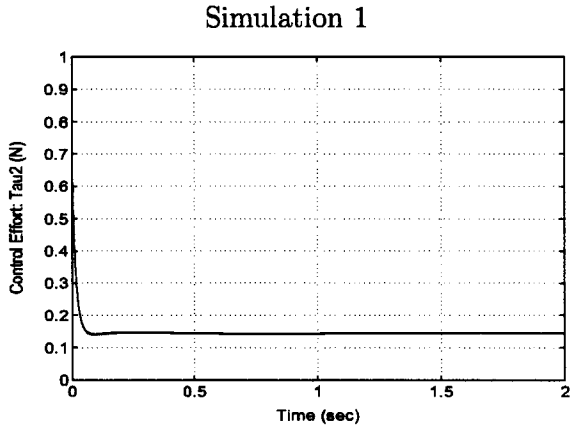

Figure 6.4: Control Effort 2, Theorem 1

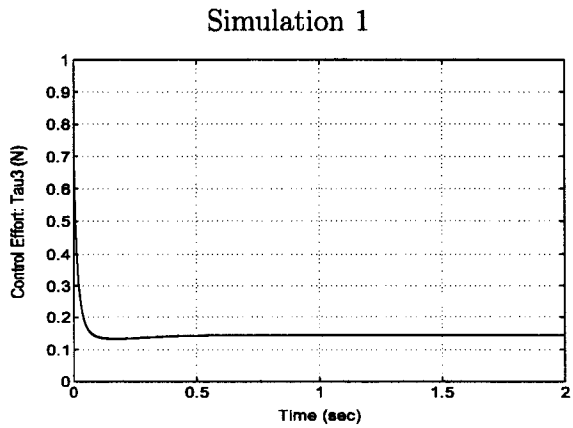

Figure 6.5: Control Effort 3, Theorem 1

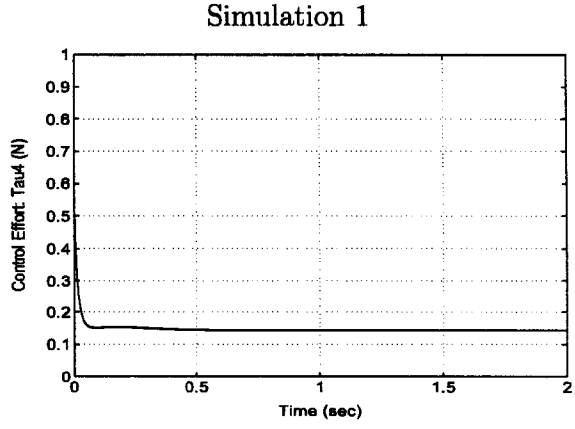

Figure 6.6: Control Effort 4, Theorem 1

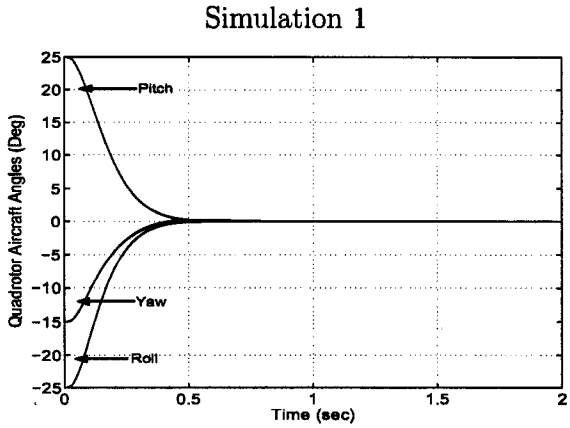

Figure 6.7: Aircraft Angles, Modified Theorem 1

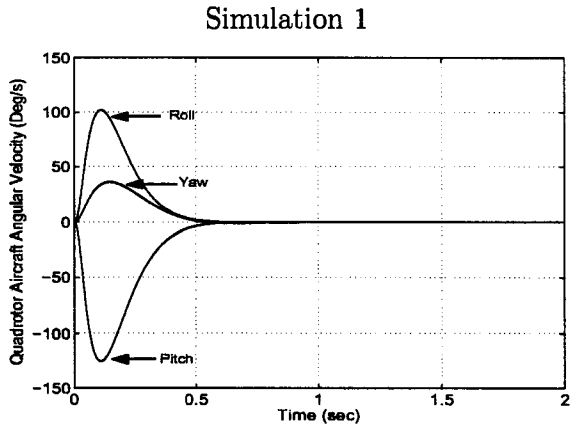

Figure 6.8: Angular Velocity, Modified Theorem 1

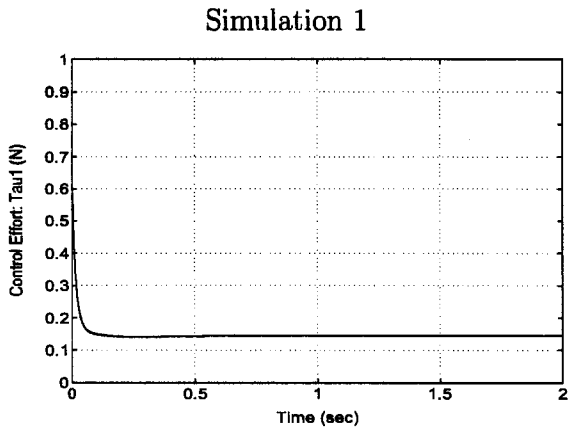

Figure 6.9: Control Effort 1, Modified Theorem 1

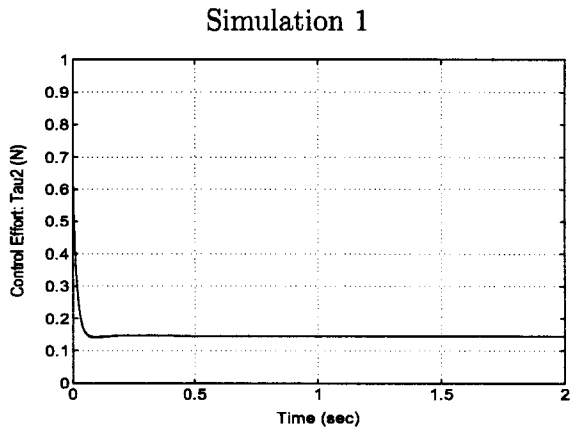

Figure 6.10: Control Effort 2, Modified Theorem 1

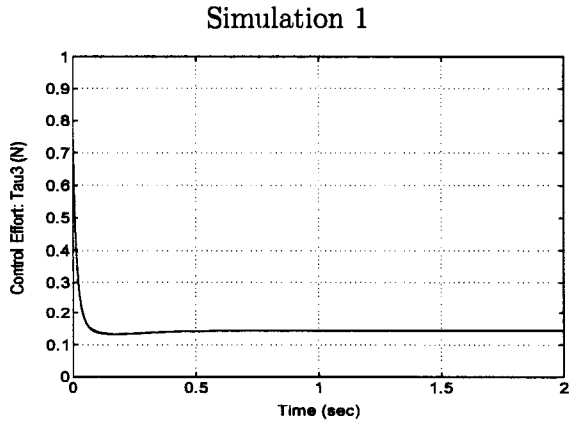

Figure 6.11: Control Effort 3, Modified Theorem 1

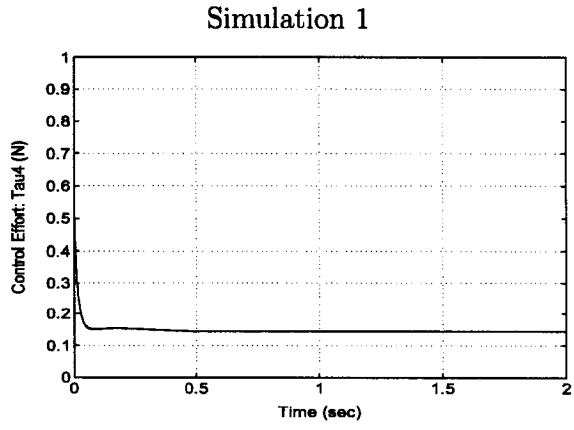

Figure 6.12: Control Effort 4, Modified Theorem 1

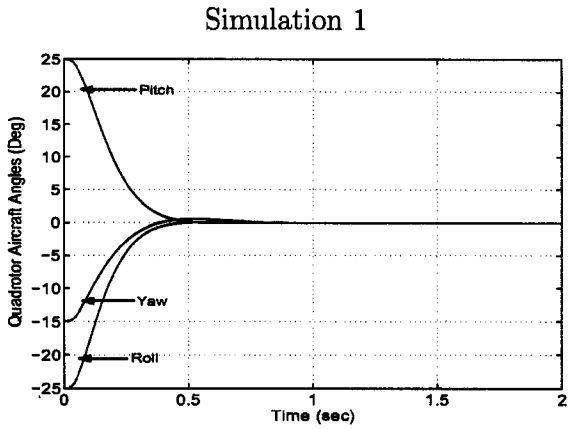

Figure 6.13: Aircraft Angles, Theorem 2

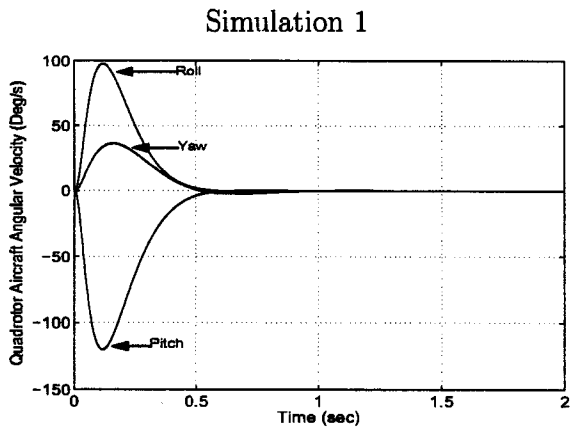

Figure 6.14: Angular Velocity, Theorem 2

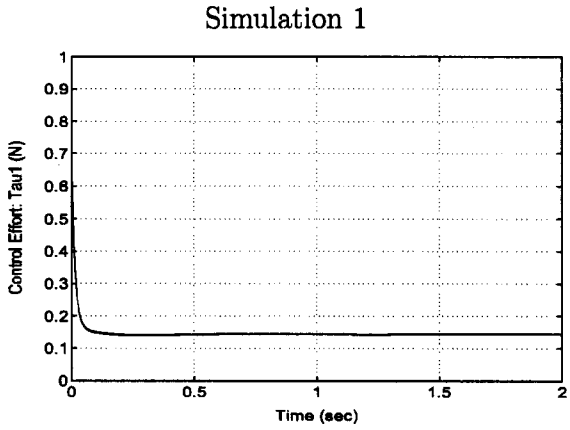

Figure 6.15: Control Effort 1, Theorem 2

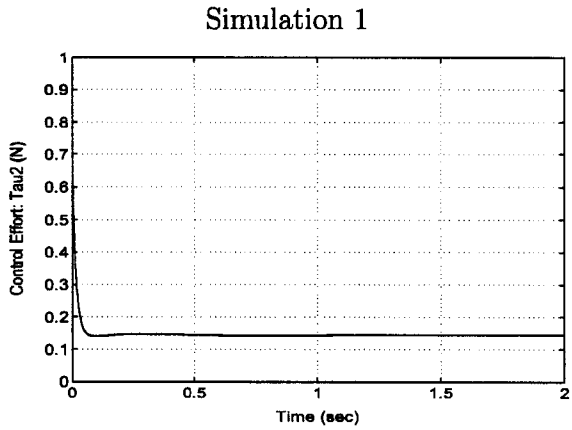

Figure 6.16: Control Effort 2, Theorem 2

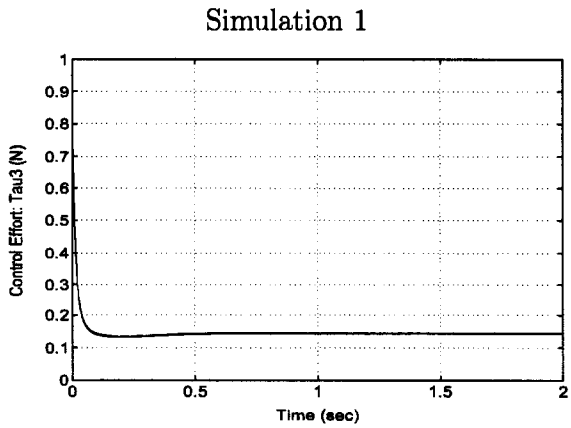

Figure 6.17: Control Effort 3, Theorem 2

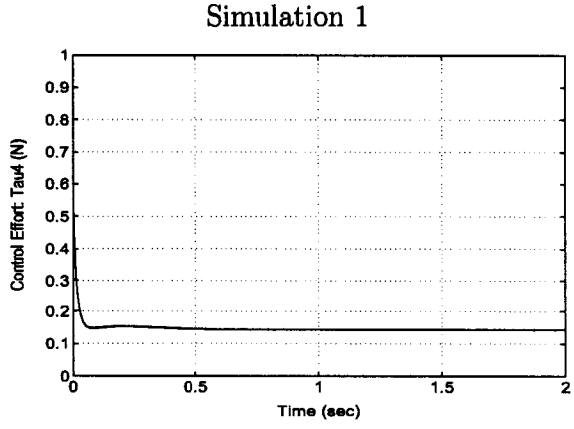

Figure 6.18: Control Effort 4, Theorem 2

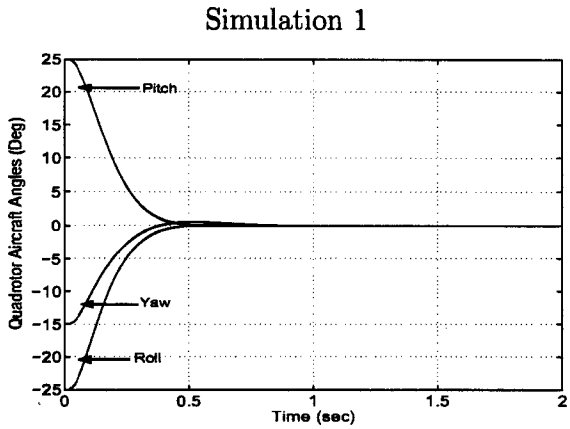

Figure 6.19: Aircraft Angles, Modified Theorem 2

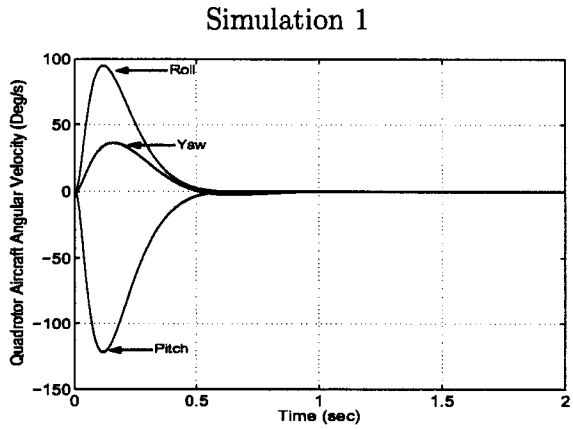

Figure 6.20: Angular Velocity, Modified Theorem 2

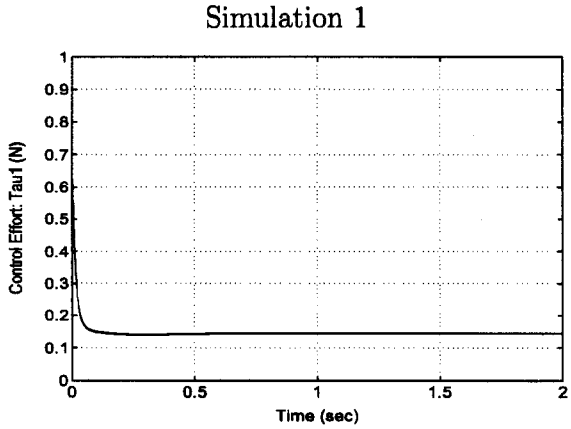

Figure 6.21: Control Effort 1, Modified Theorem 2

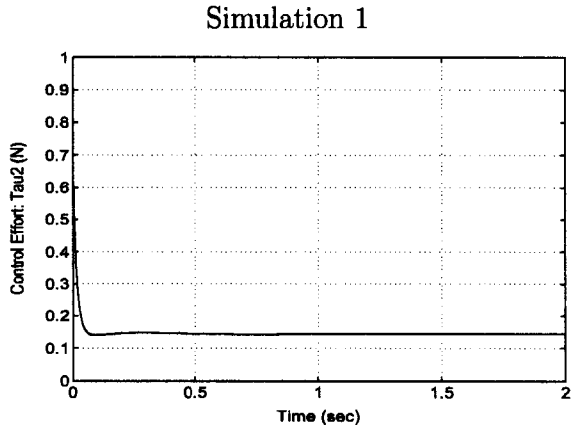

Figure 6.22: Control Effort 2, Modified Theorem 2

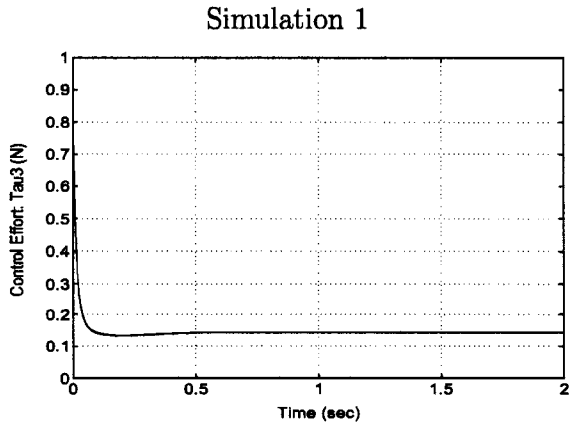

Figure 6.23: Control Effort 3, Modified Theorem 2

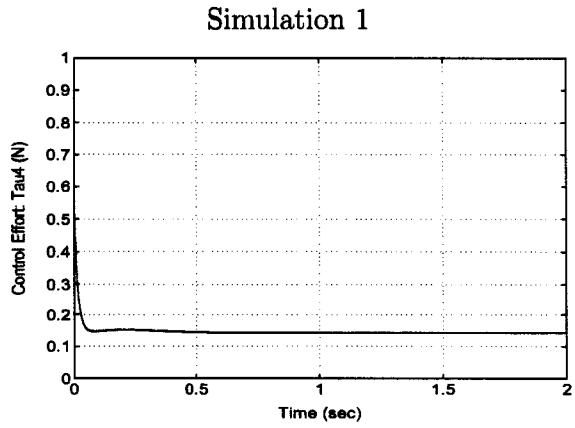

Figure 6.24: Control Effort 4, Modified Theorem 2

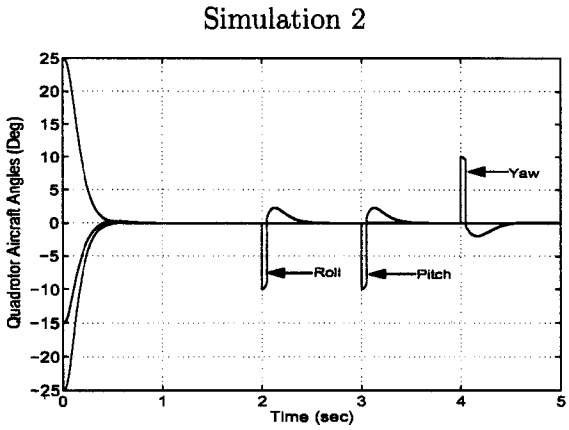

Figure 6.25: Aircraft Angles, Theorem 1

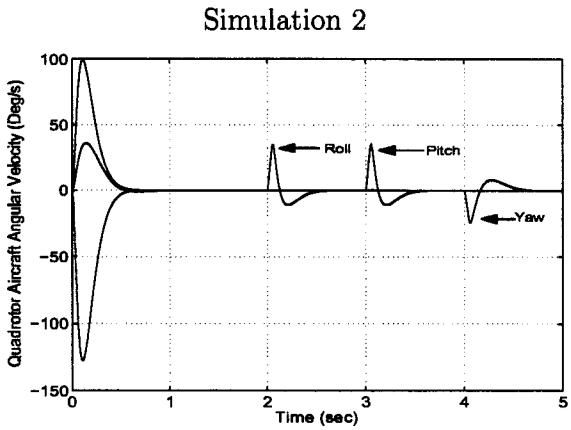

Figure 6.26: Angular Velocity, Theorem 1

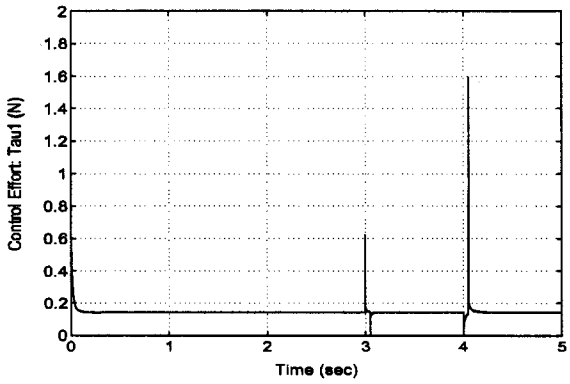

Figure 6.27: Control Effort 1, Theorem 1

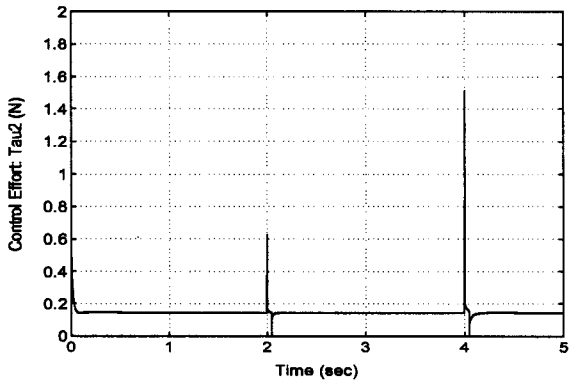

Figure 6.28: Control Effort 2, Theorem 1

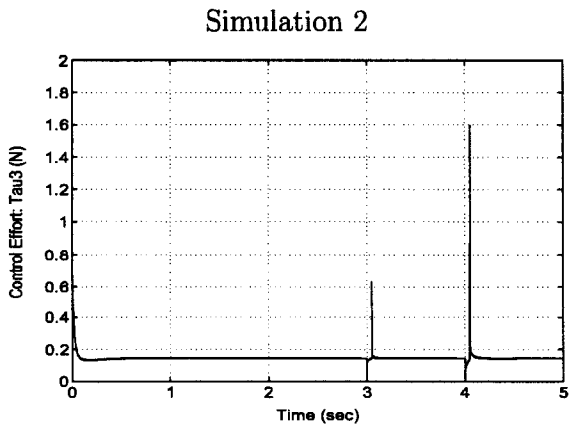

Figure 6.29: Control Effort 3, Theorem 1

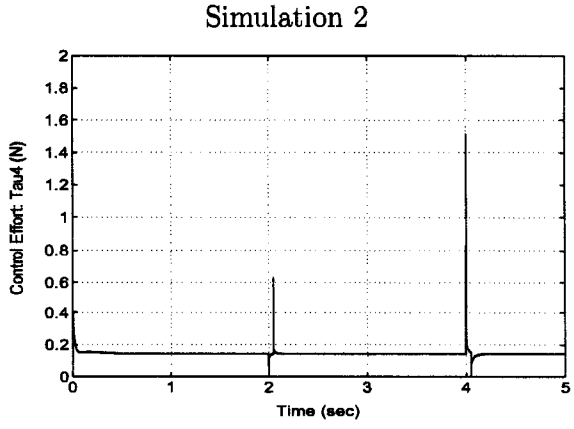

Figure 6.30: Control Effort 4, Theorem 1

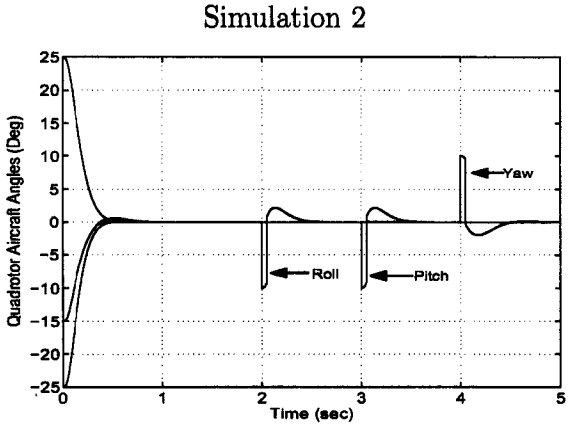

Figure 6.31: Aircraft Angles, Theorem 2

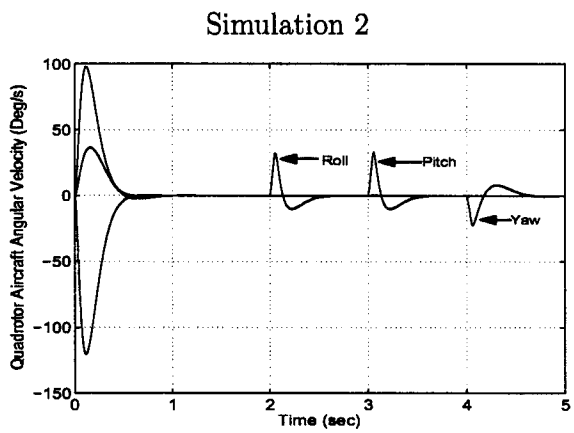

Figure 6.32: Angular Velocity, Theorem 2

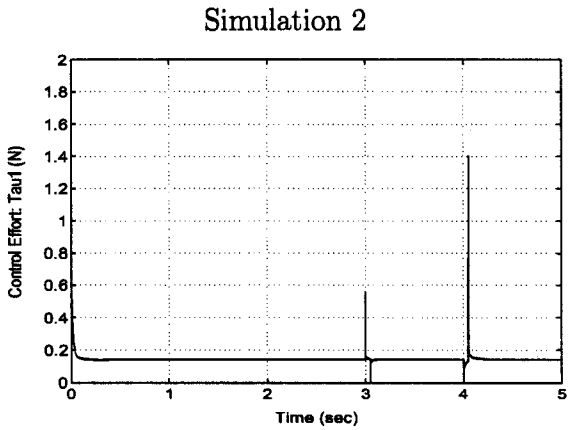

Figure 6.33: Control Effort 1, Theorem 2

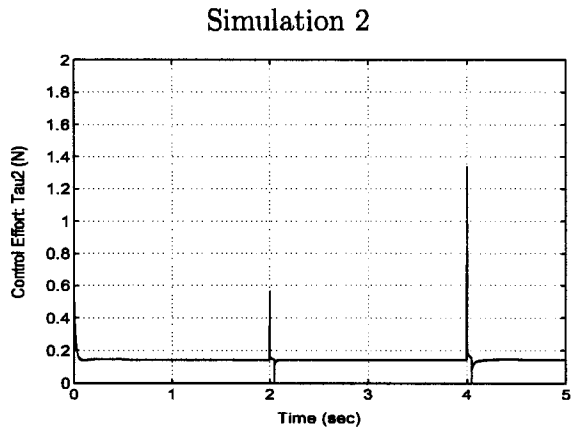

Figure 6.34: Control Effort 2, Theorem 2

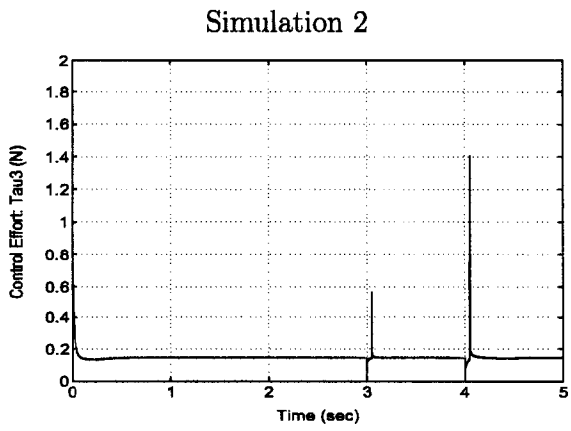

Figure 6.35: Control Effort 3, Theorem 2

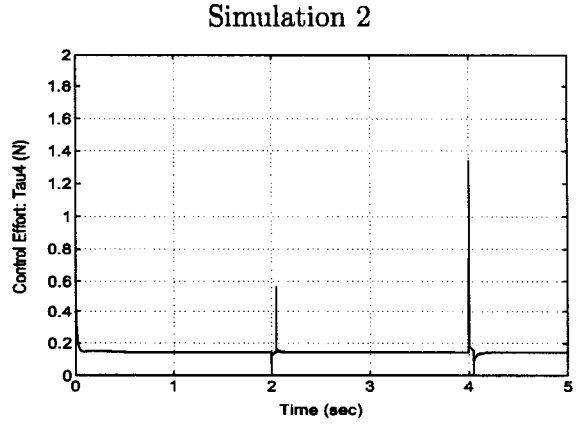

Figure 6.36: Control Effort 4, Theorem 2

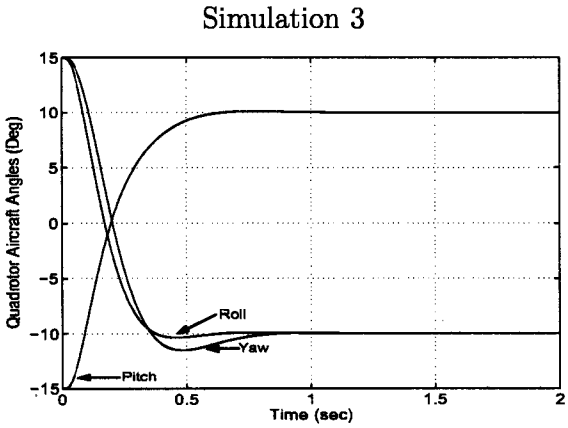

Figure 6.37: Aircraft Angles, Theorem 1

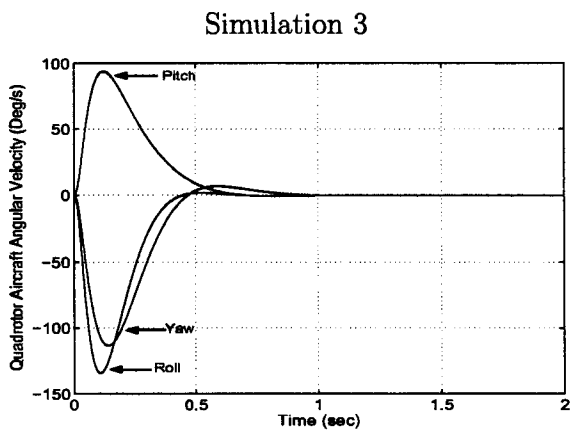

Figure 6.38: Angular Velocity, Theorem 1

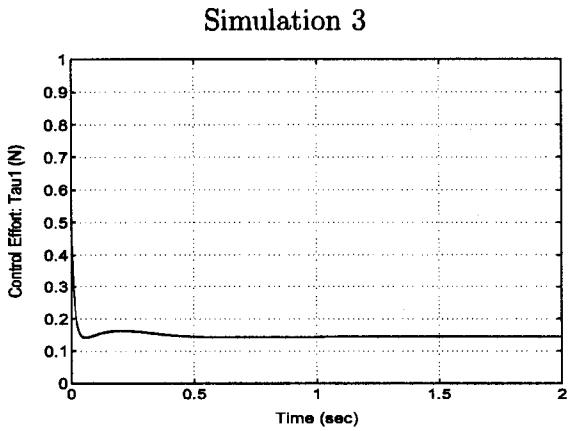

Figure 6.39: Control Effort 1, Theorem 1

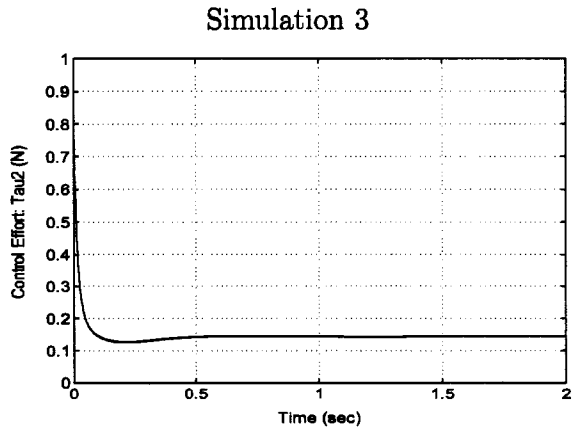

Figure 6.40: Control Effort 2, Theorem 1

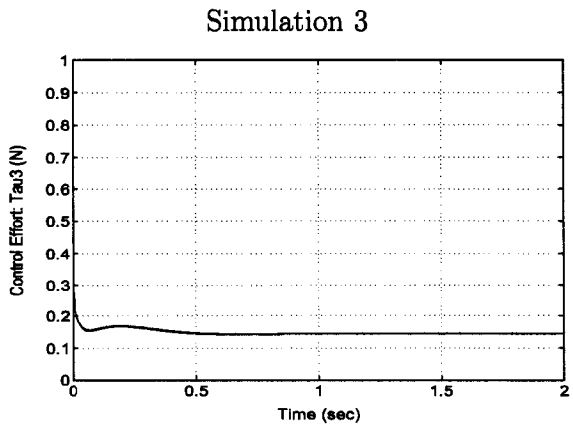

Figure 6.41: Control Effort 3, Theorem 1

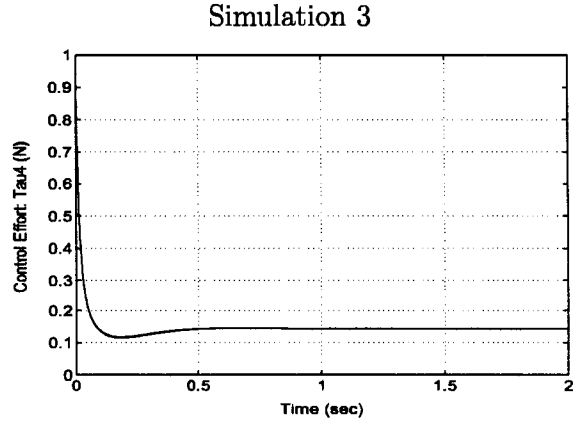

Figure 6.42: Control Effort 4, Theorem 1

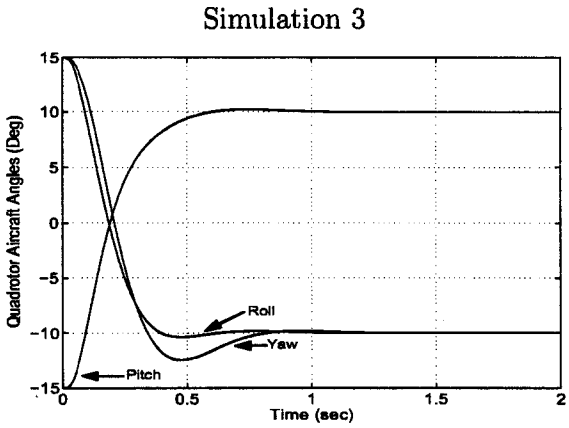

Figure 6.43: Aircraft Angles, Theorem 2

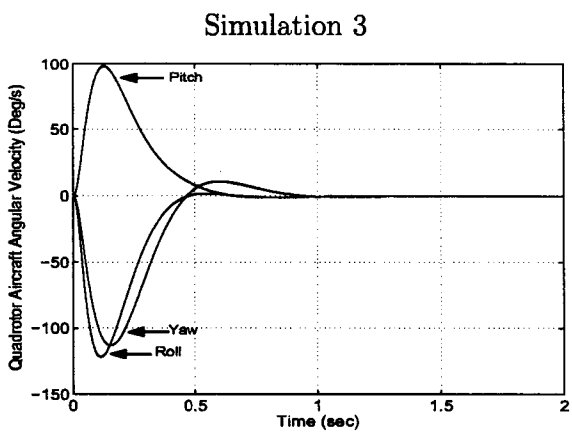

Figure 6.44: Angular Velocity, Theorem 2

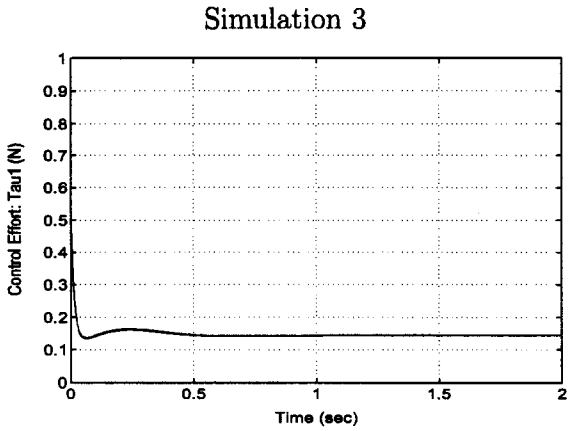

Figure 6.45: Control Effort 1, Theorem 2

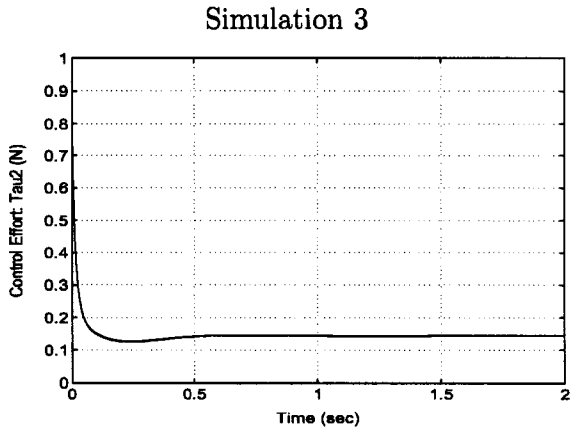

Figure 6.46: Control Effort 2, Theorem 2

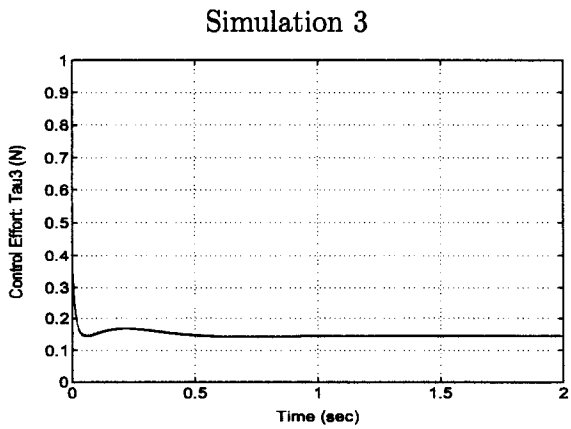

Figure 6.47: Control Effort 3, Theorem 2

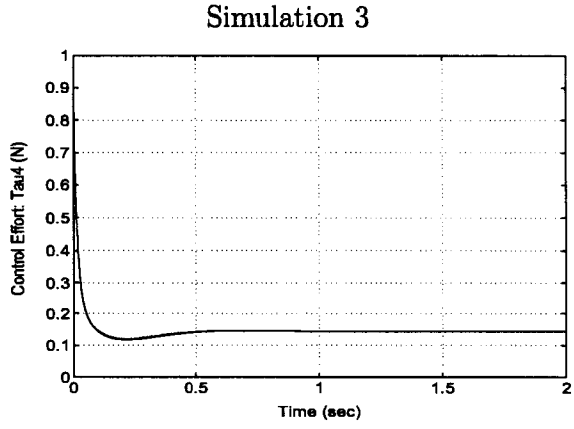

Figure 6.48: Control Effort 4, Theorem 2

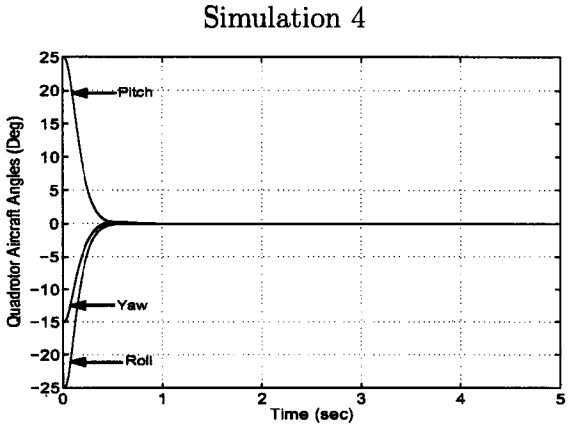

Figure 6.49: Aircraft Angles, Theorem 1

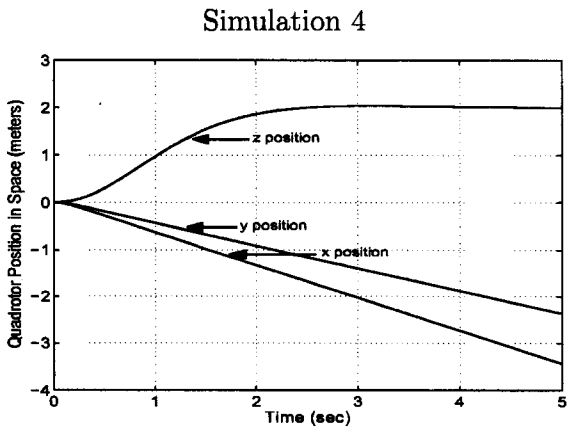

Figure 6.50: Coordinates, Theorem 1

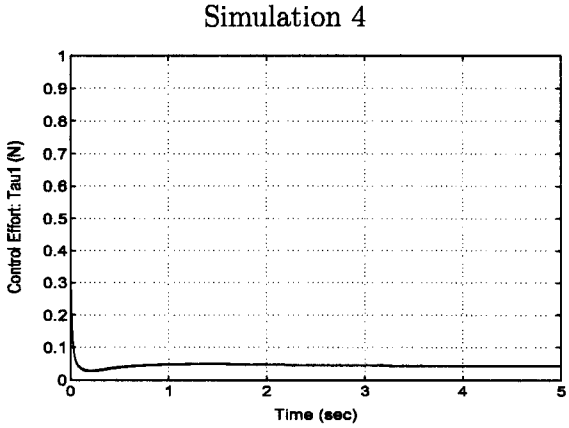

Figure 6.51: Control Effort 1, Theorem 1

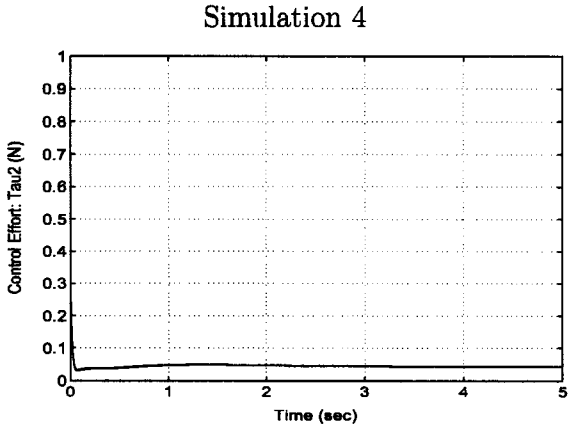

Figure 6.52: Control Effort 2, Theorem 1

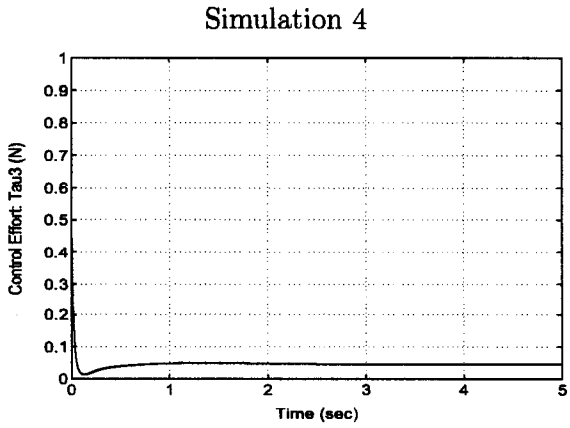

Figure 6.53: Control Effort 3, Theorem 1

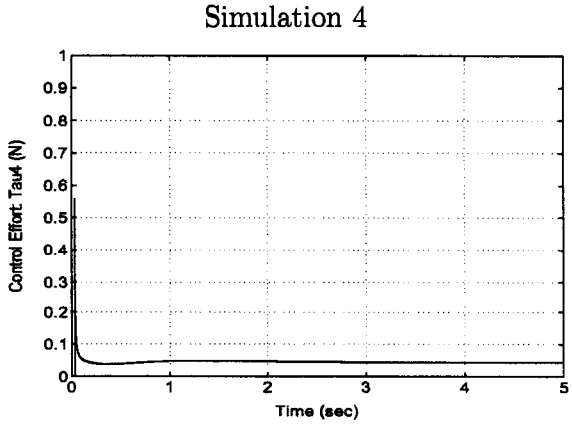

Figure 6.54: Control Effort 4, Theorem 1

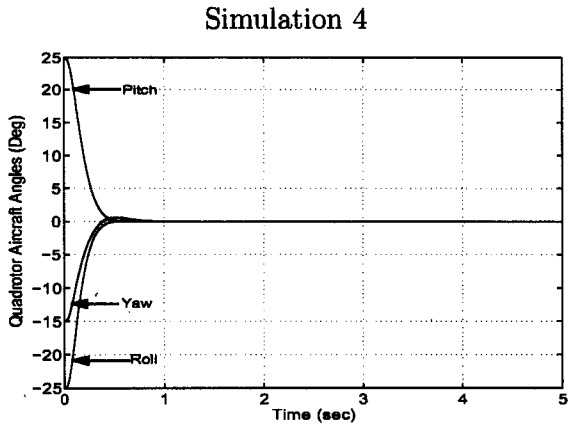

Figure 6.55: Aircraft Angles, Theorem 2

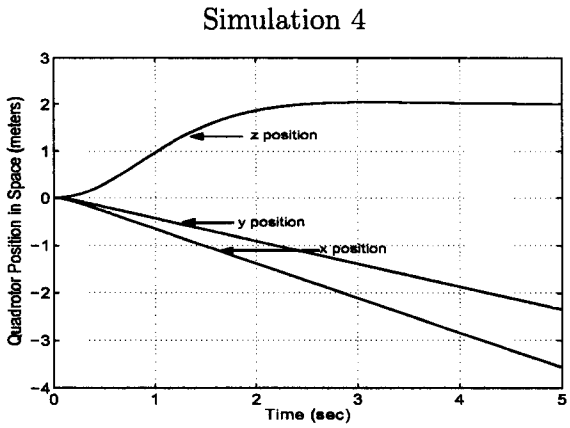

Figure 6.56: Coordinates, Theorem 2

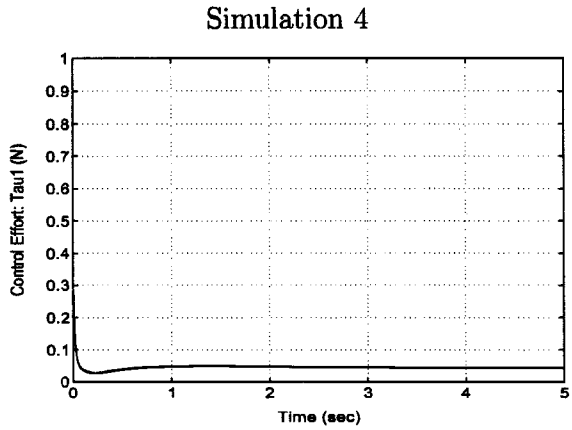

Figure 6.57: Control Effort 1, Theorem 2

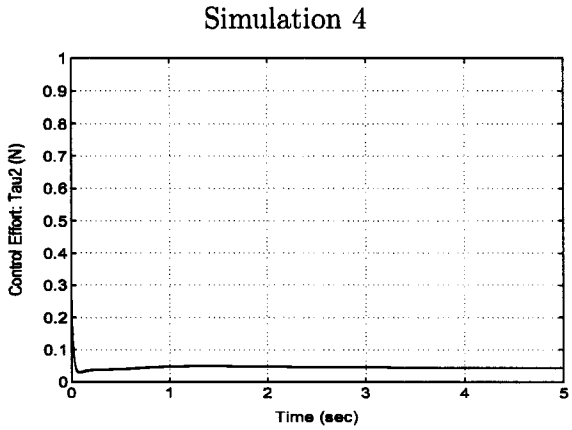

Figure 6.58: Control Effort 2, Theorem 2

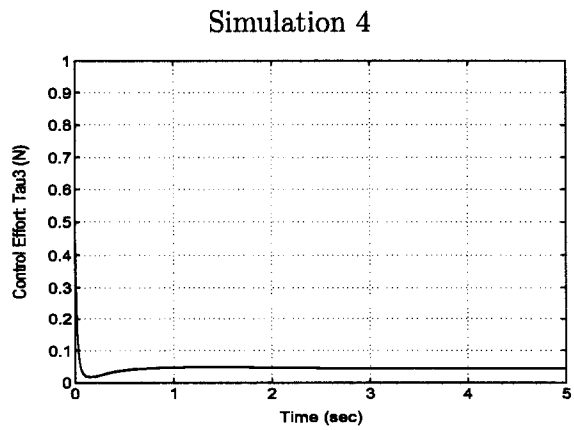

Figure 6.59: Control Effort 3, Theorem 2

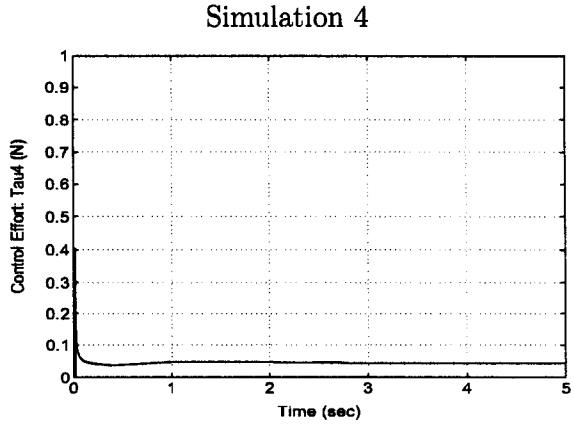

Figure 6.60: Control Effort 4, Theorem 2

Chapter 7

Experimental Setup

This chapter details the physical setup used during the experimentation for the quadrotor aircraft under consideration. An explanation of the aircraft sensors is followed by a detailed presentation of the attitude estimation technique employed to obtain the quadrotor aircraft angles. The control implementation is shown in a block diagram format followed by the plotted experimental results at the end of this chapter.

7.1 Physical Setup

The experimental quadrotor aircraft is an "in-house" modified version of the Draganflyer III from RC Toys (http://www.rctoys.com). In fact, we kept the airframe, the motors and the blades of the Draganflyer III and added our own sensors and electronic circuitry. Since, the objective was to safely test the attitude controller, we decided to use a stationary ball joint base, as shown in Figure 7.1. The ball joint is made from steel, while the lightweight socketed base is made from Teflon® to reduce the rotational friction. This base gives the aircraft unrestricted yaw movement and around $\pm 30°$ of pitch and roll, while restricting the aircraft to a fixed point in three-dimensional space.

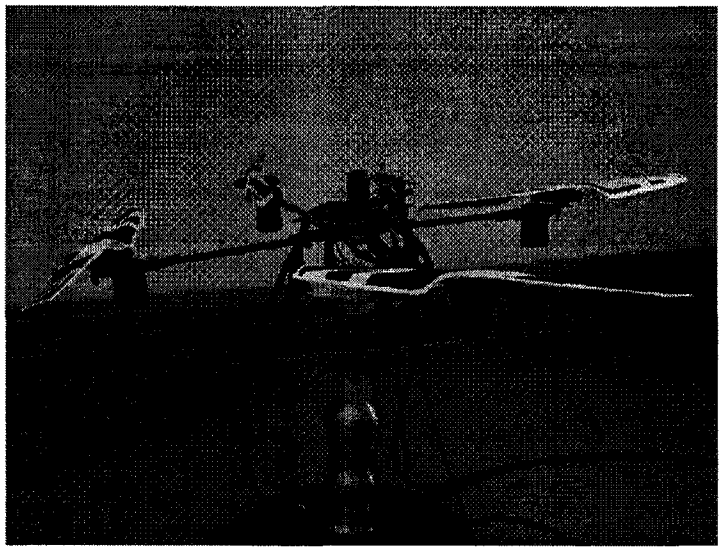

Figure 7.1: Quadrotor Aircraft Experimental Setup

Experimental testing has been performed, with a sampling frequency of 2kHz, using a DS1104 dSPACE system, which consists of a Texas Instruments TMS320C31 floating point digital signal processor (DSP) and a user-friendly graphical interface (Control Desk). The dSPACE Control Desk software in combination with Matlab/Simulink/ Real-time Workshop allows an easy implementation of the control algorithm in block diagram format via Simulink. After compilation, the program is downloaded into the DSP and the user has the possibility of real-time adjustment of the control gains.
Two independent power sources are used for the aircraft and sensors. One 12V, 7Amp-hour 'Gel-Cell' sealed lead-acid battery, not attached to the aircraft, is used to power the four motors and the Hall Effect sensors, which share a common digital ground once interfaced to the acquisition board. A single 9V alkaline battery, regulated to 5V and attached to the airframe, is used to power 3 gyroscopes and a 2-axis accelerometer sharing a common analog ground. Experimental tests using one power source with a single common ground made it difficult to achieve accurate readings from the attitude sensors due to noise generated by the motors. Using two power sources allows the digital and analog grounds to be separated and eliminates excessive noise infiltrating the sensor signals from the motors.

The four DC permanent magnet mini motors are geared to each rotor by a speed reduction ratio of 5.6:1. The motors are current amplified with a power MOSFET and driven by PWM signals at a frequency of 180Hz.

7.2 Sensors and Attitude Estimation

The rotor velocities ω_i, $i \in \{1, 2, 3, 4\}$ are obtained from Hall Effect sensors in combination with earth magnets. In fact, two magnets, placed 180° apart from each other under the main rotor gear, pass above the sensor as the gear rotates. The normally high, +5V, output signal pulses low, 0V, as each magnet passes above. The angular velocity is then obtained by first measuring the 'On' time, τ_{on} when the signal is high between pulses. Referring to Figure 7.2, we know that $\tau_{on} = 0.8737\tau_{ri}$ for any given frequency, where τ_{ri} is the time for one rotor revolution in seconds. This has been measured through experimentation and will remain constant for any frequency greater than zero. The time for one revolution of a rotor is given by

$$\tau_{ri} = \frac{2\tau_{on}}{0.8737}(s) \tag{7.1}$$

and finally the angular velocity for one rotor is given by

$$\omega = \frac{2\pi}{\tau_{ri}}(rad/s) \tag{7.2}$$

The resolution of this measurement depends on the sampling frequency and the rotor velocity. As the rotor velocity increases, the resolution of this measurement will decrease yet, with a sufficient sampling frequency, accurate measurements can be obtained. The angular velocity ω can only be calculated once τ_{ri} has been determined. If the rotor is spinning very slowly, or has stopped, then the time τ_{ri} cannot be determined, and the algorithm to calculate ω will continue waiting. To avoid this problem, a maximum time $\tau_{ri,max}$ corresponding to a minimum angular velocity is programmed into the calculation. If the calculation waits for a time greater than

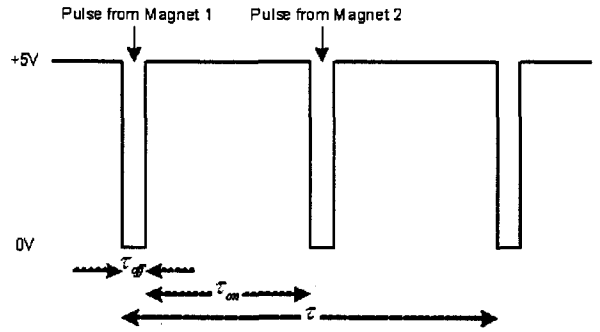

Figure 7.2: Rotor Velocity / Hall Effect Sensor Timing Diagram

$\tau_{ri,max}$, then the measured angular velocity of the rotor will be set to zero. The desired acceleration of each rotor $\dot{\omega}_d = (\dot{\omega}_{d,1}, \dot{\omega}_{d,2}, \dot{\omega}_{d,3}, \dot{\omega}_{d,4})^T$ required for the motor torques control design has been obtained by using a filtered derivative of the form $\dot{\omega}_{d,i} = \frac{s}{1+T_f s}[\omega_{d,i}]$ where $T_f = 0.008$ represents a cutoff frequency of 20Hz.

The angular velocity of the aircraft Ω is obtained from three orthogonally mounted gyroscopes. The gyroscopes employed are NEC/TOKIN CG-16D0 miniature ceramic gyros which have maximum detectable angular rates specified at $\pm 90°$/sec. The output sensitivity of each gyroscope is specified as 1.1mV/deg/sec while the output voltage at a zero angular rate is specified at 300mV at 25°C but can vary up to 800mV at any temperature. Inaccurate measurements can arise if variable temperatures occur in the testing environment however, calibrating the gyroscopes by measuring and removing the output offset prior to any experimentation, and allowing them to 'warm-up', has proven effective. High frequency noise is sufficiently removed from the Ω measurement by adding first-order low-pass software filters each with a cutoff frequency of 20Hz.

The attitude estimation of the aircraft has proven to be a challenge. Accurate measurements of the roll, pitch and yaw angles in real-time over a wide range of operating conditions is not easily achieved. Each gyroscope gives the rate of rotation around its respective axis, therefore simple integration should yield the desired angle for a planar rotation. In practice however, each signal contains a small amount of noise and offset

error. The offset error can be removed before each experiment but temperature and other factors will contribute to this error and will cause the integrated signal to grow to infinity. This problem is known as integral drift and has been observed during experimentation.

Real-time planar attitude estimation has required fusing measurements from the gyroscopes with measurements from the accelerometers. Configuring the accelerometers along the $\hat{x}_A$ and the $\hat{y}_A$ axes as tilt meters and fusing this data with the measurements from the two gyroscopes mounted along the same axes, by complementary filtering, yields relatively accurate and drift free pitch and roll angle measurements (Baerveldt and Klang 1997). Similar results are also possible for the yaw angle by fusing compass data with the yaw gyro signal, but have not been realized due to difficulties with compass readings.

A dual-axis accelerometer mounted to the aircraft has been positioned to measure the acceleration along the $\hat{x}_A$ and $\hat{y}_A$ axes. Manufactured by Analog Devices, the ADXL202AE has a full-scale range of $\pm 2g$. This low-cost, low-power device is made with Micro-Electro-Mechanical System (MEMS) technology on a single IC and weighs less than 1 gram. The dual-axis accelerometer has been configured as a tilt meter to give the roll (ϕ) and pitch (θ) angles of the aircraft up to a maximum angle of $\pm 90°$. By using the force of gravity as an input vector, the dual-axis accelerometer can be configured as a tilt meter giving the angles of the rigid body or platform on which it is installed. The objective is to extract the angle of rotation with the knowledge of the measured acceleration from the device. Assuming that the accelerations are due to gravity only, and by using the equation for torque given as

$$\tau = mglsin\theta, \tag{7.3}$$

and Newton's second law of rotation given as

$$\Sigma\tau = I\ddot{\theta}, \tag{7.4}$$

we can see that

$$I\ddot{\theta} = mglsin\theta. \tag{7.5}$$

Normalizing the above by letting

$$\theta = sin^{-1}\frac{I}{mgl}\ddot{\theta}, \tag{7.6}$$

leads to a simple expression of the angle as

$$\theta = sin^{-1}\frac{\ddot{\theta}}{\ddot{\theta}_s}. \tag{7.7}$$

The accelerometer sensitivity is denoted by $\ddot{\theta}_s$ and is obtained through measurement as a voltage in mV. To obtain this data, the aircraft is set to a 0° position, and an acceleration measurement is taken. This value will be the offset bias, and will be removed so the measurement at 0° is always zero. The sensitivity is given by

$$\ddot{\theta}_s = \frac{\mid \ddot{\theta}_{+90^\circ} \mid + \mid \ddot{\theta}_{-90^\circ} \mid}{2g} \tag{7.8}$$

Normalizing the acceleration measurement gives a value between ± 1 . However, care must be taken to ensure that this measurement is between -1 and +1 before computing the arcsine function. This is achieved by placing limits on the normalized measurement.

The angle of rotation can be calculated with the knowledge of the measured acceleration from the device, assuming that the acceleration is due only to gravity. However, accurate tilt angles are only possible with a relatively static platform. Large angular velocities as well as vibrations and translational motion of the aircraft make it difficult to read proper tilt angles. Placing a first order low-pass hardware filter on the analog output of the accelerometer with a cut-off frequency of 0.5 Hz effectively removes the unwanted noise due to high frequency vibration and angular velocities of the aircraft, and defines the dynamics of the device. Since the design of the complementary filters, to be discussed later, only requires the tilt meter to have effective dynamics in the lower frequency range, we can easily justify the use of this filter.

In fact, the roll and pitch are obtained, through the fusion process, as follows

$$x = G_t(s)[x_t] + G_g(s)[x_g],$$

where x denotes (ϕ) or (θ). The signal x_t is obtained from the tilt-meter and x_g is obtained from the gyroscope. The transfer functions G_t and G_g are calculated such that the following equality is satisfied (Baerveldt and Klang 1997)

$$H_t(s)G_t(s) + sH_g(s)G_g(s) = 1 \tag{7.9}$$

where H_t and H_g denote the transfer functions describing the dynamics for the tilt meter and gyroscope respectively. Including the known dynamics for the tilt meter, and assuming ideal dynamics for the gyroscope, we have

$$H_t(s) = \frac{1}{0.32s+1}, H_g(s) = 1. \tag{7.10}$$

Therefore, we can choose the filter transfer functions as

$$G_t(s) = \frac{0.64s+1}{0.32s+1}, G_g(s) = \frac{0.1024s}{(0.32s+1)^2} \tag{7.11}$$

The high-pass filter on the gyro branch effectively removes the low frequency signal components at 40dB per decade, sufficiently reducing the effects of drift at lower frequencies. Similarly the low-pass filter on the tilt meter branch effectively removes the high frequency signal components at 20dB per decade.

In fact, the need for additional filtering has been observed and implemented on both the gyroscope and tilt meter measurements to obtain a cleaner fused signal. The additional first order low pass filters have cutoff frequencies set at 20Hz for the roll and pitch gyro signals, 10Hz for the yaw gyro signal, and 2Hz for the roll and pitch tilt meter signals. The filter transfer functions are given as follows

$$F_t = \frac{1}{0.08s+1}, F_{g,\psi} = \frac{1}{0.016s+1}, F_g = \frac{1}{0.008s+1} \tag{7.12}$$

where F_t and $F_{g,\psi}$ denote the transfer functions for the additional tilt meter filter and yaw gyroscope filter, and F_g denotes the transfer function for the roll and pitch gyro signals. Since the fusion process considers only the roll and pitch, the addition of the filter on the yaw gyro $F_{g,\psi}$ has no effect on the complimentary filtering results. However, the additional filtering on the roll and pitch gyros and tilt meter signals

does indeed affect the overall result. Using (7.9) and the additional filter transfer funtions gives

$$H_t(s)G_t(s)F_t(s) + sH_g(s)G_g(s)F_g(s) = G_d(s) \tag{7.13}$$

where G_d denotes the transfer function describing the dynamics of the final fused signal and is given by

$$G_d = \frac{125s^3 + 1641s^2 + 9888s + 15260}{s^4 + 143.8s^3 + 2432s^2 + 11110s + 15260} \tag{7.14}$$

Bode plots showing the contribution of each branch after filtering as well as the final fused result may be seen in Figures 7.3 and 7.4 below.

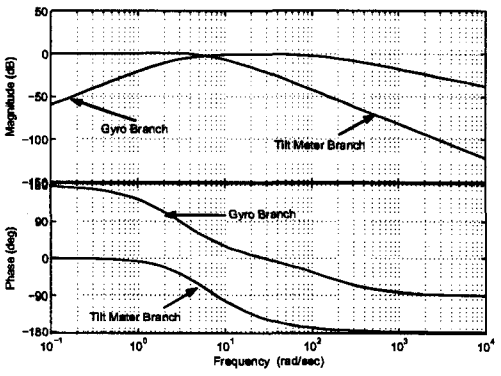

Figure 7.3: Bode Plot of Gyro and Tilt Meter.

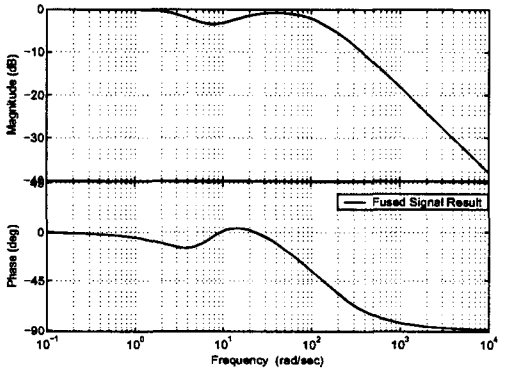

Figure 7.4: Bode Plot of Final Fused Signal.

This type of angle estimation through complementary filtering has proven effective for relatively small roll and pitch aircraft angles. However, this method is only theoretically justified for individual planar rotations. More complex rotations of simultaneous roll, pitch and yaw angles require a nonlinear fusion technique as described in (Rehbinder and Hu 2003; Rehbinder and Hu 2000), due to the relationship previously given in the kinematic equation (3.12). Considering the relative complexity, and restrictions of this method, and the fact that our experiments are controlled within restricted aircraft angles, the first linear fusion method described has proven the effective choice for the roll and pitch angles estimation.

Since the yaw angle of the aircraft is not measurable with a tilt meter, the use of a compass is a potential alternative to give an accurate yaw angle at lower frequencies.

The compass employed for this task is a Dinsmore analog sensor No. R1655 which outputs a sine-cosine curve pair. It exhibits slightly slower dynamics compared with the configured tilt meter, in that the specified response time from a 90° displacement is 2.5 to 3.5 seconds without overshoot. The sensor is designed to measure the horizontal component of the earth flux fields. However, experimental testing has shown that relatively small tilt angles, and vibrations from the four motors, induce large errors in the compass measurement. Experimentation with filtering and complex algorithms to ignore compass data when a specified roll or pitch angle is detected has been tried without success. Therefore, the drift of the integrated yaw signal from the gyro alone has been noted and considered acceptable, and experimentation has continued without compensation for the yaw drift. The yaw angle estimation (ψ) is therefore achieved by

$$\psi = F_g(s)\frac{1}{s}[\dot{\psi}] \tag{7.15}$$

where $\dot{\psi}$ denotes the measured angular rate from the yaw gyroscope. Again, simple integration of the velocity signal as described above, is only theoretically valid for planar rotation due to the nonlinear relationship of (3.12). However, when the quadrotor aircraft is stabilized to the hover orientation, any yaw rotations are strictly planar.

7.3 Control Implementation and Pilot Interface

The block diagram showing the implementation of the control algorithm with the pilot interface is seen in Figure 7.5. As discussed in Chapter 4, desired Euler angles may be specified numerically, or more practically, with a pilot interface such as a control-stick. Therefore, the pilot may use the control-stick to specify the desired altitude and vary the desired roll, pitch and yaw angles, to control the motion of the quadrotor aircraft in space. Used in conjuction with the attitude set-point regulation and altitude controller, the pilot now has an effective and stable means of controlling

the quadrotor aircraft. In fact, if no pilot command is given, the quadrotor will ideally stabilize its attitude, and hover at the given desired altitude. The altitude controller

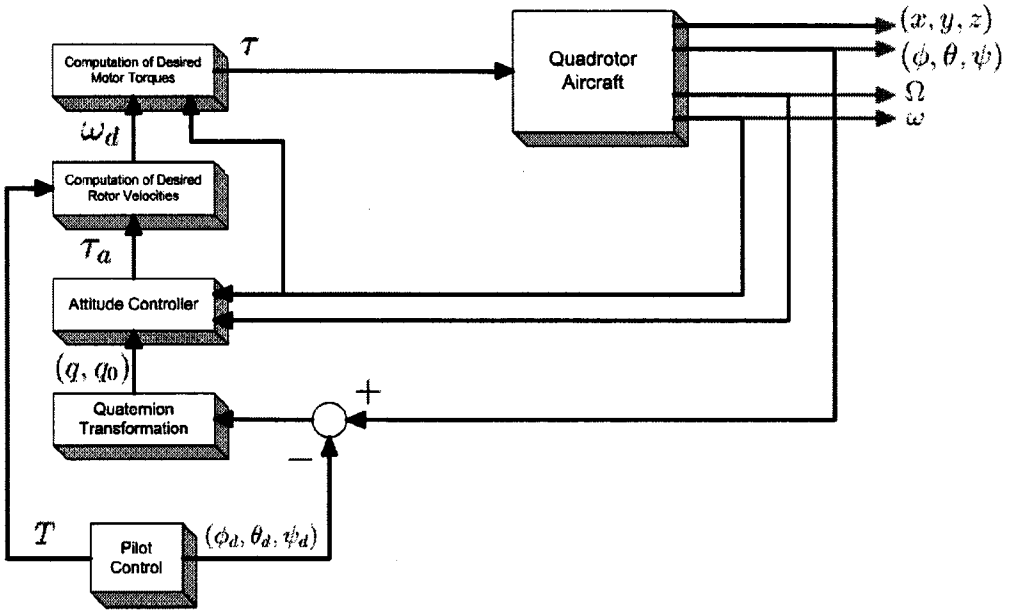

Figure 7.5: Control Implementation

gains necessary for control law (4.41), are developed below. The controller has been designed for a 3 second settling time with 2% overshoot. From this information and the well known equations for settling time and percentage overshoot, the second order characteristic equation may be numerically developed as follows:

$$\xi = \sqrt{\frac{(lnP.O.)^2}{\pi^2 (lnP.O.)^2}} = 0.78 \tag{7.16}$$

$$\omega_n = \frac{4}{\xi T_s} = 1.709, \tag{7.17}$$

where T_s, $P.O.$, ω_n and ξ denote the settling time, percentage overshoot, natural frequency and damping factor respectively for the characteristic equation given as

$$s^2 + 2.67s + 2.92 = 0 \tag{7.18}$$

The roots of the above equation are given below as P_1 and P_2, along with a third necessary pole P_3 placed five times the real part of P_1 and P_2.

$$\begin{aligned} P_1 &= -1.335 + 1.067j \\ P_2 &= -1.335 - 1.067j \\ P_3 &= -6.675. \end{aligned}$$

The controller gains are then determined to be

$$\bar{K} = [20.74, 9.35, -19.49]. \tag{7.19}$$

The attitude controller gains used for all experiments were set by trial and error through experimentation and simulation. The gains for controllers (4.1) and (4.18) of Theorem 1 and Modified Theorem 1 are given as: $\Gamma_1 = diag(240, 240, 60)$, $\Gamma_2 = 0.0025 I_{3\times3}$ and $\Gamma_3 = 4 I_{3\times3}$. The gains for controller (4.19) and (4.28) of Theorem 2 and Modified Theorem 2 are given as: $\Gamma_4 = diag(0.5, 0.5, 0.2)$ and $\alpha = 4$. The desired thrust T and gain k_i used for the motor torques control design were kept at $T = 1.5N$, $k_i = 0.002$ respectively, while the initial roll, pitch and yaw angles varied only slightly.

7.4 Experimental Results

To explore the performance of each controller, three sets of experiments have been performed. The results of each experiment allow for a comparison to be made between theorems, helping illustrate similarities or difference in graphical results. All experiments have been performed using the model parameters given in Table 5.1, and controller gains given in the previous section.

7.4.1 Experiment 1

The objective of experiment 1 is to show the stabilization of the quadrotor attitude from some initial angles for each controller. The initial conditions are roughly the

same for each experiment. The experiment commences by turning the controller to the *'On'* state at time 0 seconds, and lasts total of 3 seconds. Experiment 1 has been performed on Theorem 1 (Figures 7.6- 7.11), Modified Theorem 1 (Figures 7.12- 7.17), Theorem 2 (Figures 7.18- 7.23), and Modified Theorem 2 (Figures 7.24- 7.29). For each controller tested the aircraft angles, angular velocity and normalized control effort for each motor, are plotted separately.

From the results it appears that exponential convergence has been achieved for all controllers tested. Although not totally obvious, it appears that the controller of Theorem 1 and Modified Theorem 1 have slightly superior performance for convergence of the aircraft angles, but with a slightly higher overall angular velocity.

7.4.2 Experiment 2

In Experiment 2, the aircraft is started from an initial configuration, and then stabilized to a zero attitude. Thereafter, disturbances are introduced on the pitch, roll and yaw to explore the disturbance rejection performance. Once the controller is turned to the *'On'* state at time 0 seconds, it lasts for a total of 10 seconds. Again, Experiment 2 has been performed on Theorem 1 (Figures 7.30- 7.35), Modified Theorem 1 (Figures 7.36- 7.41), Theorem 2 (Figures 7.42- 7.47), and Modified Theorem 2 (Figures 7.48- 7.53). For each controller tested the aircraft angles, angular velocity and normalized control effort for each motor, are plotted separately.

The plotted results show the disturbance rejection characteristics for each controller tested. Each disturbance was introduced to the aircraft by hand therefore, some are larger than others. However, the results are quite similar, and each controller handles the disturbances quite well, stabilizing the aircraft to the desired attitude.

7.4.3 Experiment 3

The objective of experiment 3 is to show the stabilization of the quadrotor aircraft attitude from some initial angles to given desired angles. The experiment commences

by turning the controller to the *'On'* state at time 0 seconds, and lasts total of 3 seconds. Experiment 3 has been performed on the controller in Theorem 1 (Figures 7.54- 7.59) only, as a comparison between controllers for this experiment is not required. This experiment illustrates the attitude stabilization to the desired configuration ($\phi_d = -10°, \theta_d = 10°, \psi_d = -10°$). The results show the aircraft angles, angular velocity and normalized control effort for each motor, plotted separately.

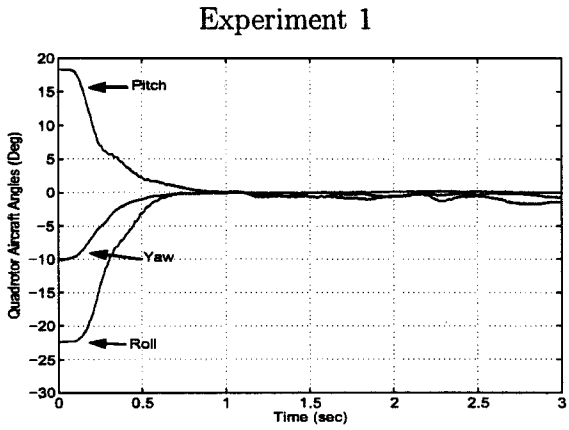

Figure 7.6: Aircraft Angles, Theorem 1

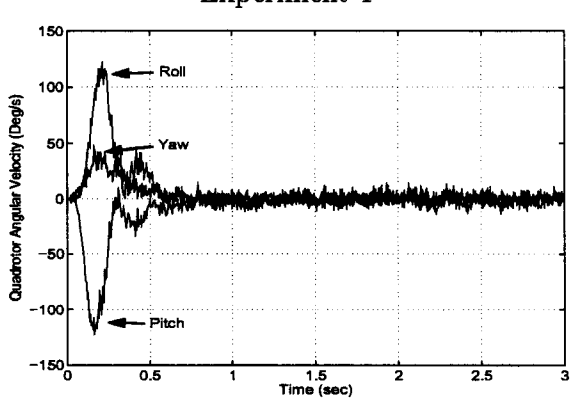

Figure 7.7: Angular Velocity, Theorem 1

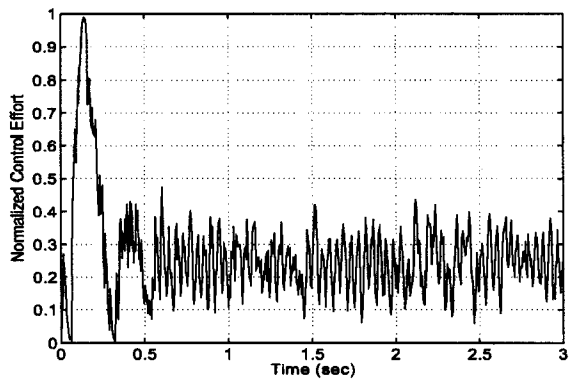

Figure 7.8: Control Effort 1, Theorem 1

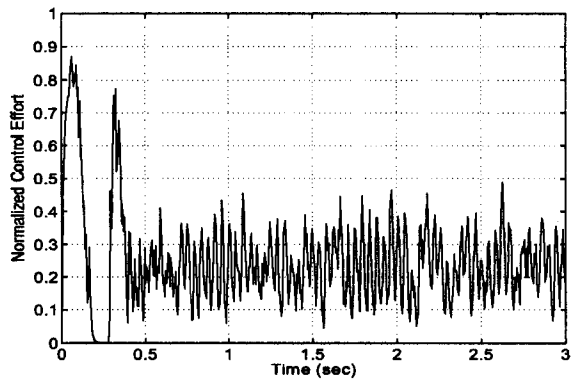

Figure 7.9: Control Effort 2, Theorem 1

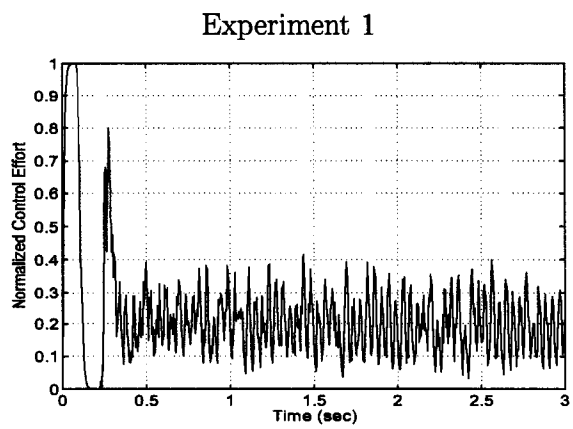

Figure 7.10: Control Effort 3, Theorem 1

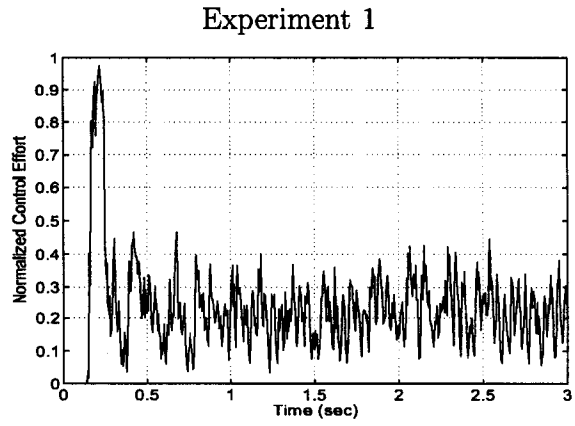

Figure 7.11: Control Effort 4, Theorem 1

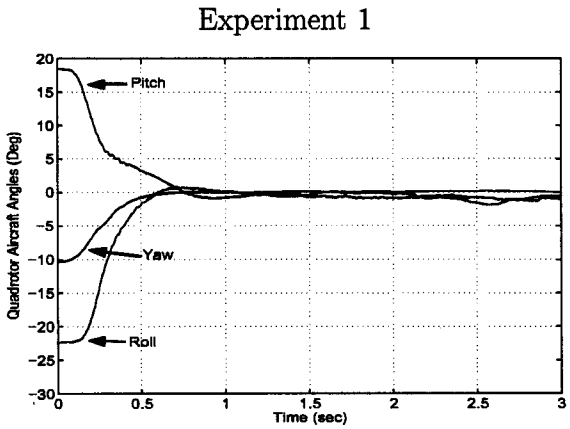

Figure 7.12: Aircraft Angles, Modified Theorem 1

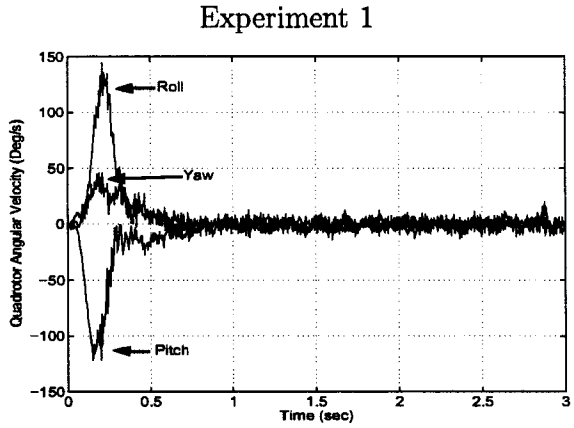

Figure 7.13: Angular Velocity, Modified Theorem 1

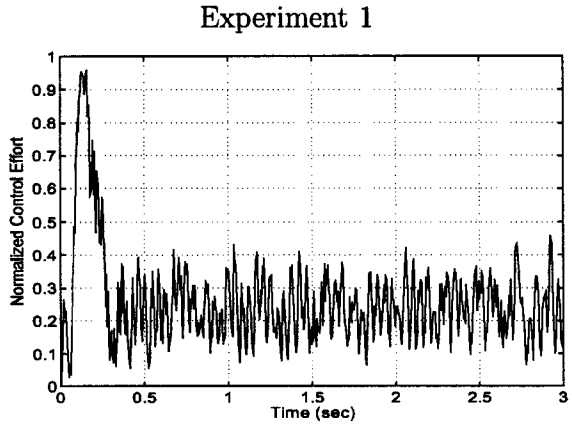

Figure 7.14: Control Effort 1, Modified Theorem 1

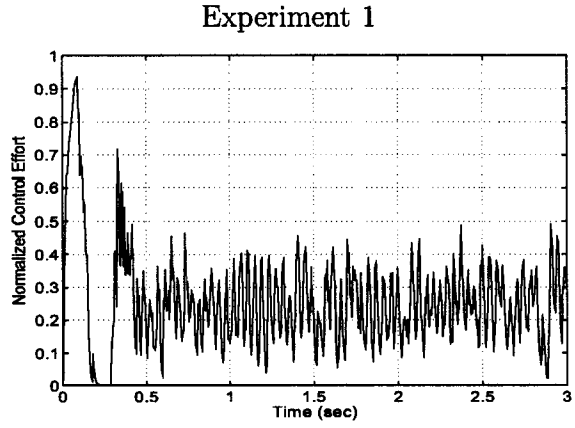

Figure 7.15: Control Effort 2, Modified Theorem 1

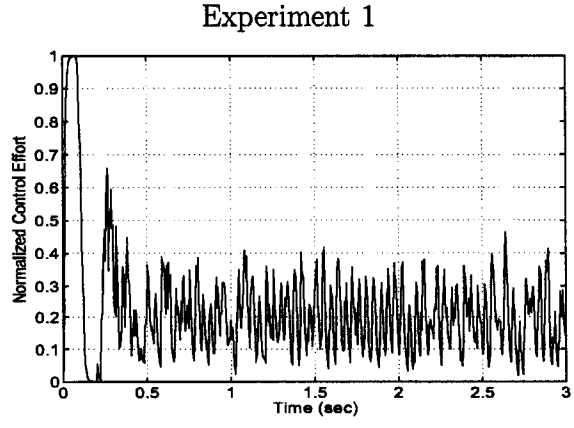

Figure 7.16: Control Effort 3, Modified Theorem 1

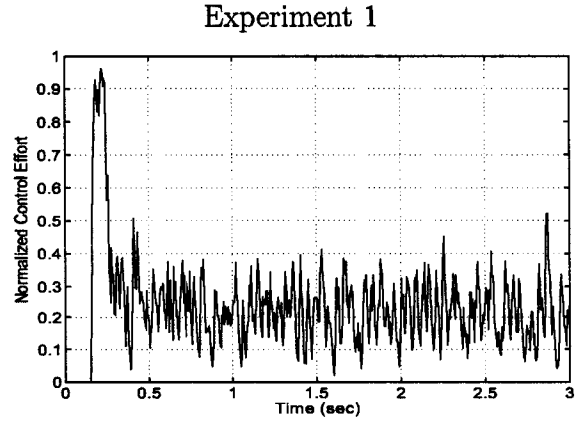

Figure 7.17: Control Effort 4, Modified Theorem 1

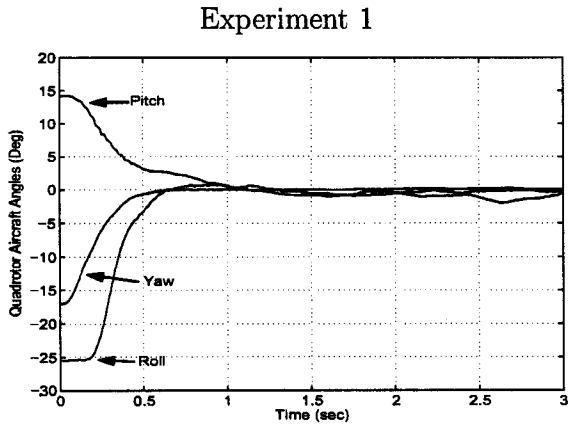

Figure 7.18: Aircraft Angles, Theorem 2

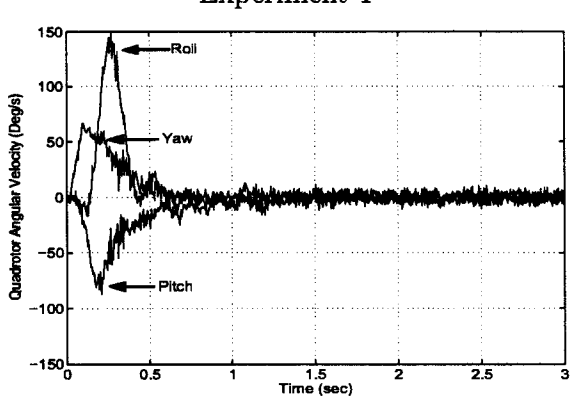

Figure 7.19: Angular Velocity, Theorem 2

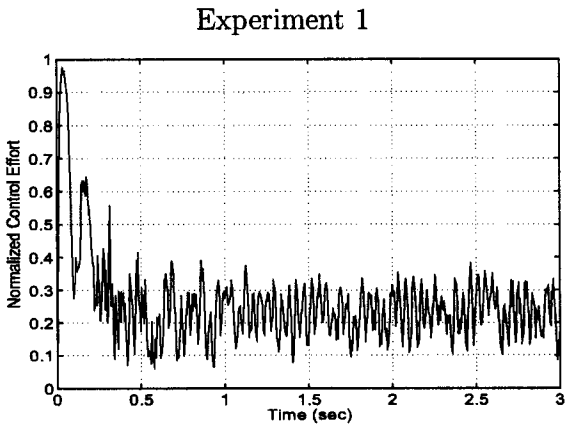

Figure 7.20: Control Effort 1, Theorem 2

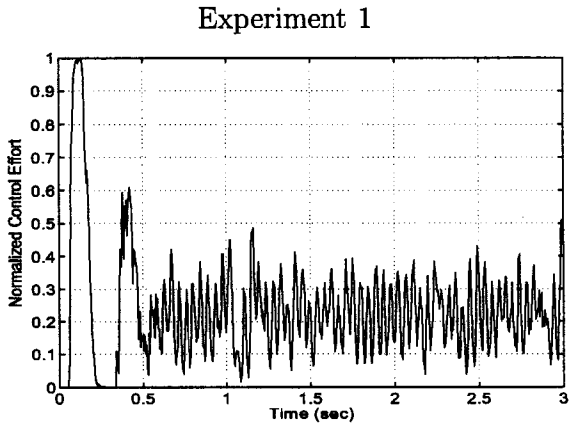

Figure 7.21: Control Effort 2, Theorem 2

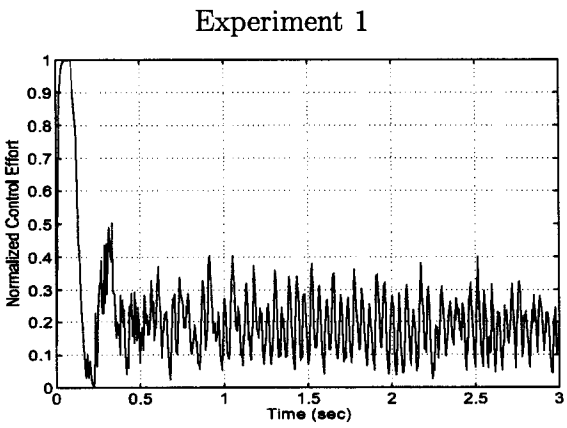

Figure 7.22: Control Effort 3, Theorem 2

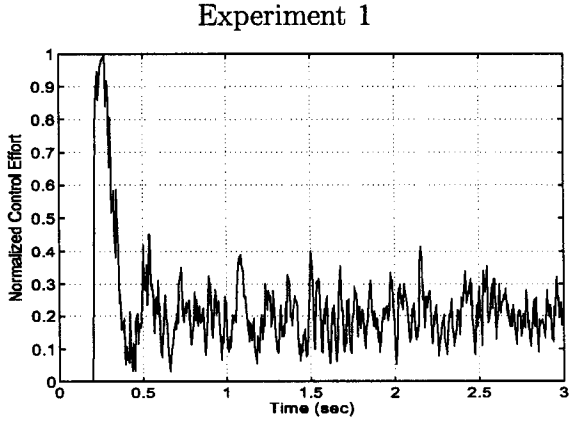

Figure 7.23: Control Effort 4, Theorem 2

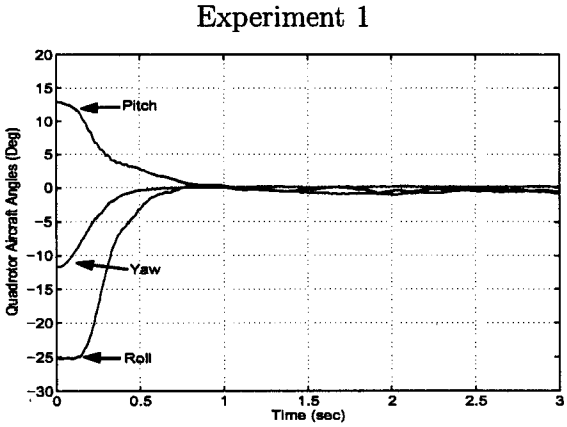

Figure 7.24: Aircraft Angles, Modified Theorem 2

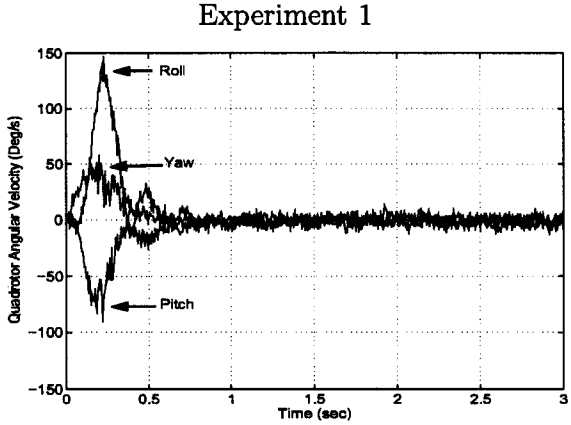

Figure 7.25: Angular Velocity, Modified Theorem 2

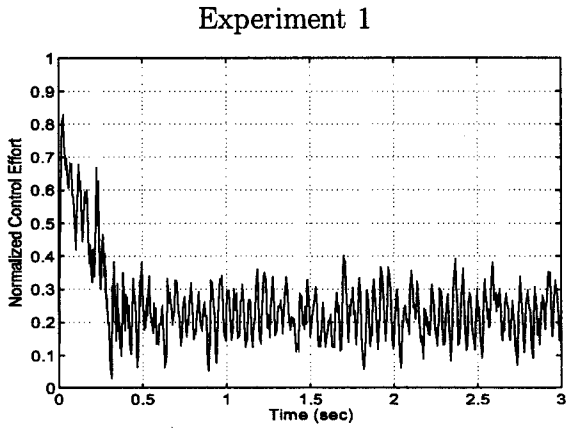

Figure 7.26: Control Effort 1, Modified Theorem 2

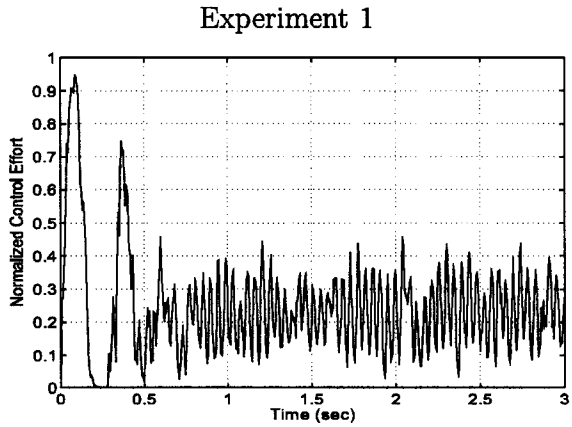

Figure 7.27: Control Effort 2, Modified Theorem 2

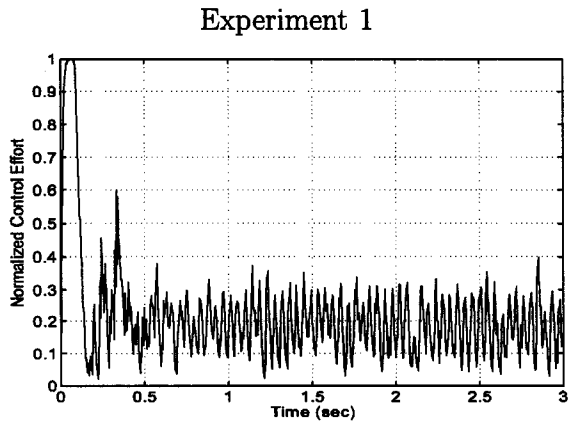

Figure 7.28: Control Effort 3, Modified Theorem 2

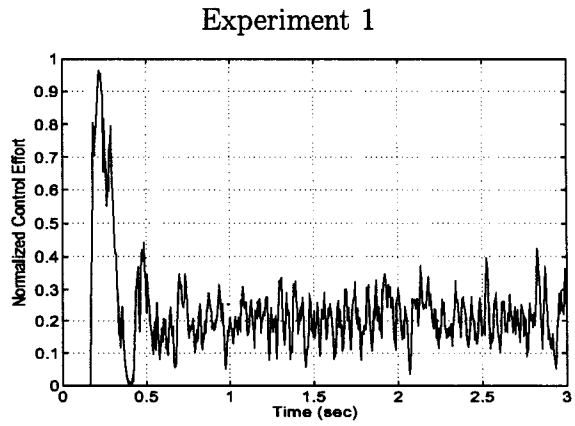

Figure 7.29: Control Effort 4, Modified Theorem 2

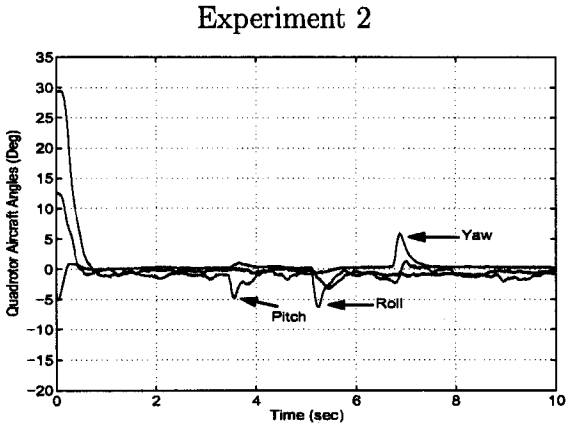

Figure 7.30: Aircraft Angles, Theorem 1

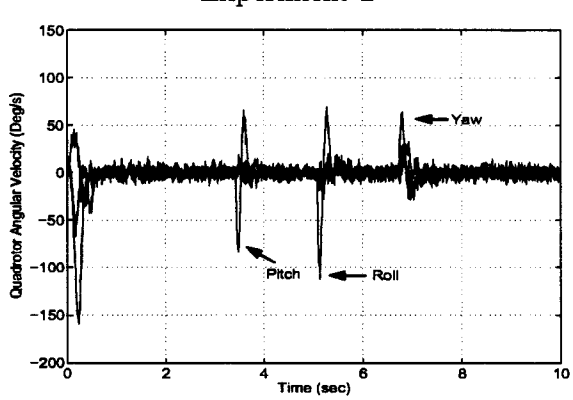

Figure 7.31: Angular Velocity, Theorem 1

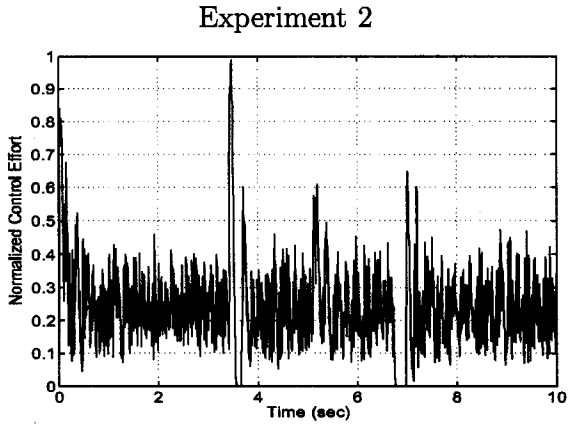

Figure 7.32: Control Effort 1, Theorem 1

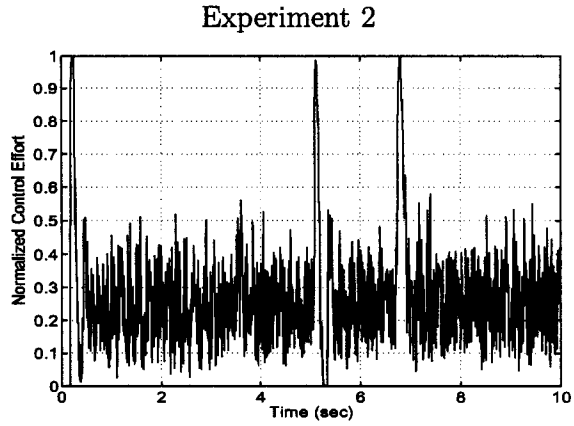

Figure 7.33: Control Effort 2, Theorem 1

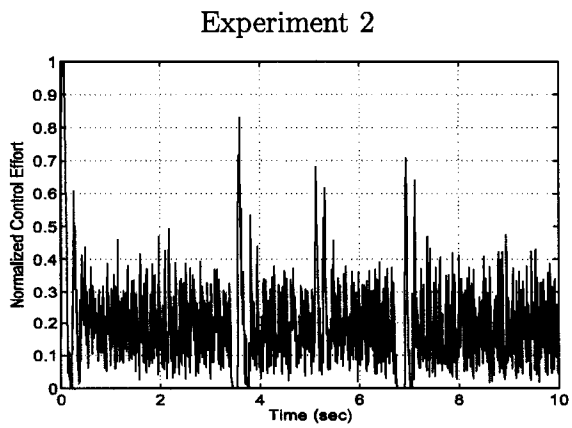

Figure 7.34: Control Effort 3, Theorem 1

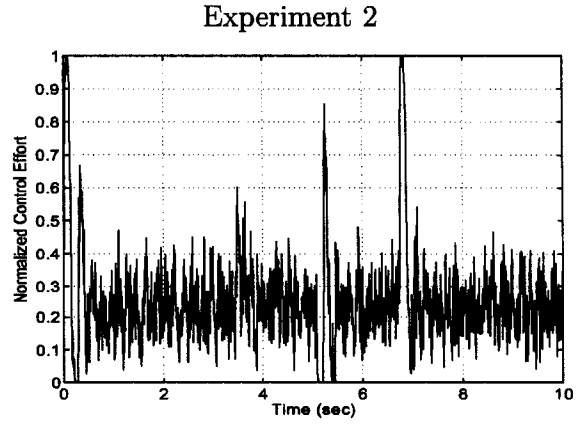

Figure 7.35: Control Effort 4, Theorem 1

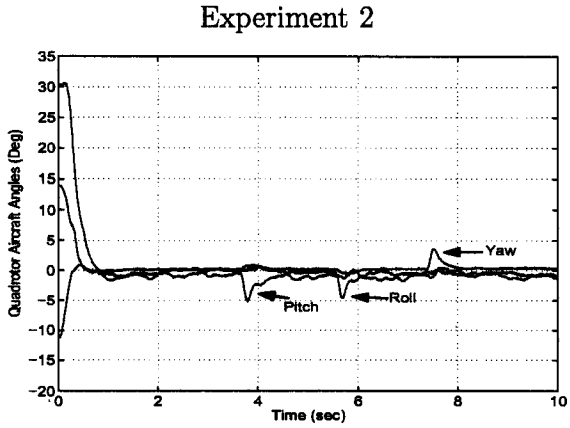

Figure 7.36: Aircraft Angles, Modified Theorem 1

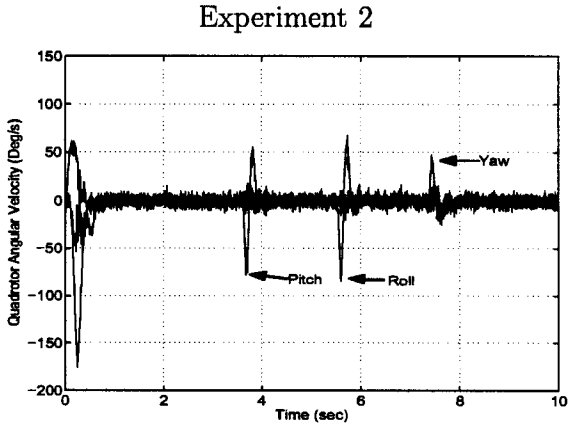

Figure 7.37: Angular Velocity, Modified Theorem 1

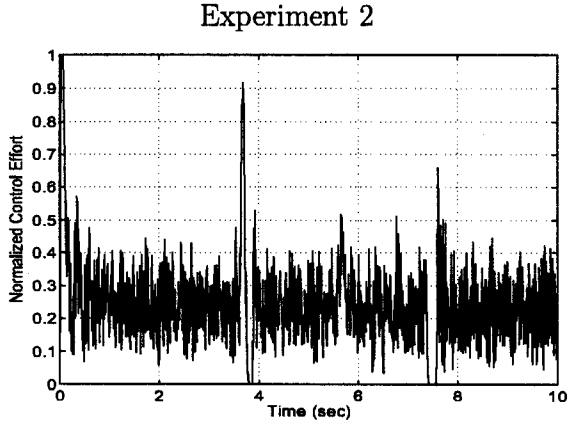

Figure 7.38: Control Effort 1, Modified Theorem 1

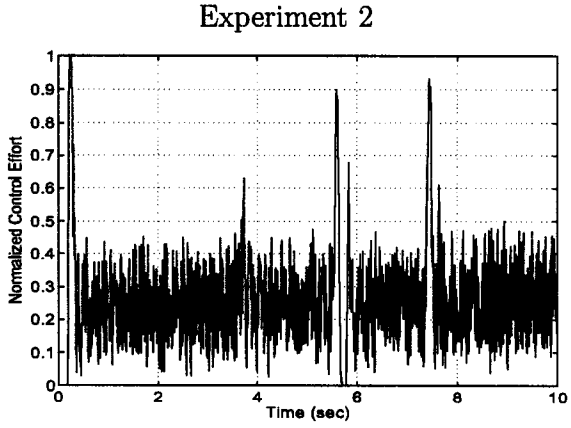

Figure 7.39: Control Effort 2, Modified Theorem 1

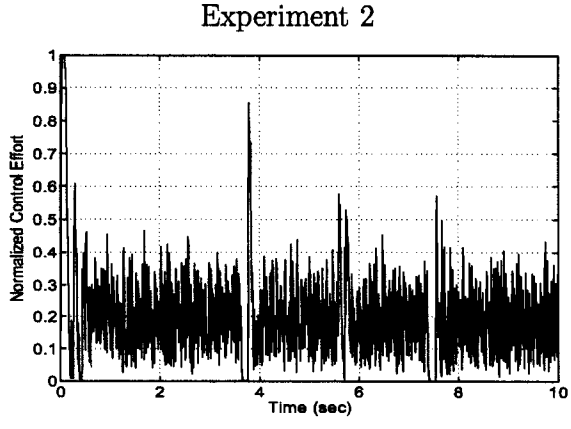

Figure 7.40: Control Effort 3, Modified Theorem 1

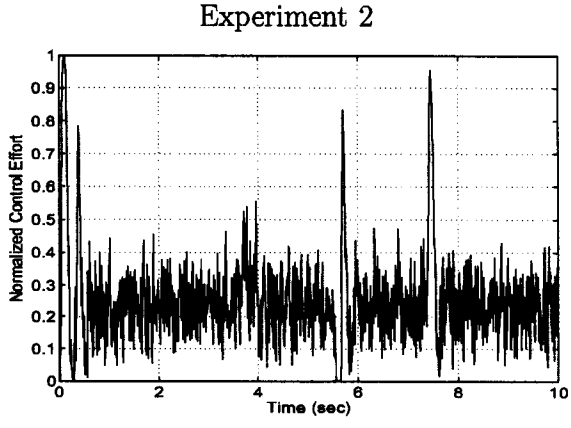

Figure 7.41: Control Effort 4, Modified Theorem 1

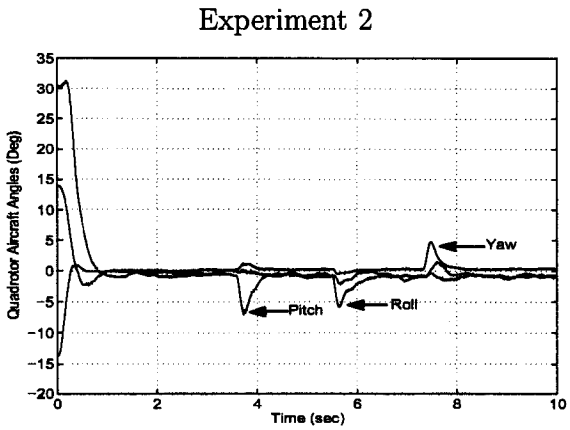

Figure 7.42: Aircraft Angles, Theorem 2

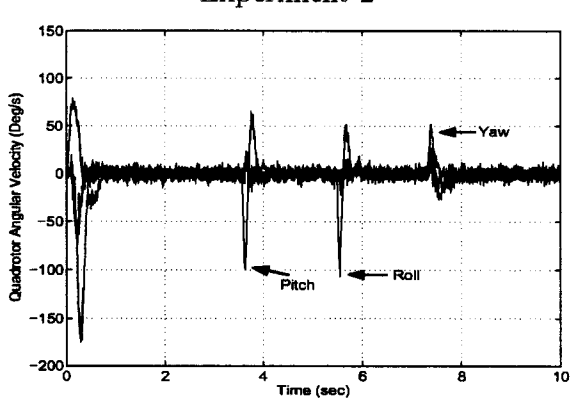

Figure 7.43: Angular Velocity, Theorem 2

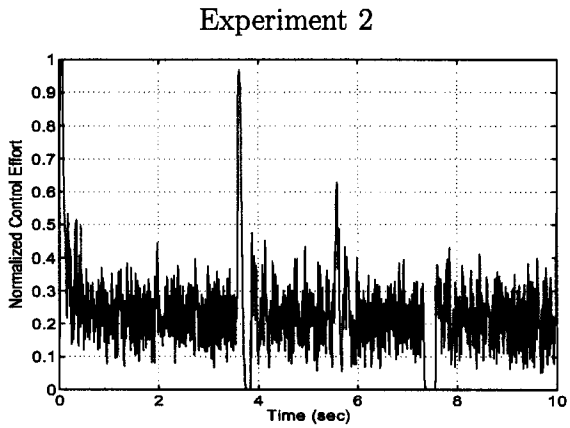

Figure 7.44: Control Effort 1, Theorem 2

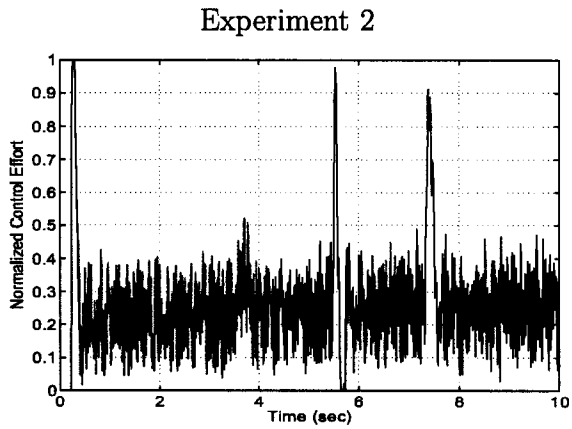

Figure 7.45: Control Effort 2, Theorem 2

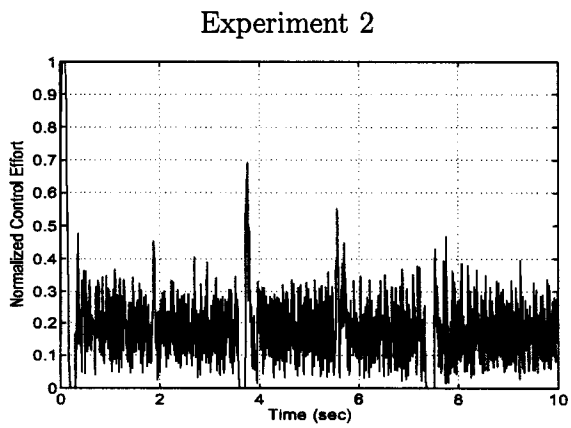

Figure 7.46: Control Effort 3, Theorem 2

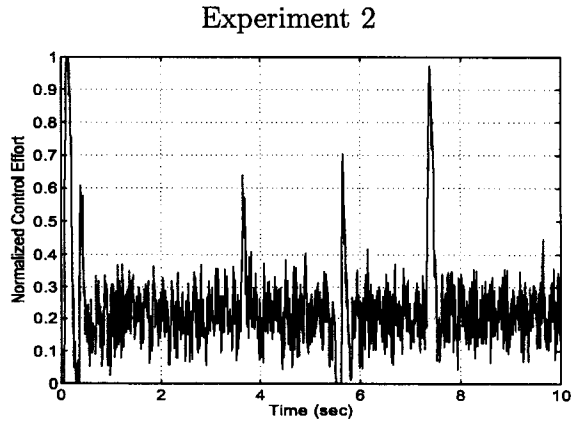

Figure 7.47: Control Effort 4, Theorem 2

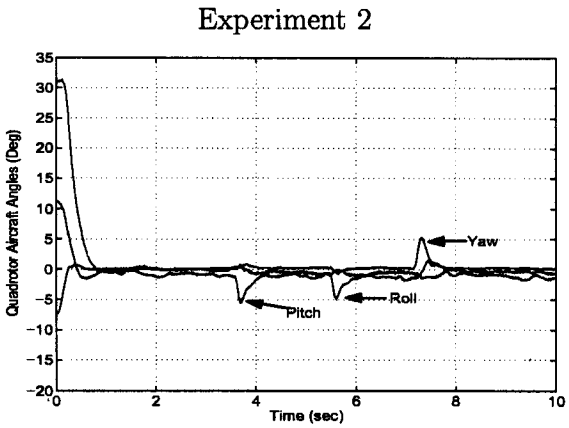

Figure 7.48: Aircraft Angles, Modified Theorem 2

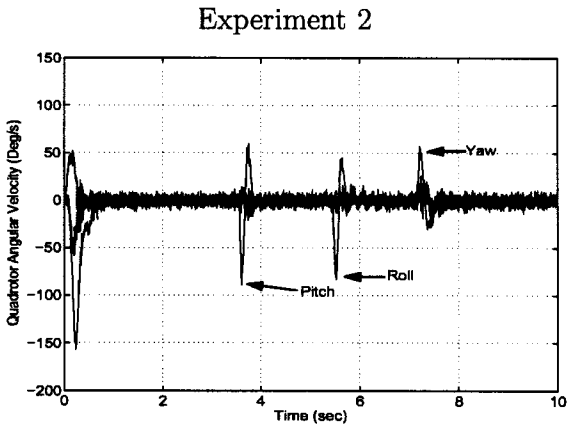

Figure 7.49: Angular Velocity, Modified Theorem 2

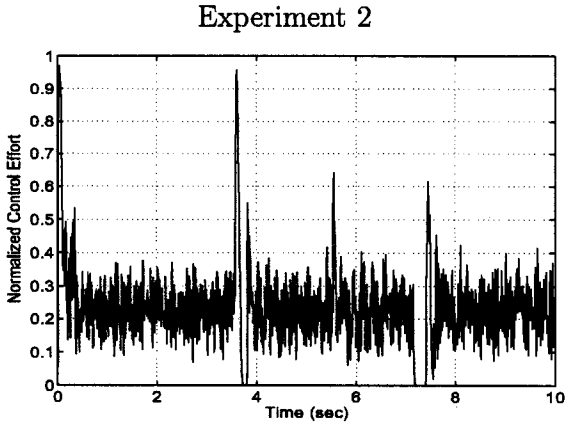

Figure 7.50: Control Effort 1, Modified Theorem 2

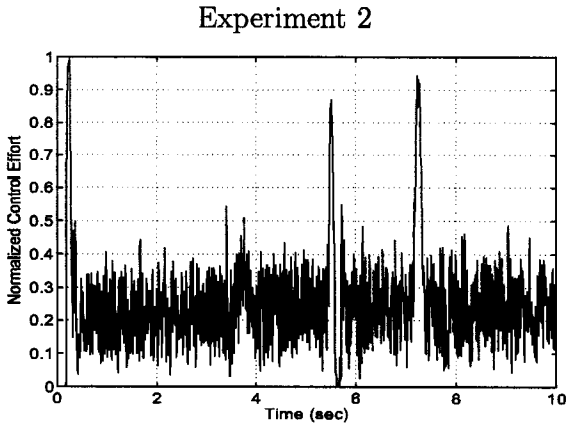

Figure 7.51: Control Effort 2, Modified Theorem 2

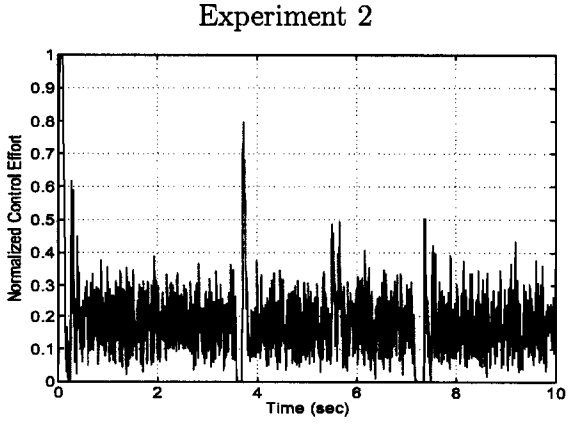

Figure 7.52: Control Effort 3, Modified Theorem 2

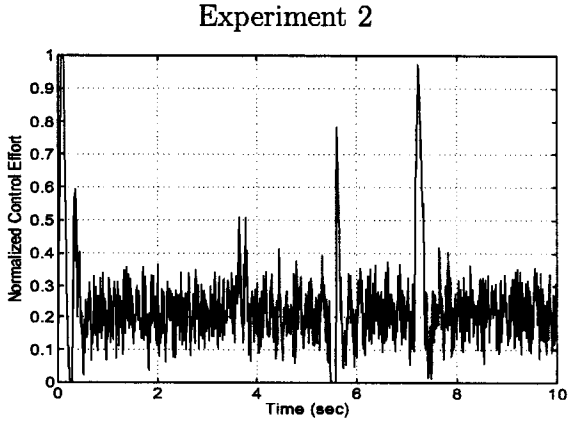

Figure 7.53: Control Effort 4, Modified Theorem 2

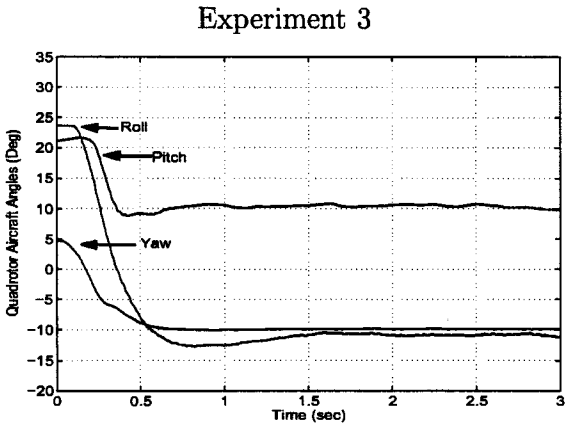

Figure 7.54: Aircraft Angles, Theorem 1

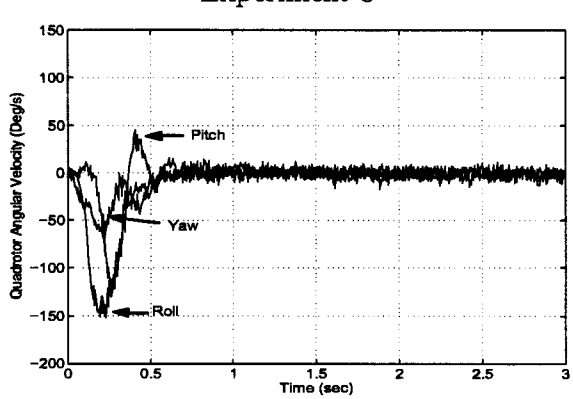

Figure 7.55: Angular Velocity, Theorem 1

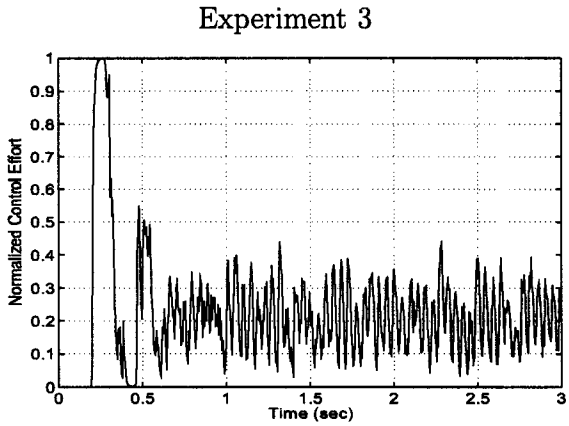

Figure 7.56: Control Effort 1, Theorem 1

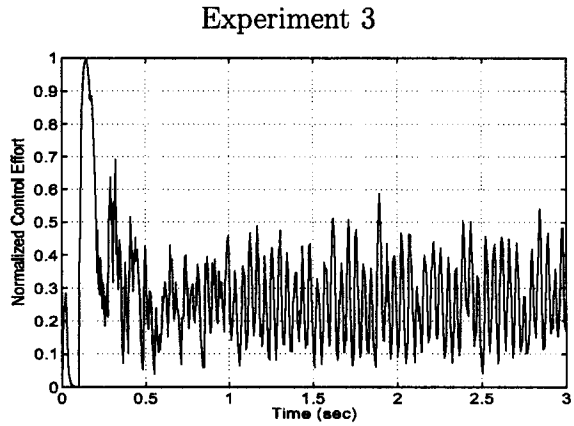

Figure 7.57: Control Effort 2, Theorem 1

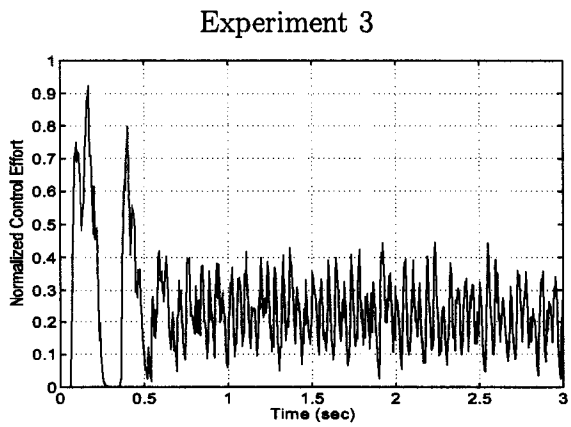

Figure 7.58: Control Effort 3, Theorem 1

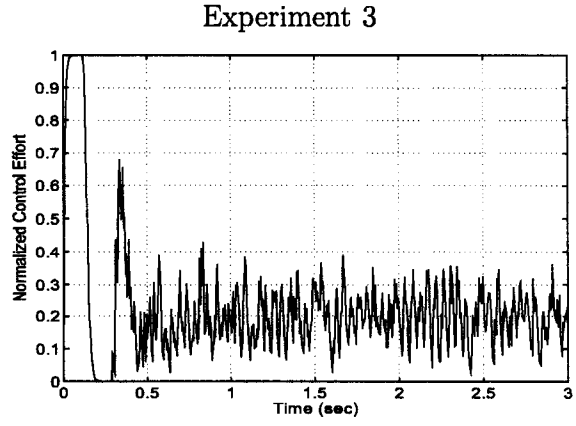

Figure 7.59: Control Effort 4, Theorem 1

Chapter 8

Conclusion

With the increasing popularity of UAV's, the desire for VTOL style aircraft, and the availability of small lightweight sensors, the quadrotor has seen an overwhelming interest in recent years. In fact, the necessity for an attitude stabilizing controller for the quadrotor has proven to be the main motivation for this research.

A review on the attitude representation of a rigid body in space has been presented detailing necessary parameterizations required for the control design, including the Euler Angles, Direction Cosine Matrix and the non-singular four-parameter Quaternion representation. Also, Chapter 5 has been presented, detailing experiments and techniques used to determine the model parameters.

The development of the quadrotor dynamical model based on the Newton-Euler formulation, has been presented. In Chapter 4, two main theorems are developed based on the work from (Tayebi and McGilvray 2004). The controller in Theorem 1 is model-dependent, and guarantees global exponential stability for the attitude stabilization problem. This theorem is based on the compensation of the gyroscopic and Coriolis torques, and has a PD^2 feedback structure, where the proportional action is in terms of the vector-quaternion, and the two derivative actions are in terms of the airframe angular velocity, and the vector-quaternion velocity. In Theorem 2, a model-independent PD controller, providing asymptotic stability, has been presented. Modifications to both theorems, by adding or removing compensation terms for the

gyroscopic and Coriolis torques, have been discussed. Moreover, the altitude control and the attitude set-point regulation problems have been addresed.

Simulations have been performed using Simulink, and have provided graphical results for each controller discussed.

The experimental setup of a model quadrotor aircraft has been presented including details regarding sensors, attitude estimation and sensor fusion. In fact, as previously mentioned, the attitude estimation of the quadrotor aircraft proved to be most challenging. Details regarding the frequency domain approach to fusing signals from gyroscopes with accelerometers have been shown, and problems with this method have been revealed and discussed.

The experimental results for the attitude stabilization controller have proven to be quite similar in terms of convergence rates and disturbance rejection. Under the experimental conditions, it is difficult to see much difference between the controllers, in terms of performance, with or without gyroscopic and Coriolis torques compensation. However, under larger initial conditions, higher speed, and more aggressive maneuvers, there is a greater influence from the gyroscopic and Coriolis torques, and although it was not possible to experiment under these conditions, it is believed that compensation of these terms will reveal the superior controller.

Upon completion of the experimental testing, a number of observations have been made. Considering any one of the attitude controllers developed in detail, there are a number of control parameters or gains that must be set for optimal performance. Of course, each of these gains have restrictions as described in the *Control Design* chapter, however, tuning each of these gains to give good results proved challenging, and was performed through simulation and trial and error.

Future work includes the programming of a microcontroller to allow untethered flight. With the addition of a lightweight Lithium battery pack supplying power to the aircraft and sensors, a lightweight landing gear for crash safety, and remote receiver for pilot input, flight testing would be possible. Adding an ultrasonic sensor to be used as an altimeter, could also allow the altitude controller to be tested experimentally.

Developing a full control solution for the quadrotor attitude and position in space could yield a fully autonomous aircraft, capable of following programmed trajectories. Of course the requirement of a coordinate positioning system, such as GPS, would also be essential. Implementation of better fusion and attitude estimation techniques would be required for aggressive maneuvers and more dynamic flight. A larger, more powerful quadrotor aircraft could also be designed with gas powered rotors. Combined with collective pitch control, the thrust of the rotors could be reversed without reversing the rotating direction of the rotor, which could yield a highly maneuverable quadrotor aircraft capable of aerobatic flight.

Bibliography

Akella M.R., J.T. Halbert and G.R. Kotamraju, 2003. Rigid body attitude control with inclinometer and low-cost gyro measurements. *Systems and Control Letters*, Vol. 49, pp. 151-159.

Altuğ E., J.P. Ostrowski and R. Mohony, 2002. Control of a Quadrotor Helicopter Using Visual Feedback. *IEEE Int. Conf. on Robotics and Automation*, Washington, D.C., pp. 72-77.

Avila Vilchis J.C., B. Brogliato, A. Dzul and R. Lozano, 2003. Nonlinear Modelling and Control of Helicopters. *Automatica*, Vol. 39, No. 9, pp. 1583-1596.

Baerveldt A.J. and R. Klang, 1997. A low-cost and low-weight attitude estimation system for an autonomous helicopter. *Proc. IEEE Int. Conf. on Intelligent Engineering Systems*, pp. 391-395.

Castillo P., A. Dzul and R. Lozano, 2003. Real-time Stabilization and Tracking of a Four Rotor Mini-Rotorcraft. Accepted to the *IEEE Transactions on Control Systems Technology.*

Crouch P.E., 1984. Spacecraft Attitude Control and Stabilization: Applications of Geometric Control Theory to Rigid Body Models. *IEEE Transactions on Automatic Control*, Vol. AC-29, No. 4, pp. 321-331.

Fitzgerald A.E., C. Kingsley, Jr., S.D. Umans, 1990. *Electric Machinery*, McGraw-Hill, Inc., New York.

Frazzoli E., M.A. Dahleh and E. Feron, 2000. Trajectory tracking control design for autonomous helicopters using a backstepping algorithm. Proc. of the *American Control Conference*, Chicago Illinois, pp. 4102-4107.

Gablehouse C., 1969. *Helicopters and Autogiros; A History of Rotating-wing and V/STOL Aviation.* Philadelphia: J.B. Lippincott Company.

Gessow A. and G.C. Meyers, Jr., 1967. *Aerodynamics of the Helicopter*, Frederick Ungar Publishing Co., New York.

Hamel T., R. Mahony, R. Lozano and J. Ostrowski, 2002. Dynamic modelling and configuration stabilization for an X4-flyer. In Proc. of *IFAC World Congress*, Barcelona, Spain.

Hughes P.C., 1986. *Spacecraft attitude dynamics.* New York: Wiley.

Ickes B.P., 1970. A New Method for Performing Control System Attitude Computation Using Quaternions. *AIAA J.*, Vol. 8, pp. 13-17.

Joshi S. M., A.G. Kelkar and J. T-Y Wen, 1995. Robust Attitude Stabilization of Spacecraft Using Nonlinear Quaternion Feedback. *IEEE Transactions on Automatic Control*, Vol. 40, No. 10, pp. 1800-1803.

Kane T.R., 1973. Solution of Kinematical Differential Equations for a Rigid Body. *J. Applied Mechanics*, pp. 109-113.

Klumpp A.R., 1976. Singularity-free Extraction of a Quaternion from a Direct-Cosine Matrix. *J. Spacecraft*, Vol. 13, No. 12, pp. 754-755.

Leishman J.G., 2000. *Principles of Helicopter Aerodynamics.* Cambridge University Press, UK.

Lizarraide F. and J. T. Wen, 1996. Attitude Control Without Angular Velocity Measurement: A Passivity Approach. *IEEE Transactions on Automatic Control*, Vol. 41, No. 3, pp. 468-472.

Mahony R. and T. Hamel, 2001. Adaptive Compensation of Aerodynamic Effects during Takeoff and Landing Manoeuvers for a Scale Model Autonomous Helicopter. *European Journal of Control*, vol. 7, pp. 43-58.

Mahony R., T. Hamel and A. Dzul, 1999. Hover Control via Lyapunov Control for an Autonomous Model Helicopter. In proc. *IEEE Conference on Decision and Control*, Phoenix, Arizona, USA, pp. 3490-3495.

Pounds P., R. Mohony, P. Hynes and J. Roberts, 2002. Design of a Four-Rotor Aerial Robot. In Proc. of *Australian Conference on Robotics and Automation*, Auckland, Australia.

Prouty R.W., 1995. *Helicopter Performance, Stability and Control.* Krieger Publishing Company, USA.

Rehbinder H. and X. Hu, 2003. Drift-Free Attitude Estimation for Accelerated Rigid Bodies. *Automatica*, Vol. 40, No. 4, pp. 653-659.

Rehbinder H. and X. Hu, 2000. Nonlinear State Estimation for Rigid-Body Motion with Low-Pass Sensors. *Systems and Control Letters*, Vol. 40, No. 3, pp. 183-190.

Riley W.F. and L.D. Sturges, 1996. *Engineering Mechanics: Dynamics.* Wiley, New York.

Shim H., T.J. Koo, F. Hoffmann and S. Sastry, 1998. A Comprehensive Study of Control Design for an Autonomous Helicopter. In proc. *IEEE Conference on Decision and Control*, Florida, USA.

Tayebi A. and S. McGilvray, 2004. Attitude Stabilization of a Four-Rotor Aerial Robot: Theory and Experiments. Submitted to *IEEE Transactions on Automatic Control.* A short version of this paper has been accepted in the *IEEE Conference on Decision and Control*, Dec. 2004 Paradise Island, Bahamas.

Spong M.W. and M. Vidyasagar, 1989. *Robot Dynamics and Control.* Wiley, USA.

Wen J. T-Y. and K. Kreutz-Delgado, 1991. The Attitude Control Problem. *IEEE Transactions on Automatic Control*, Vol. 36, No. 10, pp. 1148-1162.

Wertz J.R., 1978. *Spacecraft Attitude Determination and Control*, Members of the Technical Staff, Attitude Systems Operation, Computer Sciences Corporation. D. Reidel Publishing Company, London, England.

Wie B., H. Weiss and A. Arapostathis, 1989. Quaternion Feedback Regulator for Spacecraft Eigenaxis Rotations. *AIAA J. Guidance Control*, Vol. 12, No. 3, pp. 375-380.